Performance Characteristics of Bitumen-Emulsion Stabilized Mine-Haul roads.

by
Jan-Christiaan Kotzé

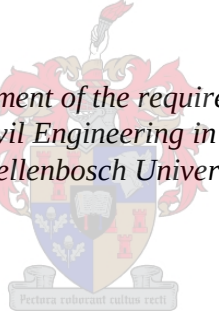

Thesis presented in fulfilment of the requirements for the degree of Master of Engineering in Civil Engineering in the Faculty of Engineering at Stellenbosch University

Supervisor:

Professor Kim J. Jenkins

SANRAL Chair in Pavement Engineering

April 2022

Declaration

By submitting this thesis electronically, I declare that the entirety of the work contained therein is my own, original work, that I am the sole author thereof (save to the extent explicitly otherwise stated), that reproduction and publication thereof by Stellenbosch University will not infringe any third party rights and that I have not previously in its entirety or in part submitted it for obtaining any qualification.

April 2022

Abstract

In the past, mine haul roads were constructed based on local mining knowledge which often resulted in unpredictable road conditions and high vehicle- and road maintenance costs. It has become crucial to reduce both operating costs and road maintenance costs to remain profitable. Recently, a viable long term and cost-effective solution was introduced by incorporating of Bitumen Stabilized Material (BSM) on Mine Haul Road Structures.

BSM incorporated into Pavement Structures have been proven to increase the life span of the road structure. Also, bitumen stabilization creates less moisture susceptible base layers which allows the given layer to be more durable under repeated loading. However, the durability of BSM technology should also be taken into consideration and how it would benefit the mining industry. To create a more standardized implementation of bitumen stabilization in mine haul roads, this research aims to investigate correlations between the performance and material characterisation. Also, this research aims to provide insight into the expected bearing capacity of the bitumen stabilized base layer through various structural testing methods such as Indirect Tensile Strength (ITS) and Dynamic- as well as Monotonic Triaxial testing.

Preliminary ITS results suggest that the current mix design under consideration meets the minimum requirements of a BSM2 material classification for both base layers on Kansanshi and Kalumbila at an average residual bitumen content of 2.2 % and 1.3 % respectively. Further monotonic triaxial analysis on the Kansanshi base indicates that the mix design has a cohesion of 240 kPa with an accompanying friction angle of 41.8 º. These parameters are in line with BSM1 classification limits. However, further analysis is required on the retained cohesion classification limits. Dynamic triaxial tests performed on the Kansanshi base also yields the BSM Base Layer's Resilient Modulus to be in the order of 2500 MPa.

Permeability testing on both Kansanshi- and Kalumbila Trolley Ramp cores evaluates durability of the haul road surfacing, however, the implementation of the dust palliative layer does improve the water-resistance of the BSM Layer. Water is still able to penetrate through the palliative layer due to surface cracking and irregularities. Through the material composition analysis, the residual

binder content for Kansanshi and Kalumbila is 2.2 % and 1.3 % respectively. Also, through grading analysis on both Mines' Trolley Ramp cores, excess fine material was observed between the 2.0 mm to 0.075 mm grading fraction.

By making use of the performance- and material composition results the expected Mechanistic-Empirical (ME) pavement life design for both Kansanshi and Kalumbila Trolley Ramp cores is modelled. The pavement life model yields that the BSM Base Layers can withstand 50+ Million Equivalent Standard Axles (MESAs) under repeated loading. Also, the stress distribution between the Base layer and underlying Subbase structure indicates that both Kansanshi and Kalumbila have well-balanced pavement structures.

Opsomming

In die verlede is mynafvoerpaaie gebou op grond van plaaslike kennis wat dikwels tot onvoorspelbare padtoestande en hoë voertuig- en padinstandhoudingskoste gelei het. Weens ekonomiese beperkings het dit noodsaaklik geword om beide bedryfskoste en padinstandhoudingskoste te verminder. In onlangse jare is die inkorporering van bitumen gestabiliseerde materiaal op mynafvoerpadstrukture as 'n lewensvatbare langtermynkoste-effektiewe oplossing beskou.

Bewyse is gelewer dat die inkorporeering van BSM materiaal in ‘n plaveisels struktuur die lewensduur van daardie struktuur verleng. Bitumen emulsie stabilisering skep ook 'n kroon laag wat minder water deurlaatbaar is, wat in ruil die laag meer duursaam onder herhaalde spannings kragte. Kan BSM-tegnologie mynafvoerpaaie bevoordeel? Om 'n meer gestandaardiseerde implementering van bitumenstabilisering in mynafvoerpaaie te skep, het hierdie navorsing ten doel om korrelasies tussen die plaveisel duursaamheid en materiële karakterisering te ondersoek. Hierdie navorsing het ook ten doel om insig te gee in die verwagte dravermoë van die bitumen gestabiliseerde kroon laag.

Voorlopige resultate dui daarop dat die huidige mengsel ontwerp voldoen aan die klassifikasie vereistes van 'n BSM2 materiaal vir beide basis lae op Kansanshi en Kalumbila met gemiddelde residuele bitumen inhoude van 2.2 % en 1.3 % onderskeidelik. Verder is die skuifparameters vir die Kansanshi kroon laag bepaal as 240 kPa vir die kohesie en 41.8 º vir die wrywingshoek. Hierdie skuifsterkte-eienskappe stem ooreen met die standaard BSM1 skuifparameters. Verdere analise word egter vereis om die behoue kohesie te bepaal. Die dienamiese drie-assige toets wat op die Kansanshi kroon laag uitgevoer is, het bepaal dat die veerkragmodulus van die kroon laag in die orde van 2500 MPa is.

Deurlaatbaarheidstoetsing op beide die Kansanshi- en Kalumbila-myn evalueer duursaamheid van die kroonlaag, maar die implementering van die stof palliatief laag is bewys om die weerstand van water in die BSM kroon laag te verbeter. Water kan steeds die palliatief laag indring deur oppervlakkige krake en onreëlmatighede op die oppervlakte. Deur die materiaalsamestellingsanalise is die oorblywende bitumeninhoud vir Kansanshi en Kalumbila bepaal as 2.21% en 1.29% onderskeidelik. Verdere graderingsanalise op beide mynafvoerpaaie se oorblywende aggregaat, is 'n gebrek aan fyn materiaal waargeneem tussen die 2.0 mm tot 0.075 mm fraksie.

Met die falinseienskappe analise en kroon laag mengsel samestelling resultate, kan die plaveisel lewe vir beide Kansanshi- en Kalumbila myn as aanvaarbaar beskou word waar die BSM kroon lae 50 Miljoen Ekwivalente Standaard Asse (MESAs) onder herhaalde spannings kragte kan dra. Die spanningskragte verspreiding tussen die kroon laag en onderliggende stutlaag struktuur dui daarop dat beide Kansanshi en Kalumbila ‘n goed gebalanseerde plaveisel struktuur het.

Table of Contents

List of Tables

List of Figures

1 Introduction

1.1 Introduction into the problem statement

In the mining industry, mine haul roads can often seem like a trivial feature that does not get the required consideration that it deserves. However, in modern times it has become essential for mines to become more cost-effective. Research indicate that the average highway dump truck is capable of carrying haulage of more than 290 tons per trip (Thompson and Visser, 2006). Thompson and Visser (2006) also state that most mining road infrastructure is constructed by local experience with no engineering background which could often lead to unpredictable road conditions and very high road maintenance costs. Furthermore, unpredictable road conditions also result in a large increase in truck operating costs.

To decrease both operating costs and road maintenance costs, it becomes crucial to focus more on the standardized mine haul road structural design methods coupled with its functional trafficability. To assess a mine haul road in terms of functional trafficability becomes difficult, as each mine implements different methods of performance evaluation and standards. Typical evaluation methods include reduced riding quality, extreme dustiness, increased tyre damage and wear, and loss in haulage productivity (Thompson and Visser, 2006).

In recent years, some mines started incorporating bitumen stabilized base layers within their road structure. Bitumen emulsion refers to the emulsifying of bitumen in water to be added to an aggregate mixture. This is a different variation as to hot mix asphalt (typically used in pavement structures) and has been around since the early 20th century used within unbound layers as a binder (Needham, 1996). The implementation of bitumen emulsion within mine haul roads has been considered due to several beneficial factors. Firstly, to apply bitumen emulsion, the aggregate is not required to be pre-heated resulting in fewer construction costs. Secondly, introducing bitumen emulsion into the aggregate layer significantly reduces the dust emissions that are produced in representative unbound layers. Emulsion mixtures (or referred to as "*cold mix*") have the capability

of being transported over long distances without influencing the structural and functional capability of the material. This provides large logistical advantages as well as reduces operating and manufacturing costs as the material can be stockpiled (Needham, 1996).

1.2 Problem statement

There are two copper mines (namely Kansanshi and Kalumbila) situated in the North-West region of Zambia. Both mines focus on copper ore extraction and processing. For the Kansanshi mine, the typical mine haul trucks can carry a capacity of approximately 180 tons of copper ore. Kansanshi also has a daily copper ore extraction rate of over 200 kilotons per day. For the Kalumbila mine, a typical mine haul truck has a carrying capacity of 400 tons with the mine having a daily ore extraction rate of over 450 kilotons per day.

Both mines make use of haulage ramps with a grade of between 9-10 %. These ramps have the capability of carrying up to 6 haul trucks at a time. On these haul ramps, both mines have implemented a version of a bitumen stabilized layer. Kansanshi mine created a road structure that consists of 2 m of rock compacted by an impact roller followed by an emulsion treated base layer, Slow Set Emulsion (SS60). Some problems have been observed within the grading of the material (i.e. material passing the 0.425 mm sieve observed to be around 36 %). Also, the material used for the emulsion treated baes layer had fractions of material larger than 40 mm. Some sections also indicated signs of block cracking and fatigue cracking.

Kalumbila mine created Trolley Lanes which also consists of a 2 m rock fill compacted with an impact crusher. The Pavement Structure is deep (approximately 2 m) and comprises of good quality overburden that was removed to enable the open cast mining to take place. The upper part of the haul road needs to have a good riding quality measured as Internal Roughness Index (IRI). Improved base layers and sometimes even asphaltic surfacings are known to improve IRI. However, there are challenges related to spillage (falling rocks) from the trucks that create damage in the surfacing. This needs to be addressed through an economical solution.

Both mines provided core Specimens of their haul ramps which are analyzed in terms of their structural capacity as well as their functional trafficability.

1.3 Research goals and objectives

For this research statement, the following goals are set out:

- The main objective of this study is to find solutions for mine haul roads, in terms of structural properties such as bearing capacity;
- To provide optimal technical and economical solutions for Zambian context and its material;
- Provide insight into the BSM-emulsion mix designs used in mining pavement structures.
- Analyze structural capacity of mine haul roads, with a focus on the base layer that includes bitumen emulsion stabilization.
- Find correlations between material properties and functional performance of the material.

To achieve the above-stated goals, the following objectives are going to be executed:

- Determine the structural performance capacity of the existing ramps through applicable test procedures (triaxial, ITS, etc.);
- Identify the composition of the current BSM-emulsion mixes on the mine haul roads, including the percentages residual bitumen content present in specimens and grading;
- Evaluate the structural performance of current BSM-emulsion on the haul roads and investigate links to the residual binder content percentages in these mixes;
- Prepare alternate mix designs of BSM emulsion that assist in identifying the optimum emulsion application rates and the comparative performance. This will include the use of virgin aggregates being used in laboratory mix designs.

1.4 Research limitations

The logistics of an investigation of mine haul roads in northwest Zambia and the transport of material samples and core Specimens to be tested at Stellenbosch University in southwest South Africa, limits by the scope of activities. Performance analysis of the mine haul roads requires Specimens to determine material characteristics such as strength and durability. For the Kansanshi mine, 9 Specimens were provided for testing, of which 2 of the Specimens were cracked. So 7 Specimens could be used for dynamic triaxial, monotonic triaxial, indirect tensile strength, dynamic indirect tensile test, permeability test, and material classification tests. Most of the Specimens also displayed visible irregularities which had to be addressed (i.e. Specimen had to be flattened by the diamond blade cutter). It was also visibly observable that most Specimens displayed signs of being in a brittle state which would influence the workability of these specimens.

1.5 Chapter overview

This section provides underlines the main points that will be discussed in each chapter.

1. Introduction: This chapter provides an introduction to mine haul roads, while also stating the research objectives. Furthermore, this chapter mentions the motivation for this research as well as the goals and objectives set out to achieve this research goal.
2. Literature Study: This chapter provides an understanding of failure mechanisms that can be expected on unpaved roads. Each failure mechanism is discussed with its applicability on mine haul roads. Additionally, this chapter will provide knowledge on Bitumen Stabilized Material (BSM). More specifically, this chapter will further discuss the history of bitumen emulsions, while also evaluating emulsion structures and manufacturing processes.
3. Methodology: This chapter provides information regarding the test procedures that were followed to obtain sensible data for analysis. Correspondingly, this chapter discusses each method in detail providing knowledge with regards to each test procedure.
4. Results: This chapter list and analysis the results obtained through laboratory testing. This chapter will also further discuss and interpret the results concerning the material properties.

5. Conclusion and Recommendations: This chapter summarizes the results discussed in chapter 4 while also highlighting the major findings that were observed. In addition, this chapter will include research recommendations for future studies in terms of the results obtained through testing.

2 Literature review

This chapter provides a brief background into the operations on mine-haul roads, such as distress mechanisms. In addition, the advantages and disadvantages of constructing unpaved haul roads versus stabilized bases, are explored. Furthermore, background information on Bitumen Stabilized Materials, including composition, preparation, conditioning, compaction, and the properties that influence the strength and performance of this stabilized material, are explained. This chapter also provides an overview of the durability of Bitumen stabilized pavement layers and the necessary performance-based tests that will determine the applicable strength parameters. Finally, this chapter will provide, background into the mix design process of BSMs which includes distress mechanisms in BSMs, mix design considerations, aggregate compatibility and mix design procedures.

2.1 Introduction

Development and maintenance of infrastructure are aligned with the performance of the global economy. In recent years, there has been an economic decline, leaving not only insufficient funding for infrastructure but also logistical and procurement issues. The importation and transportation of pavement materials face greater challenges too, based on both economic and environmental circumstances. This produces a scenario where there is a bigger demand for pavement rehabilitation than the development of new roads. These circumstances result in the need for innovative design of alternative rehabilitation solutions. These methods include the recycling of locally obtainable material, usually in-place recycling, with the addition of a stabilizing agent. This can be done at relatively low costs while also achieving the desired strength and stiffness of the required layer (Sabita, 2020).

2.2 Unpaved roads

In most developing and developed countries unpaved road networks provide a crucial element of their economic prosperity. For industries such as agriculture, forestry, tourism and most importantly mining to remain economically viable, they need access to road networks able to withstand year-round weather conditions (Ferry, 1986). For the mining industry, it is an ongoing strug-

gle to maintain unpaved road networks able to withstand the enormous amounts of stress repetitions caused by mine haul trucks. These stresses often lead to several failures such as dustiness, potholes, stoniness, corrugations, ruts, cracks, ravelling, erosion, slipperiness, impassability, and loss of surfacing (Committee of Transport Officials (COTO), 2016). Even though the main objective of this thesis is to determine the effectiveness of Bitumen Emulsion stabilized Mine Haul roads, this section aims to provide insight into the distress mechanisms that are normally observed on untreated Gravel Mine Haul roads. Thus providing more validation for the implementation of BSMs.

Typically gravel wearing courses found on mine haul roads, the major failure mechanism is shear failure as indicated in Figure 1 below (without asphalt surfacing). A granular pavement layers' stiffness is highly dependent on the actual stress state of the material. The stiffness measured in the granular layer will influence the permanent deformation behaviour of the material. Thus the higher the stress, the higher the elastic strain- and permanent strain deformation will be (Jenkins and Rudman, 2019). Typical deformations on gravel wearing courses will be discussed more in depth in this section, as they provide insight into granular-type failure mechanisms that need to be overlaid by Bitumen Stabilized Material BSM, to extend the haul road life.

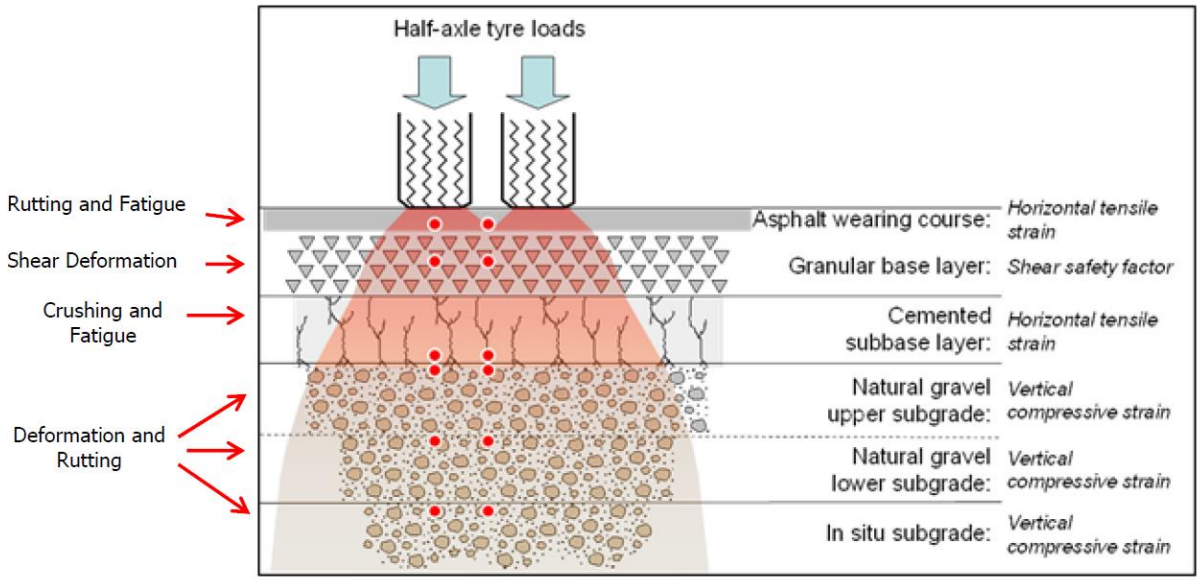

Figure 1 Critical failure parameters found in a typical pavement structure with analysis points (from Jenkins and Rudman (2019)).

2.2.1 Dustiness

Dust is created through a process in which a vehicle moves over a section of unpaved road surfacing. During this movement fine material, usually between 2 to 75 µm, is picked up by the wheels and blown around due to turbulence caused by the vehicle (Adams, 2020). Factors that influence the rate at which dust is created are a function of:

a. The speed at which the vehicle moves
b. The material properties of the surfacing layer, and
c. The aerodynamic shape of the vehicle

Dust can harm the overall safety of road networks. The dust can severely limit visibility and so doing lead to hazardous conditions to follow or pass other vehicles. In terms of health, dust has not been directly proven to cause serious negative health defects. However, the United States of America has identified that certain wearing course gravels may contain materials such as silica dust or even asbestos (which is known to cause illnesses). Dust, during wet and dry conditions, can also inflict damage on vehicles when formed as a hardened paste. This paste causes excessive wear to vehicle parts such as the wheels, thus also increasing maintenance costs to the vehicles. Dust also removes wearing course material which can lead to increased economic cost. Over time the amount of material removed can cause the wearing course material to change in strength properties and ultimately decrease the lifetime of the layer (Committee for State Road Authorities, 1990; Adams, 2020).

However, it is very challenging to predict how dusty a material will become since most materials are dusty. The main factor influencing the dustiness is the material's composition, but there are also other factors such as the speed at which the vehicle travels, the volume of the vehicles using the road, wind speeds, intervals of maintenance, looseness of the material, and moisture content of the wearing course that can affect the dustiness of the road (Committee for State Road Authorities, 1990). According to Paige-Green (1989) when the Shrinkage Product (Sp) is restricted to values between 100 and 240 acceptable levels of dust is produced. It is possible to reduce the amount of dust produced by applying palliatives. These palliatives may include water, water-absorbing suppressant, polymer emulsion, adhesive, clay additive, petroleum emulsion, and bituminous (National Resources Conservation Services, 2007).

2.2.2 Potholes

Potholes are large diameter holes that form within the road. Many factors influence the rate at which potholes form, such as poor compaction, moisture, and material variability, dispersive soils, lack of drainage, inadequate road shape, poor grader practice, and many more[1]. Potholes cause extensive damage to traffic and this damage is a factor of both the depth and diameter of the pothole. Once a pothole starts to form it is almost impossible to repair because drainage starts to deteriorate which causes water to build up in these holes and over-saturate the material. With the addition of traffic, the oversaturated material gets picked up and moved easier causing the pothole depth and diameter to increase. Potholes can be prevented from occurring by scheduled grading. If a pothole already exists the only effective method for repair is creating a larger hole around the pothole and filling it with moist gravel in layers and compacting (Committee for State Road Authorities, 1990).

2.2.3 Stoniness

Stoniness refers to aggregate larger than 37.5 mm that can be found within the road. Several problems arise as a result of excessive stoniness such as corrugation development, unnecessarily rough

Figure 2 Excessive stoniness on unpaved roads (from Unpaved Road Standards for Caribbean and Pacific Islands', 2021).

[1] Factors influencing pothole creation can be found in TRH20.

roads, areas adjacent to stones often suffering from poor compaction, difficulty maintaining with a grader and excessive fine material is required to cover the stone. Materials such as shale and hornfels, when crushed or compacted, causes sharp or flaky stones which can affect the safety of the road or even cause serious damage to vehicle tires. Certain types of Mudrock have been observed to rapidly deteriorate when exposed to the atmosphere producing smaller flaky and sharp stones and in worst case deteriorate into a fine-grained 'soil' (Committee for State Road Authorities, 1990; Kitchell, Kuchar and Viqueira Rios, 2021).

2.2.4 Corrugation

Corrugation can best be described through the "forced oscillation theory" generated by Heath and Robinson (1980). This theory can be described as wheel bounce that is caused by irregularities in the road or worn suspension components on vehicles using the road. This wheel bounce on the road causes loose non-cohesive material to recoil backwards while the material underneath the

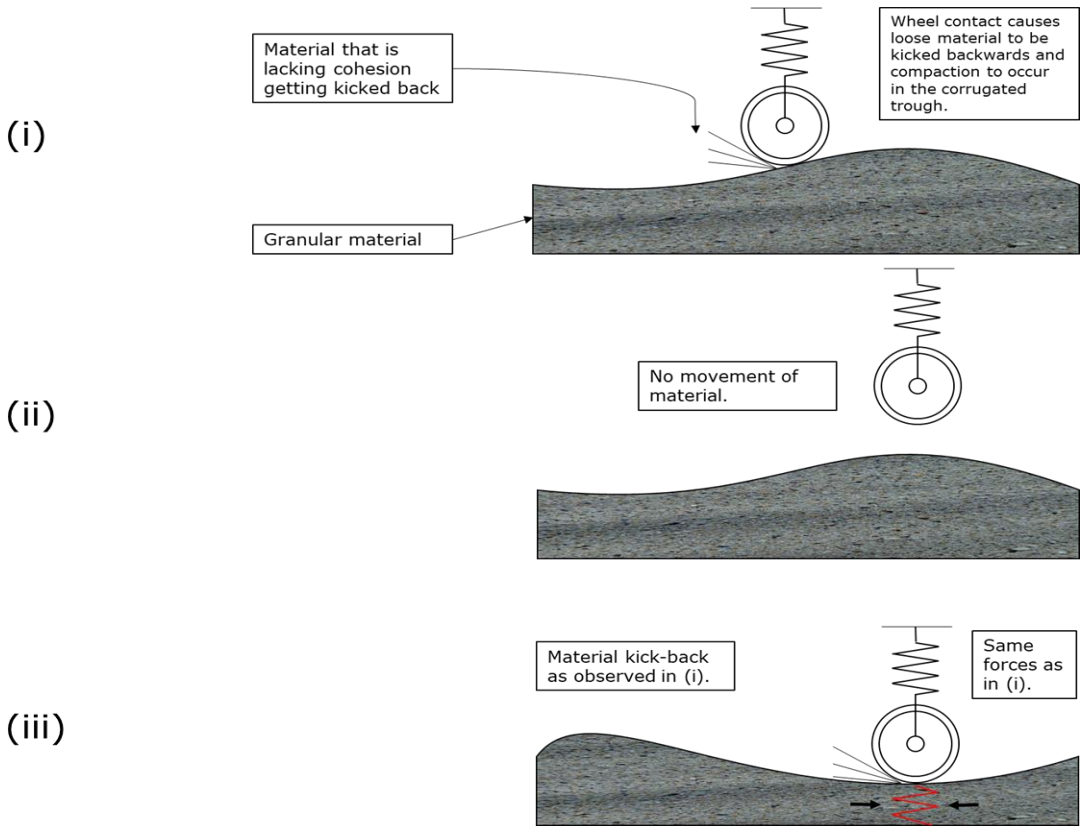

Figure 3 Forced oscillation theory (adapted from Committee for State Road Authorities, (1990))

wheel is being compressed. Paige-Green (1989) also presented research that backed the theory of Heath and Robinson and the illustration of the "forced oscillation theory" is displayed in Figure 3.

Corrugation can occur in two different states, namely loose and fixed corrugation. Fixed corrugation can be described as hard, fine-sandy material that is compacted and forms in parallel crests. It generally requires cutting or tinning with a grader to be repaired and respreads. However, loose corrugation can be described as loose, fine-sandy material which forms in parallel crests at an inclination to the direction of traffic. Loose corrugation can also easily be removed by blading. The wavelength at which corrugation occurs has also been determined to be dependent on the modal speed of the vehicles using the road (Committee of Transport Officials (COTO), 2016).

Unpaved roads with corrugation typically have high percentages of fine sandy material with low plasticity. Nonetheless, there are roads with plasticity indices of more than 9 that also produce corrugation. This can occur during the maintenance period when a grader redistributes the material that accumulates on the roads outer edge. The side material is usually lacking in binder due to environmental conditions resulting in non-plastic material causing the corrugation. During wet seasons corrugation does not tend to form as the material acts cohesive as a result of capillary suction. It has also been proven that corrugation tends not to form on roads where the modal speed is equal to or less than 20 km/h (Committee for State Road Authorities, 1990).

2.2.5 Ruts

Ruts are indents that form parallel to the wheel paths on the surface of the road. Ruts can form due to a loss of- or inadequate wearing course compaction, or even compaction (deformation) of the subgrade. South Africa is known for typically having strong, free-draining, sandy subgrade material and deep water tables, thus looking at the road performance overall localized rutting conditions are usually insignificant. However, ruts do tend to build up water that can soften the wearing course. This decreases the performance of the wearing course and allows for deformation under traffic loading which can be problematic (Committee of Transport Officials (COTO), 2016).

In South Africa, the leading cause of rutting has been identified to be the ravelling of material that has low cohesion. Deformation can also cause ruts to form in wearing course material with high

cohesive strength under traffic loading. In both cases, if maintenance becomes too expensive different types of gravel have to be used. Ruts can also form on the road that is disproportionately wide to that of roads that have a normal width. These ruts usually for in both directions and are typically deeper. The cause of the deeper ruts could be since no lateral movement is required for vehicles to pass from both directions thus all the vehicles consistently pass through the same ruts (Committee for State Road Authorities, 1990; Committee of Transport Officials (COTO), 2016).

2.2.6 Cracks

According to the Committee for State Road Authorities (1990), unpaved roads seldom display cracks but if cracks occur it could lead to the development of potholes. Cracking typically occurs during the dry season on wearing course materials that have high plasticity and are very fine-grained (Clay material). The same wearing course material acts slippery during the wet seasons. It has also been confirmed that block cracks that are 100-150 mm in diameter tend to disintegrate under loading which causes the potholes to form(Committee for State Road Authorities, 1990). It should be noted that block cracking usually refers to cement stabilized material, but in this instance block cracking refers to the formation of small clay block (high plasticity material) due to the lack of moisture. In the absence of moisture, the clay material will start to contract and result in these cracks.

2.2.7 Ravelling

Ravelling is the process in which material loosens due to traffic loading. The loose material that is produced can predominantly be found forming in windrows alongside both wheel paths of the vehicle, but can also be found distributed over the entire width of the road. Raveling occurs on roads as a result of factors such as:

a) Inadequate compaction of the road,
b) Deficiency of fines in the road material results in less cohesion, and
c) Inadequate distribution of the material's particle size.

Materials that are used for the construction of unpaved roads that have a shrinkage product[2] (S_p) smaller than 100 and/or display a grading coefficient[3] (G_c) that is larger than 34. The extent of ravelling is observed to be more in the dry season. This is due to the moisture causing capillary suction during the wet season which in turn results in more cohesion in the fines.

Several problems can occur due to ravelling. Firstly, the concentration of windrows adjacent to the wheel paths can be a safety hazard when driving. Due to the lack of fine materials, there is also the possibility of loose gravel inflicting damage on vehicles and more specifically windscreens. Vehicle operating costs along with fuel costs can increase due to the increase in rolling resistance caused by the absence of fine material. With the increase of windrows forming on the road it could also decrease the efficiency at which lateral drainage occurs on the road. However, ravelling can be mitigated by compacting the material during moist conditions or by blending the existing material with gravel with sufficient cohesion(Committee for State Road Authorities, 1990).

2.2.8 Erosion

The TRH20 guidelines from Committee for State Road Authorities (1990) describe the term erosion as surfacing material being lost due to water flowing over the road. Erosion can directly be correlated to the shear properties of the aggregate. As the normal stress within the material is zero, the shear strength is equal to the cohesion of the material. If the tensile forces of the water exerted on the material is larger than the shear strength of the material, the grains will become loose and detach causing erosion to occur. Materials with a G_c of 16 (Material that contains minimal coarse material) are more susceptible to erosion. However, the material with higher plasticity content can resist erosion but at the cost of creating a slippery surface when wet, thus decreasing the skid resistance.

Erosion can lead to numerous problems in the longitudinal and transverse directions. Erosion that occurs in the longitudinal direction can form deep ruts and erosion in the transverse direction can lead to extreme roughness. Both forms of erosion can result in a change of the material's properties

[2] Shrinkage product refers to the method used to determine the clay content in material.
[3] Grading coefficient refers to the product of the difference in percentage passing the 26.5 mm and 2.0 mm and the 4.75 mm sieves. These values are expressed as percentages.

as certain material fractions are removed by the water (Committee of Transport Officials (COTO), 2016).

2.2.9 Slipperiness

The term slipperiness refers to a material with large percentages of fine or plastic material that become slippery when subjected to moisture. Pockets of fine silty or clayey material near the surface can also result in slipperiness even if the material has a coarse grading. Drier climates can cause a form of slipperiness to occur on the road. In the absence of water, loose fines (usually between 2 and 7 mm) can build up because of ravelling. The buildup of fines causes the skid resistance to diminish to almost zero and the material particles start acting like ball bearings, rolling over each other. In wet climates, slipperiness can also occur as a result of the linear shrinkage value being greater than 365 as this provides an indication of the clay content present within the material, thus high clay would result in a slippery surface (Committee for State Road Authorities, 1990).

2.2.10 Gravel loss

Gravel loss is the term used to describe the displacement of gravel from the roads due to factors such as traffic and climate conditions. Materials that are displaced due to ravelling contribute even more to gravel loss as ravelling results in the formation of loose material and is ultimately displaced by vehicles. Although these factors are inevitable, certain actions can lead to a reduction in gravel loss. For instance, a material with a high percentage passing 26.5 mm and high plastic factor (more than 500), with good compaction can lead to a significant drop in gravel loss(Committee for State Road Authorities, 1990).

2.3 Bitumen Emulsion

2.3.1 Bitumen emulsion background

Bitumen emulsion refers to a method where bitumen is dissolved and dispersed in water. It can also be described as a two-phase, heterogeneous fluid system that contains bitumen and water that

is stabilized with an emulsifier agent (Redelius and Walter, 2005). There are two methods for creating emulsion:

I. The normal method in which bitumen droplets, that range from 0.1 to 50 microns, are mixed with water (Redelius and Walter, 2005), and
II. Inversed method where the water will be dispersed through the bitumen (Kashaya, 2013).

Redelius and Walter (2005) stated that the first patent was taken out in 1906 by Van Westrum which involved the dispersion of bitumen through water for road construction. In the beginning, they tried creating emulsions through mechanical motions, but this method soon became inferior as the demand grew. They soon after started adding emulsifiers to the emulsions to mix easier as stated by the patent created by Albert and Berend (1916). The emulsifiers were created by utilizing the occurring organic acids that are found within bitumen. To stabilize the dispersion of emulsion, an anionic soap was manufactured with sodium hydroxide or potassium hydroxide added in the aqueous phase (Bradshaw, 1960; Redelius and Walter, 2005).

Schwitzer (1972) also stated that cationic emulsions have become increasingly more used since 1950 as they attract a wider variety of surfaces. This was seen as an essential change as the adhesion properties of bitumen to aggregate are a priority for road construction. Amines, amidoamine, and imidazolines were the most commonly used cationic emulsifiers. Redelius and Walter (2005) also stated that in the mid- 1980s polymer modified bitumen emulsions were created after the development of polymer modifier binders. These enhanced emulsions were exhibited to be more durable and increased performance with superior chemical properties.

2.3.2 Advantages and disadvantages of using bitumen emulsion

When comparing bitumen emulsions to hot-applied or cut-back binders several advantages can arise in terms of environmental safety, sustainability and practicality:

i. Safety
    a. Less rolling is required thus making construction a lot easier and cheaper (Muller, Sadler and Van Zyl, 2012); and

b. Bitumen emulsions can produce a better transverse distribution with blockage when compared to a hot-applied binder which will indicate unmistakable streaks (Muller, Sadler and Van Zyl, 2012); and
c. Bitumen emulsions allow for lower application rates while also allowing additional binders to be applied with ease (Muller, Sadler and Van Zyl, 2012).

ii. Environmental factors
   a. Bitumen emulsions have low solvent content when compared to cut-back binders, thus less environmental contamination occurs (James, 2006; Muller, Sadler and Van Zyl, 2012).
   b. Bitumen emulsion produces much less carbon dioxide and other greenhouse gasses as it requires a lot less energy during the application (Meyer, 1999; Muller, Sadler and Van Zyl, 2012).
   c. There is no heat required in the application process of bitumen emulsion and hence, no burns can occur making bitumen emulsion a lot safer (Meyer, 1999; Muller, Sadler and Van Zyl, 2012).

iii. Practical concerns
   a. Since no heat is required during the storage of emulsion and no heat is applied during the application process, short-term ageing of the binder can be avoided (Kashaya, 2013);
   b. Bitumen emulsion can result in an increased production rate due to emulsions allowing a minimum road working temperature of 10ºC, ultimately extending the working time (Muller, Sadler and Van Zyl, 2012);
   c. Bitumen emulsion adhesion properties are much better as a result of the growing technology of emulsifiers (Muller, Sadler and Van Zyl, 2012);
   d. It is not necessary to use pre-coated, dry and dust-free aggregate (Muller, 2011);
   e. Bitumen emulsions (especially slow set emulsions) can be applied through labour-intensive methods as the emulsion is much easier to apply (Muller, Sadler and Van Zyl, 2012);
   f. Polymer dispersions that are water-based, such as natural- or synthetic latex and a hydraulic binder such as cement and lime is compatible with bitumen emulsions.

When a bitumen emulsion is created and includes one of these binders, a new composite binder is created with increased performance and durability properties when compared to normal bitumen (James, 2006; Pt.2).

Bitumen emulsion applications also have some disadvantages. (Muller, 2011) identified those disadvantages as:

a. The creation process for emulsion must consider aggregate type, mineralogy, reactivity and charge;
b. The viscosity of bitumen emulsion would result in higher surface runoff rates when compared to hot-applied binders; and
c. Rain can also sweep away the bitumen emulsion during the curing period;
d. The top layer of bitumen emulsion can sometimes break, causing a coating layer to form and confining water underneath the layer. This gives the appearance of a false break causing the emulsion to have a longer set time (Muller, Sadler and Van Zyl, 2012);
e. Costs of transport to site: only 60% of the load is bitumen which is what is needed in the mix. The 40% water is transported and then wasted;
f. The cost of bulk emulsion per litre is similar to the cost of bitumen per litre;
g. The breaking of emulsion is dependent on heat, mechanical pressure, amount of emulsifiers, amount of filler and fines, the plasticity of the material, moisture in the mix, so it is difficult to control the rate of breaking.

2.3.3 Bitumen emulsion structures

Bitumen emulsions can be created in three different states: a) Oil-in-water (O/W), b) Water-in-oil (W/O), and c) Multiple phases (W/O/W).

a. **Oil-in-water emulsions:** O/W emulsions have a continuous aqueous phase (water) and a dispersed phase that consists of an “oily” liquid(Redelius and Walter, 2005; Kazemi Esfeh, Ghanavati and Shojaei Arani, 2010). According to James (2006), O/W emulsions are typically taken as the industry standard and contains 0.1 – 2.5 % emulsifier, 40 – 75 % bitumen, and 25 – 60 % water.

b. **Water-in-oil emulsions:** W/O emulsions are "inverted" emulsions, with a continuous phase consisting of an organic liquid (an oil') and a dispersed phase consisting of water(Redelius and Walter, 2005; Kazemi Esfeh, Ghanavati and Shojaei Arani, 2010). Meyer (1999) stated that inverted emulsions based on cutback bitumen also have special applications.

c. **Multiple phase emulsions:** Multiple phase emulsions can have a more complex structure when compared to the W/O and O/W emulsion types. The dispersed phase droplets in a multiple-phase emulsion can contain smaller droplets with a different phase/composition to the continuous phase(Meyer, 1999; James, 2006). Kazemi Esfeh, Ghanavati and Shojaei Arani (2010) stated that emulsions used during road construction are normally considered to be O/W. However, several studies completed indicated that water droplets were found within the bitumen droplets, indicating that they should be considered as W/O/W emulsions.

2.3.4 Types of bitumen emulsion

It is possible to form an emulsion by rapidly mixing oil and water. Once the mixing stops the droplets will deform and move closer together and coalesce. To delay or prevent the two phases from separating, an emulsifier is required (James, 2006). The five different types of bitumen emulsions will be discussed in more depth below.

i. Cationic emulsions

Cationic emulsions are the most widely produced emulsions in the world. Different types and mixtures can manufacture it, such as quaternary ammonium compounds, alkoxylated amines, monoamines, diamines, and amidoamine(Redelius and Walter, 2005). These chemical structures are displayed in the figure below.

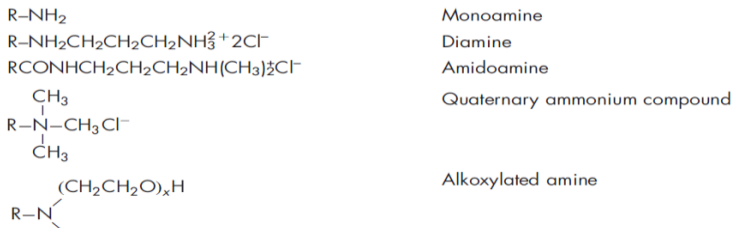

Figure 4 Chemical structures of mixtures available to create cationic emulsions provided by Redelius and Walter (2005).

Redelius and Walter (2005) also stated that these mixtures are provided with a neutral pH. Acid must be added to react with the mixtures so that the mixture can become water-soluble and cationic. Hydrochloric acid, phosphoric, or sulfuric acid is usually used to react with the nitrogen atoms that produce an ammonium ion and force the chemical structure to become a cationic soap with a pH<7. An example reaction is shown as follows

$$R - NH_2 + HCI \rightarrow R - NH_3^+ CI^-$$

(monoamine) (acid) (alkylammonium acid)

Redelius and Walter (2005) stated that the cationic emulsifying agent leaves the positively charged head behind while the negatively charged head floats around in the water. During the dissociation process, Muller (2011) also found that the molecules split into R-NH_3^+ and CI^- ions(Kashaya, 2013). The positively charged R-NH_3^+ connects to the bitumen droplets giving the droplets a positive charge. As each bitumen droplet has a positive charge, they remain in suspension as positive charges repel each other (Redelius and Walter, 2005).

ii. Anionic emulsion

Anionic emulsions are the second-largest mass-produced emulsions in the world by volume. The emulsifier used in anionic emulsions is sulfonate or fatty acids. However, fatty acids have to be treated with alkalies, such as sodium or potassium peroxide, to make the mixture alkaline with a pH>7 since it is insoluble in water (Redelius and Walter, 2005). An example of the chemical structure is displayed as follows:

$$R - COOH + NaOH \rightarrow R - COO^- Na^+ + H_2O$$

(Fatty acid) (Base) (Anionic soap) (Water)

The ‘R’ in the formula refers to a hydrocarbon tail. Most emulsifiers consist of a hydrophilic head and a lipophilic hydrocarbon tail. These hydrocarbon tails usually have 12 to 18 carbon atoms that are comprised of oils, tall oil, natural fats, wood resin, or lignin (James, 2006). These hydrocarbon tails work by aligning with the bitumen. This cause the positive region of the hydrophilic head to float around within the water, causing the surface of the bitumen droplet to become negatively charged by the remaining head (Redelius and Walter, 2005).

Muller (2011) also found that during chemical dissociation, the anionic soap molecule splits into COO^- and Na^+ ions (Kashaya, 2013). The bitumen droplet gets a negative charge from the $R\text{-}COO^-$. The anionic emulsion has a pH balance of between 7 and 14 (according to Redelius and Walter (2005), a pH between 10-11) and would normally be used with positively charged or neutral aggregate.

iii. Non-ionic emulsion

This emulsion is made with non-ionic emulsifiers. The non-ionic emulsifier has a covalent hydrophilic head group, which indicates that the atoms share electron pairs. Non-ionic emulsifiers dissolve without ionization as they are also polar (Redelius and Walter, 2005). An example of a non-ionic emulsifier structure can be seen below:

$$R - COO(CH_2CH_2O)_XH$$

According to Needham (1996), the hydrophilic head groups of non-ionic emulsifier structures consists of ethoxylate group chains (C_2H_2O). Needham (1996) further stated that the polarization of this structure is similar to that of H_2O. As the molecule becomes polarized, the electrons concentrate around the oxygen atoms giving them a negative charge. During this process the carbon atoms are left electron-deficient, thus becoming positive. An example of the chemical structure of such an emulsifier is ethoxylated nonylphenol and is shown in Figure 5 below.

For an emulsion to be classified as non-ionic, the emulsifier has to be neutral. However, James

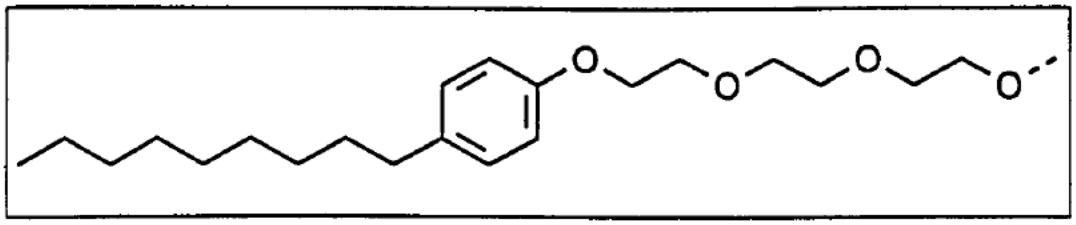

Figure 5 Nonyl phenol ethoxylate, retrieved from Needham (1996).

(2006) cited that several other studies indicated that non-ionic emulsifiers usually have a negative charge, although very small. Redelius and Walter (2005) also stated that any charge found within a non-ionic emulsion comes from the bitumen itself.

Since non-ionic emulsions are neutral, the bitumen emulsion droplets do not collide due to the emulsifier head and not the charge. This phenomenon is called steric hindrance (Suleiman, 2006). Non-ionic emulsions are not used that often and thus it is not produced in major quantities. It is mostly used to change either cationic or anionic emulsions(Redelius and Walter, 2005).

iv. Clay-stabilised emulsion

The clay-stabilized emulsion consists of material where the emulsifying agent used is a fine powder. These fine powders usually consist of natural or processed clays or bentonite. The particles are smaller in size than bitumen particles used in emulsions. Clay emulsifiers are frequently used during industrial applications and not in road construction(Redelius and Walter, 2005). The bitumen particles themselves don't have a lot of electrical charges, but they accumulate together due to mechanical protection of the bitumen's surface by the clay powder and the thixotropic structure of the emulsion (Redelius and Walter, 2005).

According to James and Zhou (2012), bentonite clay can be used to stabilize bitumen emulsions without the need for conventional organic "chemical" surface agents. However, high speeds dispenser will be necessary and this process will also consume large quantities of clay. If chemical emulsifiers were to be included in the emulsion, a lot less clay would have to be combined with the emulsion. James and Zhou (2012) also stated that the residues from the clay stabilized emulsion result in considerably higher softening points, lower penetrations and higher performance grade (PG) top grade. The lower performance grade was not significantly affected.

v. Amphoteric emulsions

Colas (2016) defines an amphoteric emulsion as an emulsion with a neutral pH, but can also be negative- or positively charged. An amphoteric emulsion is manufactured with an amphoteric emulsifier and can be used to create emulsions for micro-surfacings, tack-coats, prime- coats, and cold mixes such as grave- emulsions and standard emulsions used for soil stabilization. According to James (2006), amphoteric[4] emulsions can also exist apart from the above stated four types.

[4] According to the American Heritage Dictionary 2010 the term "amphoteric" refers to having the characteristics of both acids and a base and can also chemically react with an acid or base.

Amphoteric emulsions, depending on the pH of the emulsifier, can be either have a positive or negative charge. Amphoteric emulsifiers can possess both anionic head groups and cationic head groups. Emulsifiers can be categorized according to the electrical charge the head group adopts in water. These categories are either anionic, cationic or non-anionic, but James (2006) stated that these charges can change depending on the pH as well.

In a study completed by Needham (1996), it was found that amphoteric emulsions became cationic at low pH levels and anionic at high pH levels. It was also observed that in most emulsion tests, the point of zero charges was observed at a pH level of between 6 and 7. Needham (1996) also found that emulsions that included Ordinary Portland Cement (OPC) or lime had a zero charge point at a pH level of four.

2.3.5 Bitumen Emulsion Classification

Bitumen emulsions can be categorized in terms of chemical types, but they can also be categorized in terms of setting (breaking) rate. To be considered as a binder within a material mix, bitumen emulsion has to change back into bitumen only phase. The rate at which this process happens is referred to as the setting/breaking rate. The breaking rate can change according to the reactiveness of the emulsion and aggregate, but factors such as temperature and humidity also impede the process (James, 2006). The breaking rate can be split into four different categories which are discussed below.

i. Spray grade/Rapid Set (RS)

When rapid set emulsion comes in contact with uncontaminated aggregate that displays a low surface area, it will set quickly. An example of this type of low surface area aggregate is chippings that are used in chip seals (surface dressings)(Meyer, 1999). In the option, the process of breaking would take approximately one to five minutes according to Kashaya (2013). The reactivity of rapid set emulsions is high and therefore James (2006) suggested that it be used with unreactive aggregates. Kashaya (2013) also stated that this type of emulsion is rarely used in aggregate mixes. This grade of emulsion contains the lowest percentage of emulsifier content, at approximately 0.25 %.

ii. Pre-Mix Grade/Medium Set (MS)

Medium set emulsions set significantly lower at a rate of about 30 minutes. This is since this grade of emulsion contains more emulsifier content, approximately 0.5 %. This emulsion type can also be used with the low surface are aggregate such as the aggregate used in open-graded mixes (Meyer, 1999). This type of emulsion can also be called mixing grade emulsions occasionally, because of the binder's ability to mix with aggregate. From the Asphalt Institute & AEMA, it was also determined that this emulsion type, when mixed, can still be used after several months depending on the formulation (Kashaya, 2013). Kashaya (2013) also stated that medium set emulsion is compatible with open-graded mixes as Meyer (1999) stated, and also cold recycling, patch mixing, and also dense-graded mixes.

iii. Stable grade/Slow set (SS)

Slow set emulsions contain the highest content of emulsifier content at approximately 1.5 %, which makes the emulsion more stable. Stable grade emulsion takes the longest to set because of its low reactivity rate. These emulsions are therefore mostly mixed with highly reactive aggregates with big surface areas (Meyer, 1999). The actual setting time of this emulsion can vary depending on the technique used, the materials being used and external environmental factors. The stable grade emulsion would mostly be used with denser cold mix material that is high in 0.075 mm fines and thus resulting in its high reactivity rate (James, 2006). Kashaya (2013) also stated that the most common use for stable grade emulsions is within slurry seals, dense-graded mixes, asphalt, soil stabilization, and on rare occasions recycling.

iv. Quick setting emulsions (QS)

A quick set emulsion or cationic quick set (CQS) refers to an emulsion that is intermediate in terms of reactivity and can be categorized between the medium setting and slow setting emulsion. This type of emulsion mixture does not have to succeed in the cement mix tests. Quick set emulsions are usually used for slurry surfacing applications and micro-surfacing which requires quick setting (James, 2006). Meyer (1999) states that quick-setting emulsions used in slurry surfacing or micro-surfacing are usually polymer-modified (P) or latex modified (LM). Kashaya (2013) also stated that quick-setting emulsions can be modified to include rapid setting characteristics.

The breaking rate of quick set emulsion directly correlates with the reactiveness of the aggregate and also external elements such as mechanical action from the compaction efforts, temperature, wind speed, humidity, etc.

2.3.6 Factors influencing breaking process

There are, theoretically, six different parameters that could change the breaking rate for all four types of emulsions that were discussed. The first factor would be the bitumen content. If there were more bitumen added to the mixture, the probability of bitumen particles colliding increases the breaking rate. The second factor would be the composition of the aqueous phase. Certain studies have determined that the breaking rate would increase if there was a decrease in the acid content, increase in the emulsifier content or a decrease in the ratio between the emulsifier content and acid (Redelius and Walter, 2005).

Another factor that could influence the breaking rate would be the bitumen particle size distribution. Studies have shown that the smaller the bitumen particles, the fine the dispersion of the particle would be and this would cause the breaking rate to decrease. Just as the bitumen particle size distribution can influence the breaking rate, so can the aggregate. The aggregate must be applied

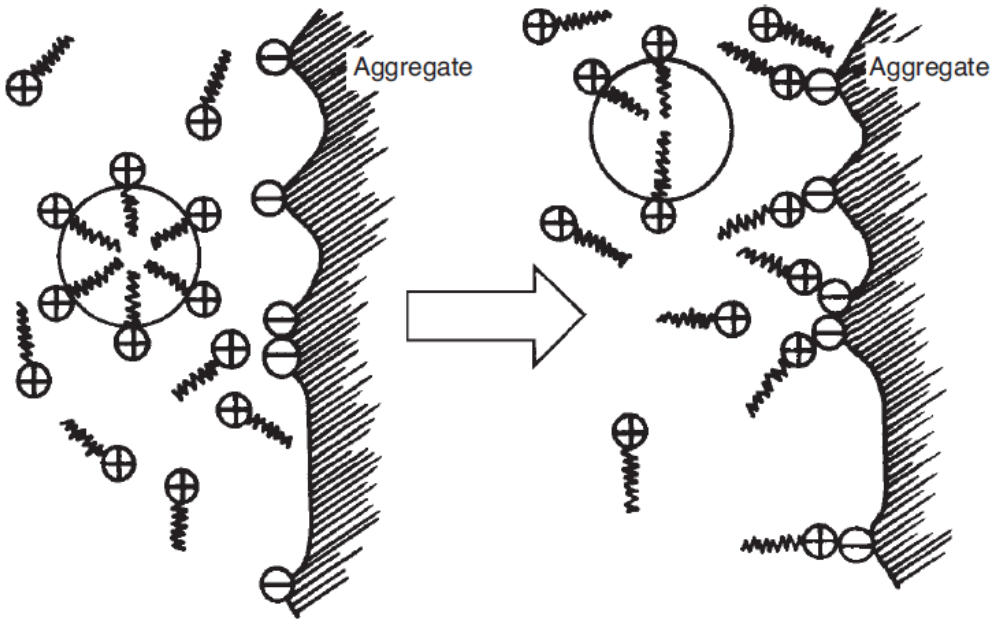

Figure 6 Schematic diagram of breaking process of emulsion (from Redelius and Walter (2005)).

to the emulsion as quickly as possible after the emulsion has been applied. This is to ensure that the emulsion is still saturated enough to cover the aggregate. As the aggregate is applied to the emulsion, evaporation has already started to occur and the aggregate would start to absorb the emulsifier. This would result in an increased breaking rate. Also, dust can cause premature breaking of the emulsion. In the presence of dust, the emulsion will tend to bind to the dust and break faster rather than binding with the aggregate. With factors such as these, the size and shape of aggregate will greatly influence the emulsion breaking rate (Redelius and Walter, 2005).

In an emulsion, there are emulsifier molecules that are attached to the bitumen droplets and can be found in the water. In a stable emulsion mixture, certain emulsifier molecules (ions) will form micelles[5] and equilibrium will exist as shown in Figure 7 below.

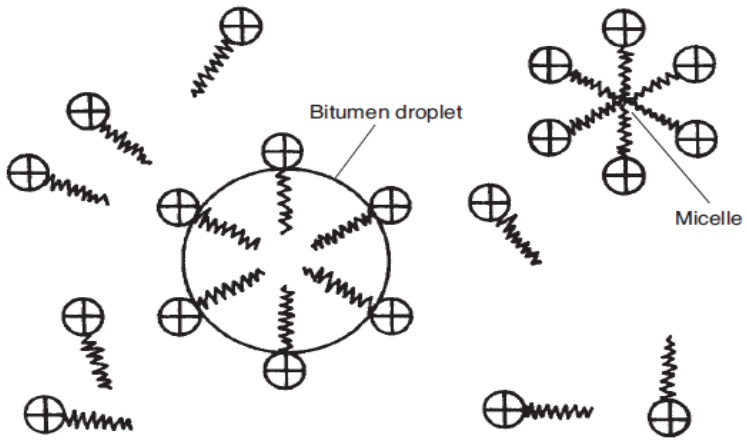

Figure 7 Emulsifiers ions resulting in the formation of Micelles in stable solution, (from Redelius and Walter (2005)).

However, once the emulsion touches the aggregate, some of the emulsifier ions will be lost. The emulsion can regain ions from the bitumen droplets or the micelles. During this process of ions being absorbed from the emulsion solution to the negatively charged aggregates, the breaking process is initiated as shown in Figure 6 (Redelius and Walter, 2005).

[5] Micelles refers to particles of colloidal dimensions. The term colloidal refers to a mixture that is phase separated with microscopically dispersed particles are suspended within a different substance (Anon, 2019. Colloidal Suspensions. Available at: https://chem.libretexts.org/@go/page/41598)

According to Redelius and Walter (2005), when the charge on the bitumen droplets is minimal, rapid coalescence will occur. During this process, hydrocarbon chains attach to the aggregate which creates a firm bond between the bitumen and the aggregate.

There is also the possibility of using a breaking agent to induce breaking. While an emulsion is applied to a surface dressing, a chemical agent can be added to excel the breaking process. Caution is however advised as adding too little breaking agent could have little to no effect. Applying too much breaking agent (or poor distribution of the breaking agent) could cause the emulsion to break too fast. This increased breaking rate may negatively affect the adhesiveness of the emulsion (Redelius and Walter, 2005).

2.3.7 Bitumen classification systems

To incorporate both the setting factor and chemistry factor of bitumen emulsions, South Africa and the United State of America introduced a naming system. This will be discussed in more detail below.

1. American modifier binder classification

Table 1 below displays the methodology used by the United States of America to categorize their emulsions according to different factors such as setting rate, viscosity, residue properties, solvent content, etc.(James, 2006).

Table 1 American classification system (from James (2006)).

Classification characteristic	Description	Identifying Codes
Type of application	Spray seal	S
	Asphalt	A
	Crack sealant	|
Emulsion Viscosity	1	Low Viscosity
	2	High Viscosity
Residue Properties	H	Hard Bitumen Residue
	S	Soft Bitumen Residue
	HF	High Float
Modification	P	Polymer Modified
	LM	Latex Modified
Solvent Content	S	High Solvent Content
Emulsions with Specific Uses	AEP	Bitumen Emulsion Prime
	PEP	Penetrating Emulsion Prime
	ERA	Recycling Agent Emulsion

According to information provided by Sabita (2020), high float emulsions refers to the manufacturing of an emulsifier that will form a gel-like structure within the bitumen residue (Kashaya, 2013). This gel structure will cause the bitumen to be applied in thicker films, resulting in a bitumen layer that can perform better at a wider variety of temperatures. The thicker bitumen film that is created would also result in less run-off from the surface of the road which makes these emulsions ideal for cold mixes and chip seals (Kashaya, 2013).

2. The South African bitumen emulsion classification system

The South African modified binder classification system, as specified by Herrmann and Bucksch (2014), was created to classify a binder according to its performance requirements. This classification system does not make it possible to select a binder based on the type and concentration of polymer used in specific applications. Thus according to this information, a general classification system was developed to classify the binder according to four categories based on information from the application type, application temperature, type of polymer used, and numerical value(Sabita, 2014). This system is described in more detail below in Table 2. It should be noted that an additional code can be added to the classification system below to indicate whether a cutter or fluxing agent is allowed. A cutter or fluxing agent can be denoted by the letter ”t” and is always added in brackets afterwards (Sabita, 2014). An example to explain this system is SC-E2(t).

- S |Refers to the binder being used as a surfacing seal,
- C |Refers to the binder being used as an emulsion,
- E |Refers to the elastomer polymer modifier being used,
- 2 |This binder has a higher softening point than a 1, and
- (t) |A fluxing agent or cutter can be used.

Table 2 South African binder classification system (adapted from TG1, 2019).

1. Type of application		
1.1)Spray Seal (S)	1.2)Asphalt (A)	1.3)Crack sealant (C)
2. Type of Binder System		
2.1)Emulsion (C)	2.2)Hot applied (No letter used for indication)	
3.Predominant polymer modifier used		
3.1)Elastomer (E)	3.2)Plastomer (P)	3.3)Rubber (R)	3.4)Hydrocarbon (H)

4.Level of modification	This factor is indicated by a numerical value. As the number increases, so will the softening point values for the binder increase. However, this does not imply that there will be an improvement in performance properties.

2.3.8 Typical uses of different emulsions

Some typical uses for different emulsions are shown in Table 3 below, but they can also differ according to local best practices (James, 2006). Choosing an emulsion for a specific application is dependent on whether the emulsion's reactivity can match the reactiveness of the aggregate and

Table 3 Typical uses of Anionic and Cationic emulsions (from James (2006) and Meyer (1999)).

	Anionic			Cationic			
	Rapid Set	Medium Set	Slow Set	Rapid Set	Medium Set	Slow Set	Super-stable
Slurry Surfacing							
Slurry seal			X			X[b]	X
Cape seal			X			X[b]	X
Microsurfacing						X[b]	
Spray Applications							
Surface Dressing	X			X			
Fog Seal		X	X		X	X	X
Tack Coat		X[a]	X	X	X[a]	X	
Prime Coat			X	X		X	X
Penetration Macadam				X			
Dust Palliative			X			X	
Mulch			X				
Plant Mixes							
Open Graded/ Dense Mix		X[a]			X		
Dense Graded			X			X	X
RAP		X				X	X
Stockpile Mix		X[a]			X[a]		X
Pre-Coated Chips					X	X	
In Place Mixes							
RAP		X[a]			X[a]	X	X
Soil Stabilisation			X				X
Dense Graded			X			X	X
Mix Paving							
Open Graded					X[a]		
Other							
Waterproofing Coatings			X[c]				
Driveway and Footpath sealers			X[c]			X[c]	

[a] Emulsion may contain solvent.
[b] Emulsion does not have to pass the cement mix test.
[c] Emulsion may contain clay.

external factors. James (2006) specified that aggregate reactivity is largely dependent on the materials smaller fractions (the fines) as the fines account for the largest contribution towards the surface area.

As an example, unreactive low surface area aggregate used in chip seals would make use of a Rapid Set (RS) emulsion to counter the un-reactivity of the aggregate. The same would occur for aggregate with reactivity and high surface area. High reactivity aggregate would make use of Slow Set (SS) emulsions. These emulsions are usually used in dense cold mixes and with aggregate that has high 0.075 mm content (James, 2006). For environmental conditions, James (2006) indicated that high temperatures can increase the chemical reactions taking place in the emulsion. This increase in reactions can lead to an increase in the physical process that takes place during the emulsion setting period. For this type of situation, a slow setting emulsion would be applicable(James, 2006).

Aggregate and environmental factors can influence the bitumen's performance, but the manufacturing process. The percentage emulsifier and bitumen droplet charge can also affect the emulsion reactivity. Thus, if the bitumen droplet charge increases, so will the emulsion reactivity increase(Kashaya, 2013). As James (2006) also stated, during the process of manufacturing emulsion, there are huge amounts of mechanical energy needed, thus as the mechanical energy increases so will the emulsion reactivity increase.

It should be noted from Table 3 that North America typically uses anionic emulsions and in some cases used on mine haul roads.

2.3.9 Manufacturing of Bitumen emulsion

Bitumen emulsion is typically created by rapidly and rigorously mixing bitumen and water resulting in the bitumen being dispersed in the aqueous phase. The water phase used in the mixing process does need an additional emulsifier agent to ensure that the mixture does not segregate once the mixing stops. To ensure that the bitumen droplets are adequately and finely dispersed in the water phase in a high shear colloid mill mixer (Needham, 1996). Redelius and Walter (2005) state that a colloid mill reduces a solids' particle size that is suspended within another liquid or a liquid suspended within another liquid. A typical colloid mill is made out of a rotor that spins at between

1000-6000 rpm and a stator. The gap in which the liquid is emulsified is usually between 0.25-0.50 mm, but can also be modified if necessary. When adjusting the emulsion gap, it should be taken into consideration that the emulsion must always be kept at a viscosity of 2 Poise (Ps) or lower. (Redelius and Walter, 2005).

However, the colloid mill can be customized as there are a few different mill heads that can be used. The most generally used, and simplest mill head is the normal "grinding" mill. This mill head consists of two plates that are closely spaced together. The bitumen and water (or aqueous) phase is then injected into the area between the two plates to create a mixing process(Needham, 1996). A typical example of a simple colloid mill is displayed in Figure 8.

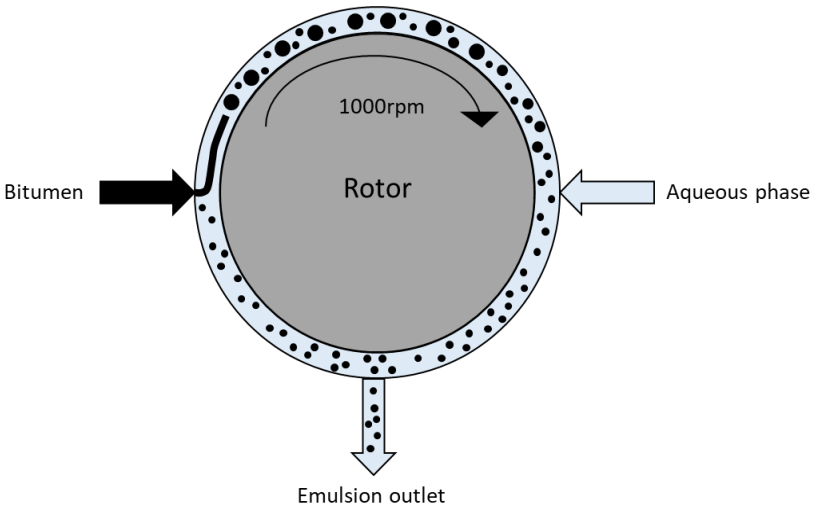

Figure 8 Colloid mill (Adapted from Needham (1996)).

Needham (1996) also stated that there is a second type of high shear mill head consisting of two circular plate type structures that have interlinking circulate teeth attached to them. The one set of teeth rotates constantly relative to the static second row of teeth. The rotating teeth are usually referred to as the rotor and the teeth that are fixed are referred to as the stator. The third type of mill head was created by Esso which is a subsidiary company for the petroleum giant in France known as ExxonMobil. This mixing process is called the SMEP (static mixer emulsion process). Instead of using high shear mill head to mix the bitumen, this process includes the dispersion of bitumen droplets by high-pressure injectors. The high pressure creates turbulence which induces mixing in the water phase. There are also claims that this mixing process has the capability of adjusting the bitumen particle size distribution, creating narrower droplet sizes. This gives the

mixing process the ability to control the physical and performance properties of the emulsions(Needham, 1996; James, 2006).

When bitumen emulsion is produced, as shown in the colloid mill figure, the emulsifier agent should be added to ensure the bitumen and water phase does not split. Two techniques can be used to infuse the emulsifier called batching or in-line mixing(Needham, 1996; James, 2006). The batching process usually consists of two steps- the water phase mixing step and the actual emulsion mixing step as stated by James (2006). The water phase can be created by mixing water, emulsifier and emulsifier chemical and applying heat(James, 2006). Batch plant mixing can be manually completed, but for quality assurance adding automatic or semi-automatic mixing will result in a less human error during the mixing process. Adding an automated mixing procedure will also decrease the risk of exposure to hazardous or corrosive chemicals(James, 2006). A schematization of a batch mixing plant can be seen in Figure 9.

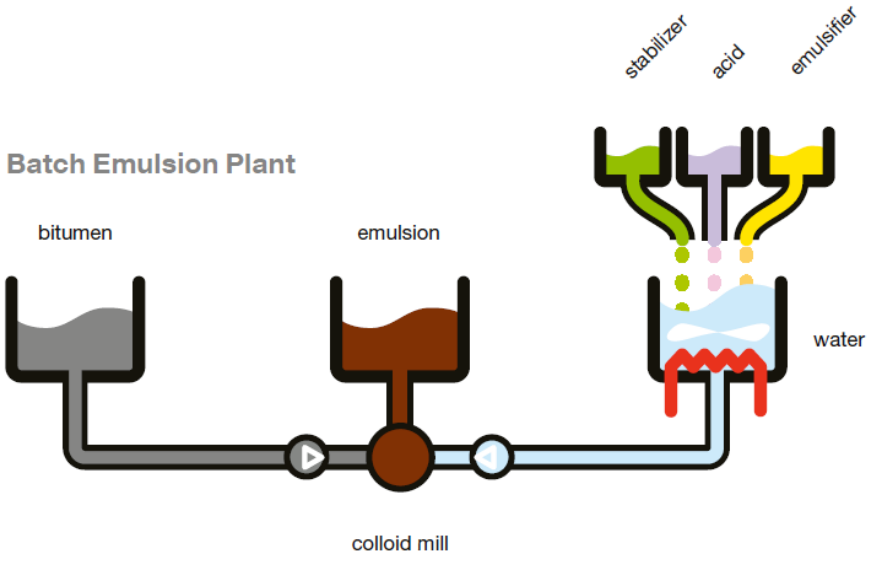

Figure 9 Batch mixing emulsion plant (from Meyer (1999))

The in-line mixing process is a continuous system, rather than a batch mixing system, that works through a system that automatically manages the water heating and material dosages needed to create the emulsion. The in-line mixing process requires that the emulsifier agent, base or acid, must be added to the water that is on its way to the colloid mill. This method, however, does require that the bitumen should be heated up until it achieves a liquid state. Bitumen, in this liquid phase, has a low enough viscosity which will allow it to flow and be pumpable.

The temperature necessary to lower the bitumen's viscosity is all dependent on its penetration grade(Needham, 1996; James, 2006). Herrmann and Bucksch (2014) describe the penetration of bitumen as a test to define the hardness or consistency of different bitumen blends. The test can be completed by measuring the time it takes a needle (of standard size and weight) to penetrate the bitumen sample to a specified depth. This penetration distance is microscopic and measured in dmm ($1/10^{th}$ mm).

Consequently, if the bitumen is hard the penetration depth will be shallow and the bitumen will have a lower penetration grade. Needham (1996) provided an example to explain the effect of temperature on the penetration grade of bitumen. For this example, the 100 pen bitumen was heated up to a temperature between 140-160 ºC. If a different pen bitumen should be used, the bitumen should be heated up until the viscosity reaches 200 cps (centipoise). A general guideline can be followed which states that 200 cps can be reached at about 100 ºC above the softening point (Needham, 1996). An example of an in-line mixer can be seen in Figure 10.

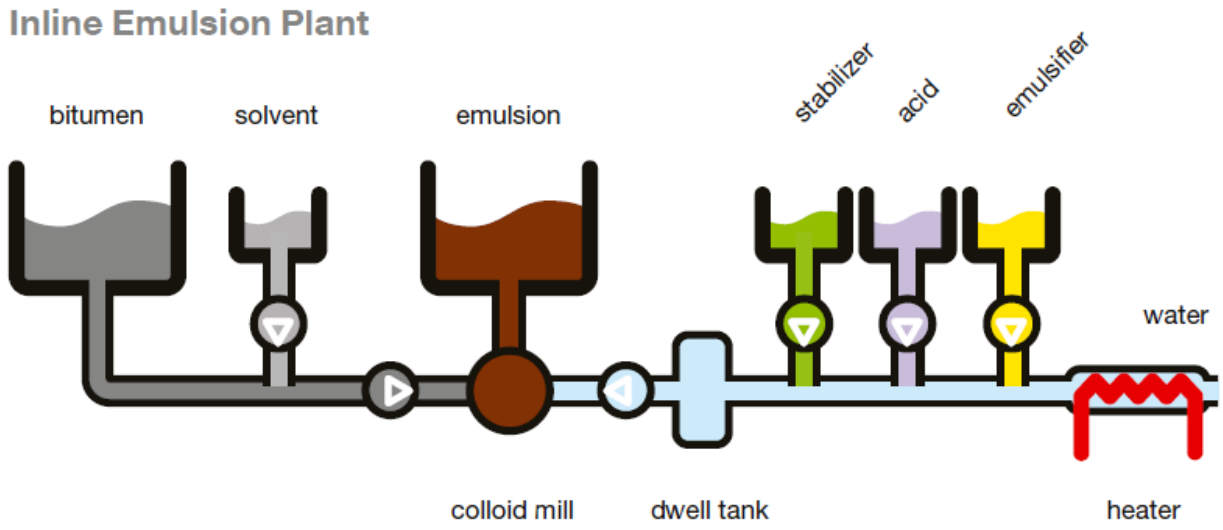

Figure 10 In-line emulsion mixing plant (from Meyer (1999)).

As seen in Figure 10, Needham (1996) stipulated that the water phase section and the mill head should be preheated to ensure that the bitumen does not solidify as a result of excessive cooling. Marchal and Boussad supported this by stating that when hot bitumen comes into contact with cool water, thermal shock will occur. During this thermal shock, course bitumen droplets can start to form in the emulsion(Needham, 1996).

With the water phase and mill head preheated, the bitumen and water phase are pumped towards the colloid mill. Once reaching the colloid mill, the two substances start to mix and form bitumen droplets ranging between 1-5 µm that is suspended in the water phase. The mixture remains stable because the surfactant molecules orientate themselves according to the bitumen-water mixture. With the mixing process complete, the emulsion can pass out of the system, but at a temperature below 95 ºC. This is to ensure that the water does not boil which can cause the bitumen droplets to rise to the surface(Needham, 1996). Redelius and Walter (2005) agreed with this statement but stated the temperature should not be above 90 ºC.

Under certain circumstances, the components used in the emulsion process are at such high temperature (such as polymer modified or oxidized bitumen working at temperatures of between 180-200 ºC) that the emulsion would not be able to fully cool down to prevent boiling in the finished product(Needham, 1996). To prevent this boiling from occurring, James (2006) suggested that the production line/process should be pressurized to prevent boiling and Redelius and Walter (2005) suggested that a head exchanger be added to the outlet and inlet to cool the mixtures.

The third type of emulsion manufacturing was stated by Kashaya (2013) and is called a semi-continuous emulsion production process. This production method consists of two soap tanks feeding into the colloid mill rather than one. This is to ensure as the first tank runs out, the process automatically switches over to the second tank so that the mill could potential run indefinitely. A schematization of this production process can be seen in Figure 11.

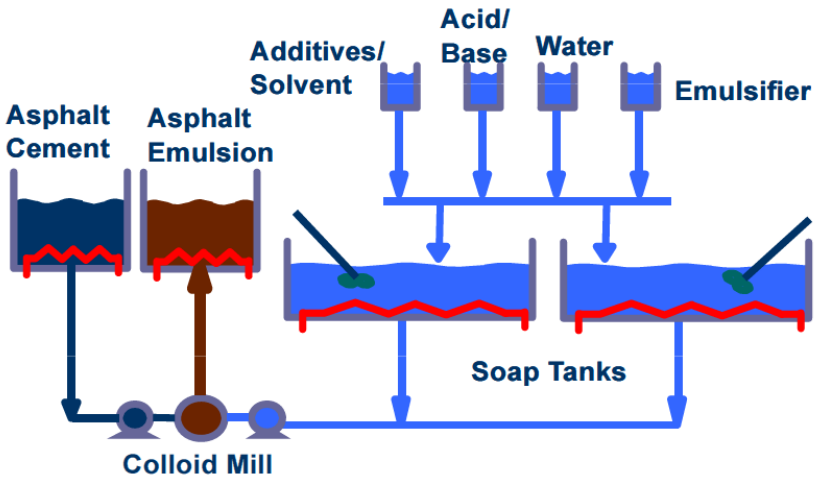

Figure 11 Semi-continuous emulsion manufacturing plant (from Kashaya, 2013).

Moreover, Manolis (2010)proposes that the layout of this manufacturing plant changes in terms of solvent input. According to Manolis (2010), the solvent should be added to the system, but from a separate batch tank. Solvents such as diesel and water are immiscible liquids, with diesel being the less dense liquid. If an emulsifier is added to these 2 liquids, the emulsifier will bond to the solvent and not the bitumen. This would cause the solvent to be ineffective at dissolving the bitumen, rendering it useless. Manolis (2010) further observed that if the emulsion is manufactured and the emulsifier is only added afterwards, the flocculation and coagulation processes are delayed. To anticipate the temperature of outgoing emulsions the following equation can be used (Manolis, 2010).

$$Emulsion\ Temperature\ (^0F) = \frac{[(AC_{wt}) \times (AC_{temp})] + [(Soap_{wt}) \times (Soap_{temp})]}{[(AC_{wt} \times 0.5) + (Soap_{wt})]}$$

Where:

AC_{wt} |refers to the Asphalt Cement proportion in the mixture, and

$Soap_{wt}$ |refers to the soap proportion.

All temperatures should be Fahrenheit (ºF).

2.3.10 Bitumen emulsion settlement

Emulsions that consist of small percentages of bitumen or have low viscosity are susceptible to settlement. This settlement can occur at ambient temperature as a result of bitumen having a higher density than the water phase it is suspended in. This phenomenon can cause a bitumen layer to form on the bottom of the mixture and a bitumen deficient layer to form on the top of the mixture(Redelius and Walter, 2005). The velocity at which these bitumen particles can be calculated by making use of Stokes' law.

$$v = \frac{2}{9} \times gr^2 \times \frac{\varsigma_1 - \varsigma_2}{\eta}$$

Where:

G |gravitational force,

R |radius of the particle,

ς_1 |first phases' specific gravity,

ς_2 |water phases' specific gravity, and

η |water phases' viscosity.

Stokes' law can best be described as a mathematical equation that explains how the forces are exerted on a particle moving through an inactive, viscous liquid at a specific velocity. Three forces are acting on this spherical particle as stated by Kashaya (2013). These forces are i) mg (the weight of the spherical particle), ii) F_b (the buoyancy force), and iii) F_d (the drag force). Consequently, if drag and buoyancy forces are smaller than the own weight force of the particle, the particle will start to move downwards (Kashaya, 2013). However, Redelius and Walter (2005) pointed out that Stokes' law applies to a particle that has no inter-particle forces and can freely move around, and bitumen does not always meet this criterion.

There are several methods available to reduce the amount of settlement that occurs. Holleran (2009) stated that emulsions stored over a long period need to be agitated at least once in two weeks. By disturbing the emulsion mixture, the settled bitumen droplets become re-suspended, leading to an increase in the shelf life that can be expected from the drums. Holleran (2009) also advised that emulsions stored in the big tank should be circulated every five days for winter periods and every 7 days during summer periods.

Another method that can be used to minimize settlement in the emulsion, would be to equalize the density of both the water phase and the bitumen as identified by Redelius and Walter (2005). To achieve equilibrium, calcium chloride ($CaCl_2$) can be added to the water phase. Nevertheless, this can only be achieved at a single constant temperature, as the coefficient of thermal expansion for the water phase and the bitumen are unequal. The bigger the bitumen particle, the faster it will tend to settle and the smaller the particle, the slower the particle will tend to settle. Thus, the rate of settlement can be influenced by the range of particle sizes. Another method to decrease settlement would be to increase the water phases' viscosity (Redelius and Walter, 2005).

The stability of bitumen emulsion during the transportation, heating and pumping phases can also be problematic. If two bitumen particles, suspended within an emulsion, come into contact with each other it will cause the particles to coalesce. However, the emulsifier agent can prevent this from occurring utilizing mechanical protection and electrical charge repulsion. Forces; such as pumping, heating and transportation; that are strong enough to overcome the electrical and mechanical safeguards, will cause flocculation and coalescence to occur within the emulsion. There are a few emulsifier agents that also tend to foam. The foaming can also be a potential factor to

cause coalescence as the bitumen particles found on the surface of these ‘bubbles’ are exposed to surface tension forces (Redelius and Walter, 2005).

2.3.11 Storing of bitumen emulsion

To keep up with the ever-increasing demand for bitumen emulsions, storage facilities are created to store emulsions for long periods. These facilities allow the production plant to run for longer and as a result, the plant’s production rate can improve. New technological innovations in bitumen emulsion have also resulted in emulsions being able to be stored for months at a time(Redelius and Walter, 2005). Redelius and Walter (2005) also recommended that for the storage process, vertical storage tanks should be used with a small horizontal diameter. These types of storage tanks should also include a dip tube filling pipe that extends to the lower part of the tank.

The main advantage of a vertical storage tank over a horizontal storage tank is the area that is exposed to air. Vertical tanks are designed to take the same volume as horizontal tanks, but with a higher height to diameter ratio (h:d). This is to limit the amount of emulsion exposed to the air on the top surface. If the emulsion is exposed to the air for a prolonged period, it will start to form a crust that will not liquefy or be absorbed during the pumping of emulsion. Nonetheless, horizontal tanks must be used in certain circumstances and to minimize the probability of a crust forming, the tank should always be kept full(Redelius and Walter, 2005).

2.4 BSM Mix design considerations

The first section provided information regarding the failure mechanisms observed in unpaved mine haul roads. The second section provided information regarding bitumen emulsion as a viable option to stabilize material to improve overall layer performance. With these factors in mind, this section will provide some insight into the mixed design procedures for BSM-emulsion layers.

2.4.1 Distress mechanism

For a BSM mix design, there are two primary distress mechanisms, namely: a) permanent deformation, and b) moisture susceptibility. Permanent deformation can be described as the shear deformation that gathers over a longer period. Repeated loading causes shear deformation and directly correlates with the shear properties of the material with accompanying densification. On the other hand, moisture susceptibility is a measure of damage that occurs to a BSM layer. The moisture damage in a BSM layer is caused by excessive exposure to moisture content with accompanying pore pressures and traffic loading. The moisture damages the cohesion bonds between the aggregate and the bitumen which leads to a decrease in shear strength (Sabita, 2020). Table 4 below indicates factors that can be incorporated (or improved on) to reduce both permanent deformation and moisture susceptibility.

Table 4 Factors which can reduce permanent deformation and moisture susceptibility in BSM (from (Sabita, 2020))

Permanent Deformation	Moisture Susceptibility
-Improve aggregate grading, shape, angularity, roughness and hardness;	- Increase the bitumen content while also keeping in mind the 3 % tolerance specified for permanent deformation;
-Increase the maximum particle size;	
-Reduce the moisture content through curing;	- Addition of active filler (but no more than 1 % as specified for permanent deformation).
-Improve on the compaction effort;	
-Include less than 3 % residual bitumen content. Permanent deformation tends to increase with higher bitumen contents;	- Improve the compaction effort which would result in higher field density during construction; and

-Maximum of 1 % active filler is allowed. Higher filler content would lead to material becoming brittle. Also, with higher filler content, fatigue cracking would occur which declassifies the material as a BSM.	-Implement a smooth continuous grading.

2.4.2 Mix Design considerations

To determine the type of BSM mixture that is required for a specific pavement structure, the following criteria have to be taken into account according to the TG2 guidelines by Sabita (2020) as they have a direct influence on the mix design proportions which include bitumen content and active filler:

- Design traffic which takes account of the number of heavy vehicles and the vehicle loads the BSM layer or structure should be able to carry over years;
- Quality of aggregate available, which includes Reclaimed Asphalt (RA) and material blending; and
- Climate or more specifically what the moisture conditions are specific to the site where BSM should be incorporated;
- The Stiffnesses and condition of supporting layer structures.

For a BSM mixture, the virgin aggregate used has a big impact on the long term durability of the layer. For higher quality BSMs, the material is required that would meet the prerequisites of a G1 – G5 material. In extraordinary circumstances, a G6 material can also be used if no other material is available. However, G6 material can only be considered if it meets the durability requirements of BSM mix design in terms of *a)* Soaked CBR, *b)* Percentage passing 0.075 mm sieve, *c)* Plasticity Index, and *d)* Grading.

2.4.3 Compatibility of Aggregate and Bitumen Emulsion

As previously discussed, the durability of BSMs is largely influenced by aggregate quality. However, it should also be taken into account that certain parent material types are only compatible

with either Cationic or Anionic emulsions. Table 5 below indicates the compatibility of general aggregate types with both anionic and cationic emulsions. The aggregate listed in the table below all contain alkali content below 35 % and silica content above 65 % which indicates that they are acidic rocks (Sabita, 2011; Sabita, 2020). Sabita (2011) also stated that for bigger projects emulsion manufacturers can formulate emulsions that are compatible with the aggregate that is encountered on site.

Table 5 Aggregate compatibility with cationic and anionic emulsions (from Sabita (2020) and Sabita (2011))

Aggregate Type	Compatible with	
	Cationic emulsion	Anionic emulsion
Dolerite	YES	YES
Quartzite	YES	NO
Hornfels/ Greywacke	YES	YES
Dolomite	YES	YES
Granite	YES	NO
Andesite	YES	YES
Tillite	YES	VARIABLE
Basalt	YES	YES
Sandstone	YES	NO
Rhyolite	YES	NO
Marble/ Norite	YES	YES
Syenite	YES	NO
Amphibolite	YES	YES
Felsite	YES	NO

2.4.4 BSM Mix Design Procedure

The mix design procedure for BSMs can comprise numerous steps depending on the traffic design life and the importance of the road. Figure 12 below displays the typical mix design procedure which should be followed for BSM (Wirtgen GmbH, 2012). To start a mix design for BSM, the material is tested for compatibility with bitumen emulsion. Standard preliminary testing includes moisture/density relationship testing, Atterberg limits, and sieve analysis. The results from these tests would indicate if the material requires blending or pre-treatment before bitumen emulsion can be introduced (Wirtgen GmbH, 2012; Sabita, 2020).

If the material has been classified as suitable for mixing with bitumen emulsion, the next phase of the mix design can commence. The next phase of testing will determine whether the material will require additional active filler. To determine if the percentage active filler, standard ITS on 100 mm diameter Specimens are conducted. The next phase of the mix design would be to determine the amount of bitumen that is required to achieve optimal strength conditions. This is achieved through mixing different 150 mm diameter Specimens with increasing bitumen content and using these Specimens to conduct ITS tests. The Specimens are tested under both soaked and unsoaked conditions. With the ITS test the optimum bitumen content can be calculated which will

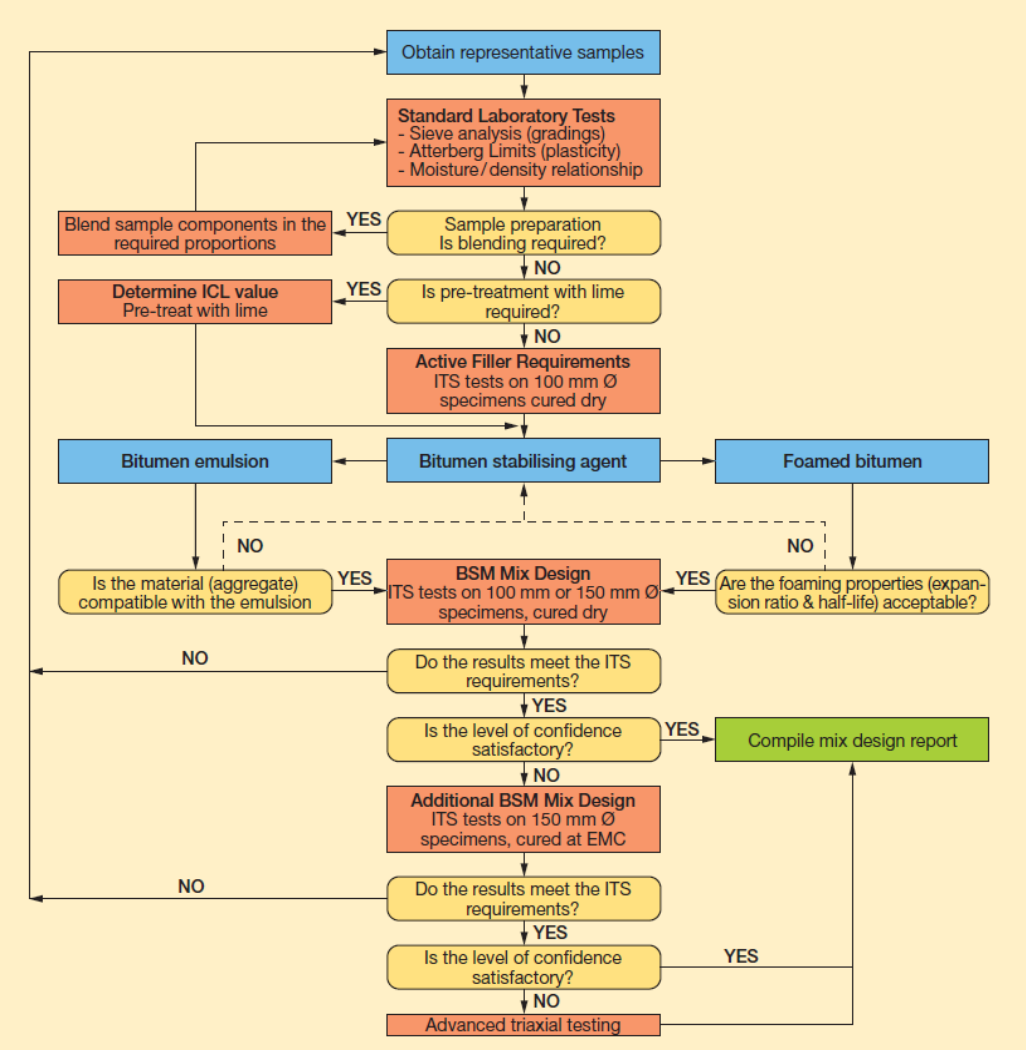

Figure 12 Typical mix design procedure for BSMs explained in a flowchart (from).

provide the desired level of strength (Wirtgen GmbH, 2012).

As seen in Figure 12, if the ITS results do not meet the requirements, the entire procedure should be started again until a mix is constructed that would meet the requirements set out for either a BSM1 or BSM2 classification. If a higher level of confidence is required for the desired structure, additional tests can be performed on more 150 mm diameter specimens. Wirtgen GmbH (2012) also mentions that in certain cases, additional sensitivity testing can be performed at this stage to determine what effect the decrease in active filler (from 1 % to 0.75 % for example) will have on the performance of the mix (Wirtgen GmbH, 2012; Sabita, 2020).

At this stage, if the results from the ITS test indicates the materials meets the requirements of either a BSM1 or BSM2 material, and also meet the level of satisfaction, the mix design report can be compiled. If the mix meets the ITS requirements but does not meet the requirements for the level of confidence, further testing ITS testing can be conducted at Equilibrium moisture condition (EMC). If the mix design passes the second phase of testing at EMC, the mix design report can be compiled, otherwise, further advanced triaxial testing should be conducted (Wirtgen GmbH, 2012; Sabita, 2020).

2.5 BSM Mix Design and Performance Properties evaluation

As mentioned by both Wirtgen GmbH (2012) and Sabita (2020) to support a desired design traffic life, a BSM mix design should incorporate the optimum aggregate, bitumen content, and active filler. However, Jenkins and Collings (2017) also states that the material's shear properties should be understood to provide an accurate and optimal pavement design. According to Figure 12 the BSM mix design procedure requires Indirect Tensile Strength (ITS) testing as a base to determine the most optimal mix between various potential mix designs. Furthermore, shear properties are determined for the most optimal mix through Monotonic- and Dynamic Triaxial testing. This section will discuss the basic principles of these various test methods and the interpretation of results. Also, factors that could influence the results will also be highlighted and discussed.

2.5.1 ITS Test

The ITS test method is a standard procedure specified both in the TG2 Guidelines from Sabita (2020) and the Wirtgen Cold Recycling Technology manual from Wirtgen GmbH (2012). The aim of this test is to determine the optimal amount of binder and active filler required to reach a desired level of strength. Due to the size of the specimens, the ITS test does not provide results that directly reflect tensile strength. Nonetheless, ITS results do provide insight into effect of bitumen and active filler additions on the applied force response of the specimens (Ebels and Jenkins, 2007). in addition, by soaking the ITS specimens in water for 24 hours, it is possible to measure the durability of potential mix designs against moisture damage. The ratio calculated between the wet- and dry ITS results, known as the Tensile Strength Retained (TSR) ratio, is used to describe this measure of mix durability (Sabita, 2020).

According to research conducted by Kennedy and Hudson (1968) the ITS test procedure is a relatively easy and cost effective manner to estimate the indirect tensile strength of a material type. As illustrated in Figure 13, a compressive force is a applied to a cylindrical specimen on its circumference. The forces exerted onto the specimens results in the formation of tensile stresses in the centre of the specimens, causing the specimen to split along the loading plate (Kennedy and Hudson, 1968). This indicates that the ITS test procedure does also to some extent provide insight into shear properties of BSM mixes. When a load (indicated as F) is applied to the ITS specimen, the Vertical- and Horizontal Stress is both in compression between points '*A*' and '*B*'. At depth '*B*' in the specimen, the Horizontal Confinement Stress (σ_h) is zero while vertical compressive stress (σ_v) is still observed. This stress combination between points '*A*' and '*B*' results in a wedge formation which indicates shear failure.

Between points '*B*' and '*C*', σ_h is in tension as indicated on the right side of Figure 13. The Horizontal Stress to Vertical Stress ratio usually reaches 1:3 ratios at depth C in the specimen. Thus the specimen will fail approximately in the centre of the specimen as the combination of vertical compression stress and horizontal tensile stress will force the specimen to fail in tension.

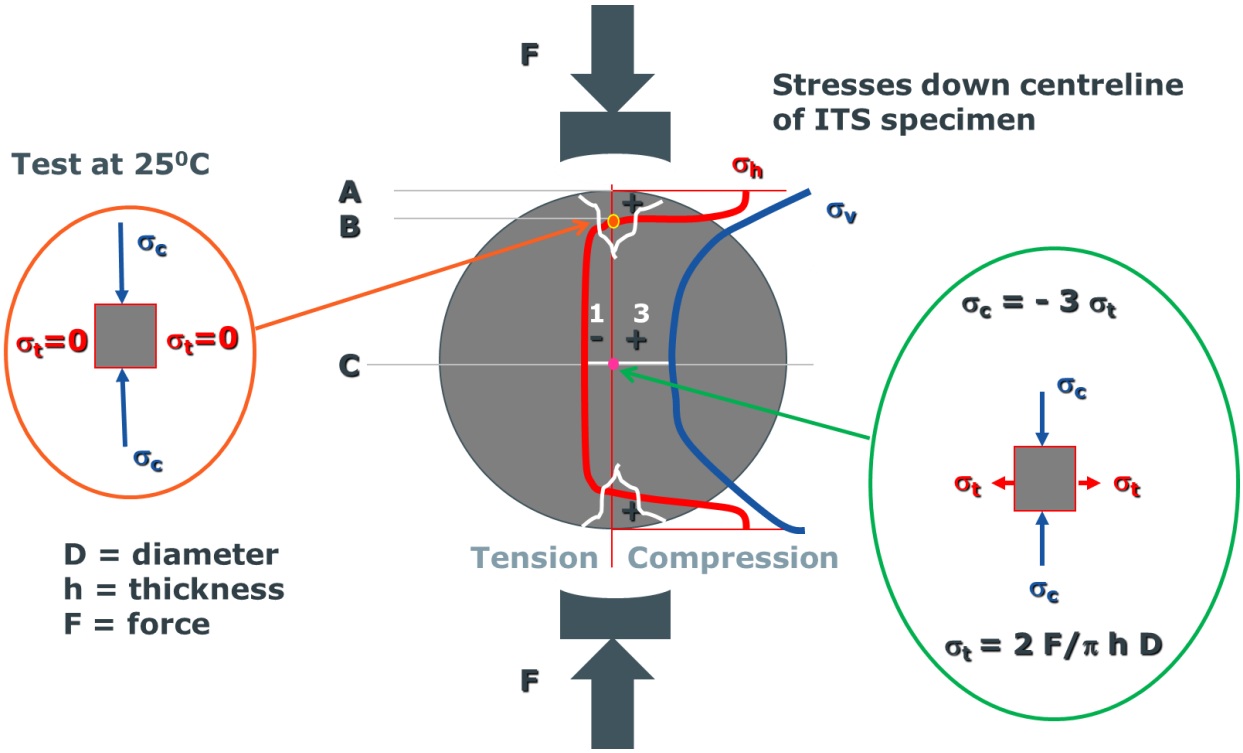

Figure 13 Illustration of the Compressive and Tensile stresses exerted on an ITS specimen (from Jenkins (2021)).

Mazibuko (2020) also states that the width of the loading strip, specimen size, testing temperature, and loading rate can all influence the ITS results and thus ITS results are not repeatable and do not resemble field loading. However, it is possible to achieve a low coefficient of variance (COV) through specimen testing. Testing completed by Ben and Jenkins (2014) measured lower ITS results at higher temperatures, thus proving that BSM mixes are temperature dependent. Standard testing procedures afterwards determined that BSM mixes should tested at a constant deformation rate of 50.8 mm/min and a temperature of 25 ºC (Wirtgen GmbH, 2012; Sabita, 2020).

2.5.2 Monotonic Triaxial Test

Once the optimum BSM mix design is determined according to the specifications mentioned in section 2.5.1, further testing is suggested to determine the shear strength properties as illustrated in Figure 14. The method used to determine the shear strength is the monotonic triaxial test and was developed and validated at the University of Stellenbosch as the Simple Triaxial Test (STT)

(Mulusa, 2009). According to the Specifications in the cold recycling manual and the TG2 guidelines by Wirtgen GmbH (2012) and Sabita (2020) respectively, to perform a monotonic triaxial test a specimen which is 150 mm in diameter and 300 mm in height is required which takes account of the large aggregates used in pavement structures (Mazibuko, 2020).

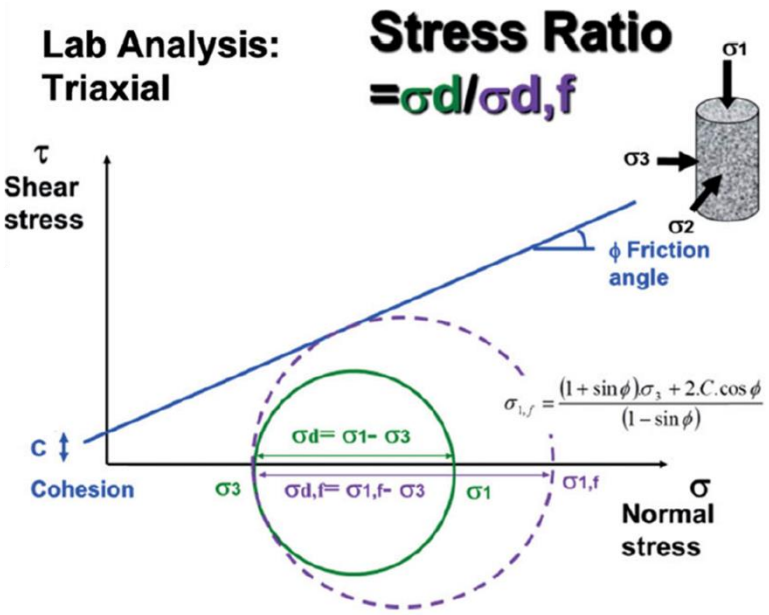

Figure 14 Shear parameters that are measured through the Monotonic Triaxial Test (from Jenkins and Collings (2017)).

The test procedure makes use of a rubber bladder which applies the confinement stress to the specimen, indicated as σ_2 and σ_3 in Figure 14. A vertical impact load is applied to the specimen at a constant displacement rate of 3 mm/min to achieve a major principle stress, indicated by the σ_1. Jenkins and Collings (2017) also states that the test method has been simplified for commercial use and provides more consistent results.

From the monotonic triaxial, the shear strength of a BSM mix design is determined through the calculated cohesion (C) and internal friction angle (θ) parameters. The calculation of these parameters are discussed further in Section 3.3.5. The shear properties determined through monotonic triaxial testing is dependent on density, curing period, and moisture content of the specimen (Sabita, 2020). The durability of the BSM mixes can also be tested by soaking Triaxial specimens

in water for up to 24 hours. From testing the soaked specimens, it is possible to measure the Retained cohesion (RC). The RC provides insight into how the mastic bond between larger aggregates are weakened due to moisture damage (Wirtgen GmbH, 2012).

The monotonic triaxial data is analyzed with a Mohr-Coulomb failure envelope model which is used to determine the cohesion and internal friction angle (Jenkins, 2000). By adding more bitumen to the mix design, the cohesion will increase within the unbound granular aggregates. Also, an increase in the cohesion will cause the failure envelope so shift upwards. With an increased failure envelope, the principal stresses at failure ($\sigma_{1,f}$) increases resulting in a mix design with higher shear strength properties (Ebels and Jenkins, 2007). The internal friction angle on the other hand is influenced by the aggregate type being stabilized. The internal friction angle represents the failure envelope as shown in Figure 15. It is visible in this figure that the quality of the BSM mix declines gradually based on the natural gravels and sands used.

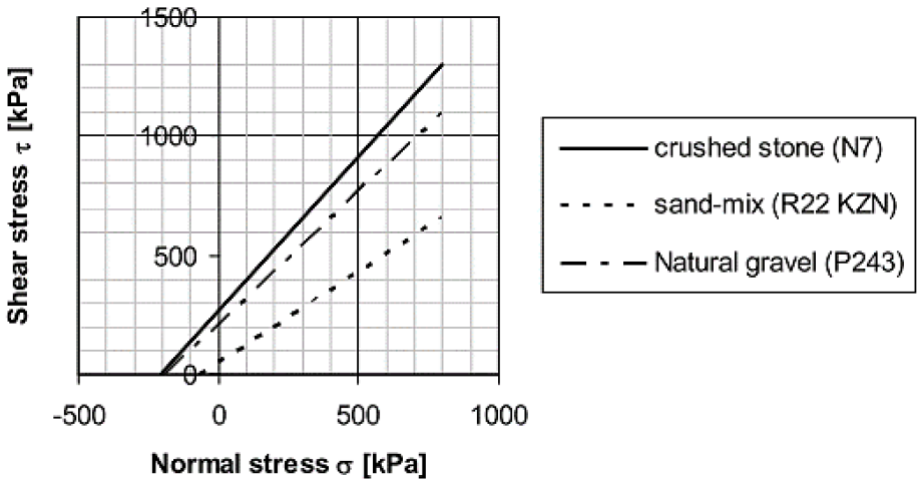

Figure 15 Example Mohr-Coulomb failure envelopes with varying aggregate type (from Ebels and Jenkins (2007)).

Previous studies completed by Ebels and Jenkins (2007) determined that BSM mixes created with crushed rock displayed cohesion values as high as 400 kPa with an internal friction angle of 55 º. Thus considering crushed rock as the main source of aggregate for mine haul roads, good quality BSM mix designs can be expected. Also, higher maximum principal stresses at failure can be expected as a result of the higher shear parameters of the mix design (Jenkins, 2000). Subsequently, the increase principal stresses lead to increased Deviator Stress Ratios (DSRs) as shown in Figure

14. Thus using monotonic triaxial testing to determine the shear parameters provide a good indication of the mode of failure of the mix design and can also predict the expected life of the BSM mix design with specific transfer functions (Mazibuko, 2020).

2.5.3 Dynamic Triaxial Test

The dynamic triaxial test, also known as the cyclic loaded triaxial test, measures the resilient modulus (Mr) response parameter of the material to repeated loading. The damage parameter, however is measured through permanent deformation (ε) (Dal Ben and Jenkins, 2014). The TG2 guidelines do not specified a standardized dynamic triaxial test method up to date. For the purpose of researching new materials, the dynamic triaxial test provides good insight into the materials' response to loading. The resilient modulus of a BSM mix design generally provides an indication of the materials load spreading capability under simulated repeated loading. Correspondingly, the resilient modulus is used as an input parameter in the Mechanistic-Empirical structural design life model of a layer (Anochie-Boateng, Paige-Green and Mgangira, 2009).

2.5.3.1 Typical Dynamic Triaxial Test Setup

To complete a standard dynamic triaxial test, a loading frame, triaxial cell, load cell, linear variable displacement transducers (LVDTs), and a control and data acquisitions system is required (Anochie-Boateng, Paige-Green and Mgangira, 2009; Mazibuko, 2020). To simulate traffic loading on the specimen, a cyclic impact load is applied (σ_1) followed by a resting period. Variable impact loads are applied to the specimen at a constant confinement pressure (σ_3), where after the confinement pressure is also changed and the test is repeated. This scenario simulates different a range of predetermined deviator stress ratios (DSRs) on the specimen as shown in Figure 16. The predetermined DSRs are chosen to simulate different traffic loads on potential BSM mix designs (Anochie-Boateng, Paige-Green and Mgangira, 2009). However, a conditioning load is applied to the specimen prior to testing to stabilize the specimen. The conditioning has an influence on the materials response, thus providing more accurate results (Mazibuko, 2020). To ensure that no permanent deformation occurs to the specimen, the DSR is controlled so that the cyclic impact loads will not cause any failure (Anochie-Boateng, Paige-Green and Mgangira, 2009).

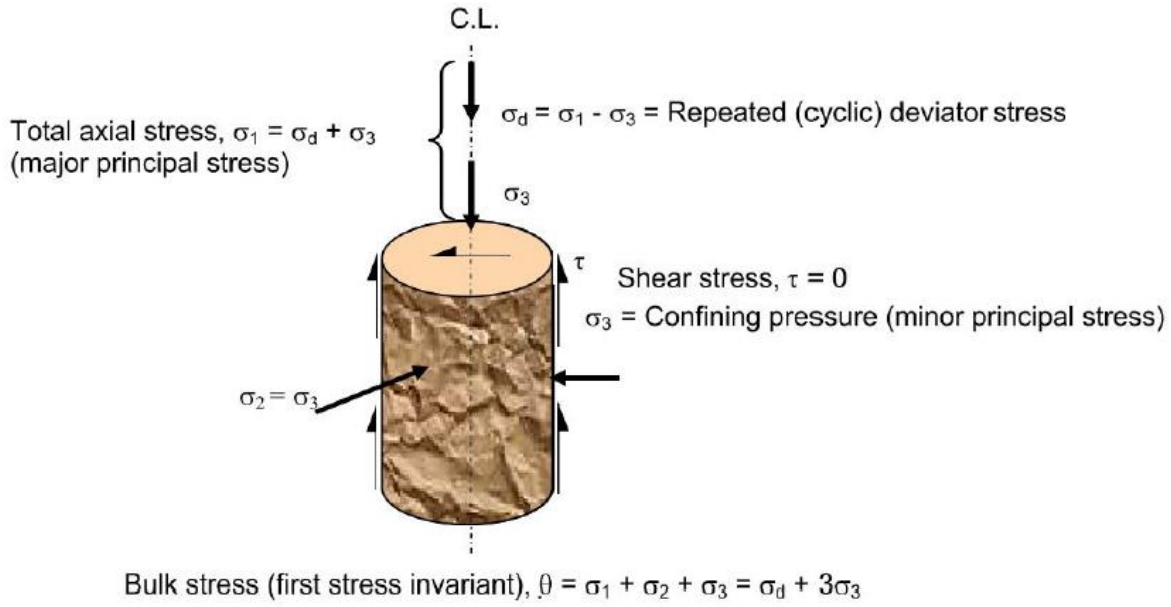

Figure 16 Dynamic Triaxial Stresses induced on the specimen (from Mazibuko (2020)).

2.5.3.2 Deviator Stress Ratio

The DSR of a BSM mix can be calculated through the shear parameters obtained by Monotonic Triaxial testing. A typical DSR range of between 40-60 % can be expected for granular materials and BSMs. Applying cyclic impact loads which would increase the DSR above these ranges would lead to rapid deformation within the specimen, which leads in premature failure (Long and Theyse, 2004). Also, the higher the DSR ratio of a potential BSM mix, the higher loading the material will be able to support. However, Higher DSR ratios with a reduction in loading can also result in longer pavement life (Ebels and Jenkins, 2007). There are also other factors which can influence the Mr results such as the moisture content and density of the specimen. Furthermore, external factors such as stress levels (i.e. DSR), stress history, conditioning sequences and load repetitions (Anochie-Boateng, Paige-Green and Mgangira, 2009).

2.5.3.3 Resilient Modulus Models and Interpretation

The relationship between the calculated Mr and the bulk stress (which is equal to $\sigma_1 + \sigma_2 + \sigma_3$) will illustrate how the BSM mix performs under repeated loading. Generally, an increase in the calculated Mr is observed when there is an increase in the bulk stress in coarse grained material, which is referred to as stress stiffening. However, it has also been observed for fine-grained material, that the Mr will decrease as the bulk stress increases, which is referred to as stress softening (Anochie-Boateng, Paige-Green and Mgangira, 2009). Ultimately, the calculated Mr can be modelled to relate with the confining pressure, DSR, and Principle Stress Ratio (PSR) (van Niekerk, 2002). Jenkins (2000) stated that four models exists that are commonly used to describe the resilient response of stress dependent granular- and BSM material. These models are presented in Table 6 below.

Table 6 Mr models (from Jenkins (2000)).

K-θ Model	Mr-σ_3-σ_d Uzan and Witzack Model
$Mr = k_1\left(\frac{\theta}{\theta_0}\right)^{k_2}$	$Mr = k_1\left(\frac{\sigma_3}{\sigma_{3,0}}\right)^{k_2}\left(\frac{\sigma_d}{\sigma_{d,0}}\right)^{k_3}$
Parabolic Mr-σ_3 –σ_d	Mr-θ-$\sigma_d/\sigma_{d,f}$
$Mr = k_1\left(\frac{\sigma_3}{\sigma_{3,0}}\right)^{k_2} \times \left(-k_3\left(\frac{\sigma_d}{\sigma_{d,f}}\right)^2 + k_4\left(\frac{\sigma_d}{\sigma_{d,f}}\right)^2 + k_5\right)$	$Mr = k_1\left(\frac{\theta}{\theta_0}\right)^{k_2} \times \left(1 - k_3\left(\frac{\sigma_d}{\sigma_{d,f}}\right)^{k_4}\right)$

Where

Mr	|Resilient Modulus of the layer (MPa),
σ_3	|Minor principal stress in the layer (kPa),
$\sigma_{3,0}/\sigma_{d,0}$	|Reference stresses (kPa),
σ_d	|Deviator stress [σ_1-σ_3] (kPa),
$\sigma_{d,\,f}$	|Deviator stress at failure [$\sigma_{1,\,f} - \sigma_3$] (kPa),
θ	|Bulk stress [$\sigma_1+\sigma_2+\sigma_3$] (kPa),
k_1, k_3, k_5	|Regression coefficients (MPa), and
k_2, k_4	|Regression coefficients (unit less).

A non-linear regression analysis method is used to fit the measured data to the models. The characteristics of each model is discussed in more depth in (TABLE). The Mr-θ is the most commonly

used model due to its simplicity of describing the stress stiffening of the material. This model does however not incorporate the confining pressure, nor the deviator stress, thus the Mr-σ_3-σ_d model was created (Ebels and Jenkins, 2007). On the other hand, the Mr-σ_3-σ_d model does not consider the effect of the confining pressure and deviator stress individually on the resilient modulus. van Niekerk (2002) furthermore created a model which considers both stress stiffening and stress softening as the bulk stresses increases.

Table 7 Mr models descriptions and coefficient interpretations (from Jenkins (2000); van Niekerk (2002); Ebels and Jenkins (2007)).

Mr-θ Model	
Characteristics	Coefficient Interpretation
- Easy to use, - Describes stiffening, but not stress stiffening of stress softening, - Does not measure the effect of confining pressure of deviator stress.	- k_1 is directly proportional to Mr - k_2 indicates the slope of the line
Mr-σ_3-σ_d Model	
Characteristics	Coefficient Interpretation
- Describes Mr in terms of confining stress and deviator stress, - Physically correct in comparison to the Mr-θ model, - Model cannot differentiate between stress stiffening and stress softening.	- k_1 is directly proportional to Mr - k_2,k_3 indicates the slope of the line
Parabolic Mr-σ_3-σ_d Model	
Characteristics	Coefficient Interpretation
- Model can describe both stress stiffening and stress softening, - Model can consider the effect of the confining stress and deviator stress individually.	
Mr-θ-σ_d/$\sigma_{d,f}$ Model	
Characteristics	Coefficient Interpretation
- Model can describe the influence of both stress stiffening and stress softening, - Physically incorrect, - Cannot consider the effect of confining stress and deviator stress separately on the resilient modulus.	- k_1 describes the stress stiffening of the material, - k_2 describes the decrease in resilient modulus in relation to the stress increase, - k_3 describes the relative decrease of Mr at higher stresses, - k_4 describes the shape of the resilient modulus decrease.

2.6 Chapter Summary

This chapter begins by discussing the major pavement distresses that influence unpaved road networks with emphasis on mine haul roads. Furthermore, this chapter considers and discusses bitumen stabilized base layers as an upgrade to the durability of mine haul roads. This section includes the bitumen emulsion selection process, advantages and disadvantages of bitumen emulsion, classification systems, chemical compositions, manufacturing as well as handling and storage procedures of bitumen emulsion. Additionally, this chapter discusses the mix design procedure stipulated for BSMs which include distress mechanisms, mix design considerations, aggregate compatibility, and the mix design process.

3 Methodology

3.1 Introduction

To find solutions for mine haul roads' structural capacity problems, structural capacity testing had to be completed, with accompanying permeability testing, binder analysis, and material characteristics analysis. Each mine would follow a similar experimental design but would differ for some test procedures.

- Kansanshi

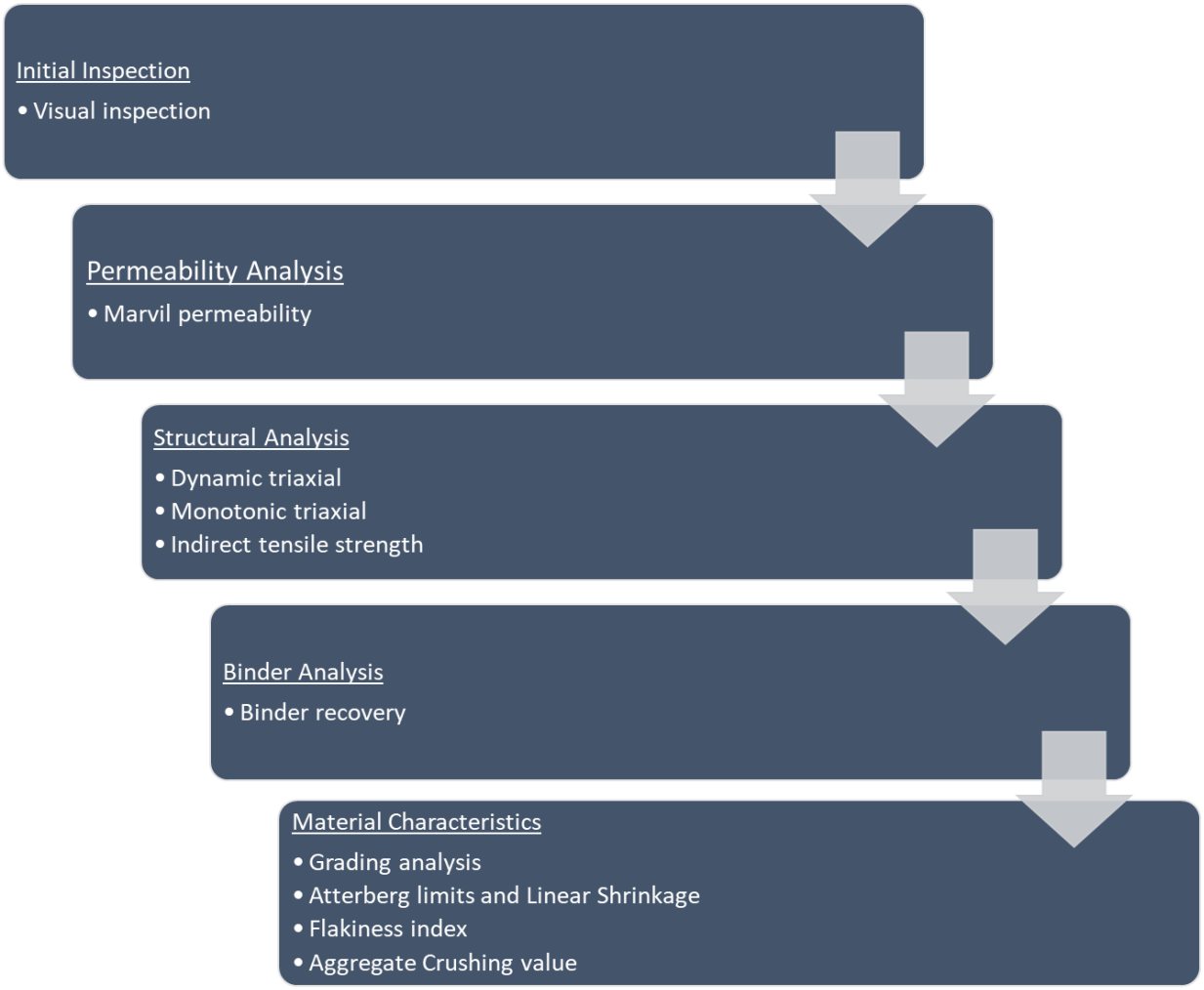

Figure 17 Experimental design proposed for Kansanshi.

For Kansanshi, an experimental design is proposed in Figure 17. Firstly, an initial visual inspection is conducted on the specimens. The inspection would observe the current condition of Specimens and take into consideration the location of each Specimen on the respective ramp. The inspection also provides an indication of which Specimens are structurally compromised and which can be studied for structural analysis.

After the inspection, the Specimens remaining are used to perform the destructive tests, such as Indirect Tensile Strength, Dynamic Triaxial, and Monotonic Triaxial. These tests provides comprehensive results which can be used to describe the structural capacity of the Kansanshi Mine Hual roads. Certain Specimens have also been allocated to permeability testing. Permeability testing provides a broad relationship between structural integrity in soaked conditions. Also, permeability testing allows for testing the viability of the waterproofing layer used on these roads.

With the destructive tests complete, binder analysis is executed. With the data collected from this procedure, a good understanding can be achieved of the correlation between residual binder content and structural performance. Once the binder analysis has been completed, the excess aggregate is used to perform material classification tests. These tests will include grading analysis, Atterberg limits and linear shrinkage, flakiness index, and aggregate crushing value. The results collected with these tests will provide a good indication of the material's performance characteristics.

- Kalumbila

For Kalumbila, an experimental design is proposed in Figure 18. Firstly, an initial visual inspection is conducted on the specimens, just as applied on the Kansanshi mine. The inspection would observe the current condition of specimens and take into consideration the location of each Specimen on the respective ramp. For Kalumbila, two ramps were identified and examined. The inspection also provides an indication of which specimens are structurally compromised and which can be studied for structural analysis.

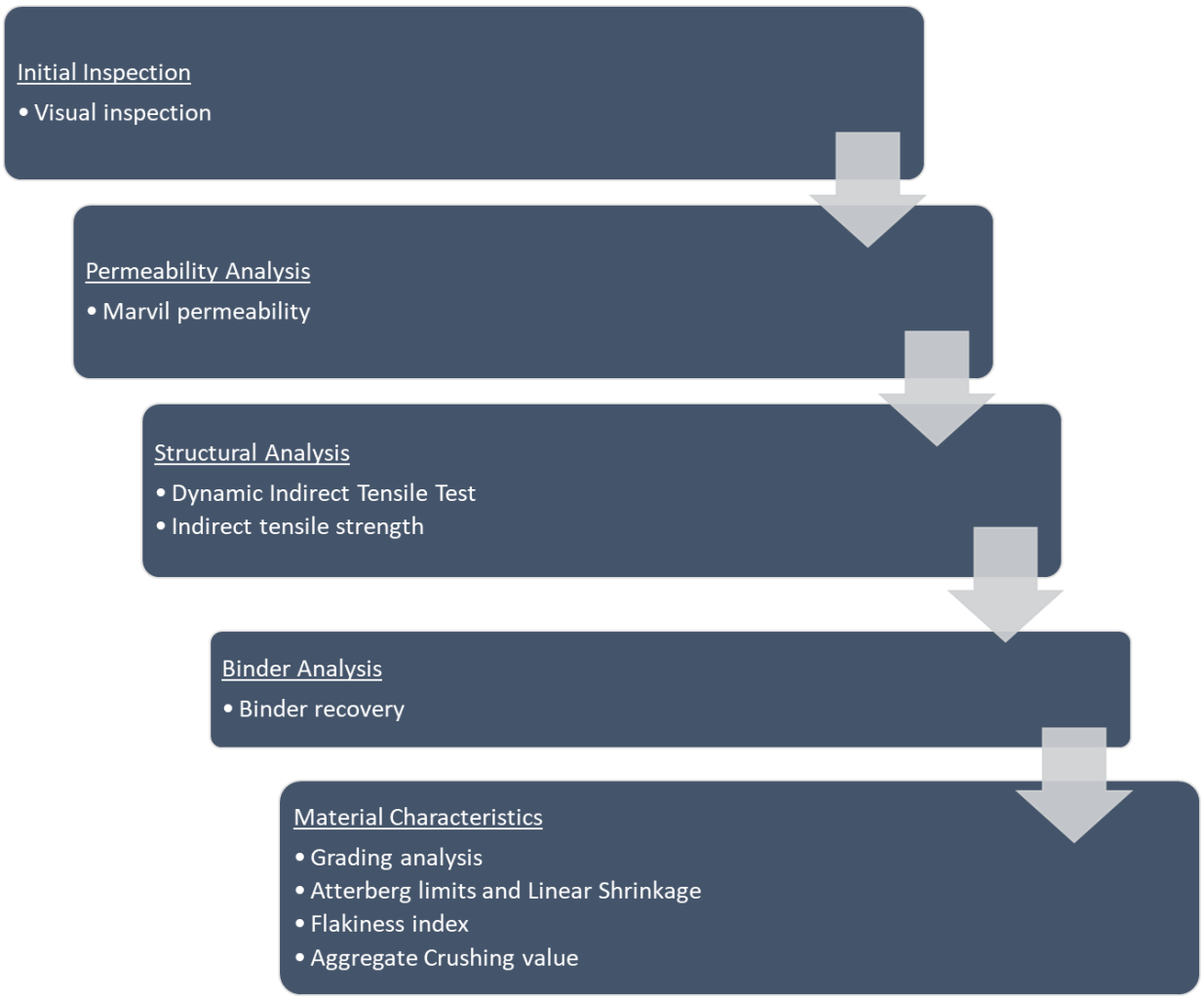

Figure 18 Experimental design proposed for Kalumbila.

After the inspection, the Specimens remaining will be used to perform the destructive tests, such as Indirect Tensile Strength and Dynamic Indirect Tensile Testing. No monotonic- or dynamic triaxial can be performed on the Kalumbila ramps as no Specimens were meeting the height requirements for these respective tests. The test that will however be used, will provide insight into the structural capacity of the two Kalumbila ramps.

Certain Specimens have also been allocated to permeability testing. Permeability testing will provide a general relationship between structural integrity in soaked conditions. Also, permeability testing will check the viability of the waterproofing layer used on these roads.

With the destructive tests complete, binder analysis will be executed. With the data collected from this procedure, a good understanding can be achieved of the correlation between residual binder

content and structural performance. Once the binder analysis has been completed, the excess aggregate will be used to perform material classification tests. These tests will include grading analysis, Atterberg limits and linear shrinkage, flakiness index, and aggregate crushing value. The results collected from these tests will provide a good indication of the material's performance characteristics.

3.2 Indirect Tensile Strength (ITS)

For the Kanshanshi mine, 3 specimens were identified to be tested, namely Specimen 1, 5, and 6. These specimens were chosen because of their increasing bitumen content. Also, the height of each Specimen closely approximated the ITS specimen height requirements, thus less alterations to the specimen is required. According to the information provided by Kanshanshi, Specimen 1 has the lowest residual bitumen content at 2.1 % followed by Specimen 6 with 2.3 % and finally Specimen 5 with a residual bitumen content of 2.7 %.

3.2.1 Stress conditions for ITS test

3.2.2 Testing apparatus

According to Asphalt Academy (2009) and Williams (1969), the following equipment will be needed to complete an Indirect tensile strength (ITS) test. The test equipment includes a compression testing machine, ITS load frame, load transfer plate, drying oven, water bath, digital thermometer, and carrier plates. The specifications of each apparatus are discussed in depth in Appendix A.

3.2.3 Specimen Preparations

Standard procedures for bitumen stabilized base materials on a road network would include a mix design composition and a design emulsion content with or without active filler. In this case, however, for the mine haul road, the design binder content was not selected via a mix design. Core

specimens were obtained from the mines, enabling the actual residual binder contents to be obtained through the recovery of the binder. 5 Cores from Kansanshi were identified for ITS_{dry} and ITS_{wet} testing and only 3 cores from Kalumbila were identified. All the information as specified by the Mine is detailed in Table 8 below. These specimens were chosen for their increasing percentage in bitumen content.

Table 8 Measurements observed for Kansanshi Specimens.

ITS Specimens			
Specimen number	Specimen Height (mm)	Specimen Diameter (mm)	Residual Bitumen content (%)
Kansanshi ITS_{dry}			
1	100	143	2.11
6	100	143	2.27
5	106	143	2.67
Kansanshi ITS_{wet}			
2	150	143	2.60
4	165	143	2.39
Kalumbila ITS_{dry}			
1	53	143	2.11
2	60	143	2.11
6	40	143	2.11

1. Specimen conditioning
   1.1. Firstly, trim all three Specimens using a diamond blade cutter to achieve the required ITS Specimen height of 95 mm.
   1.2. Place each Specimen on a carrier plate and mark each Specimen with an identifying marker.

2. Curing
   2.1. Take each Specimen off their respective carrier plate and weigh. Record the mass of the Specimen and place it back on the carrier plate.
   2.2. Place each Specimen in a forced draft oven at 40 ºC for 72 hours. Ensure that there is at least 25 mm of spacing between each Specimen.

2.3. After 72 hours, each Specimen was weighed to determine if there was any moisture loss. If the mass of each Specimen displayed a difference of more than 10 g, the Specimens were put back into the oven for another 24 hours. This cycle continues until the Specimens reach a constant mass.

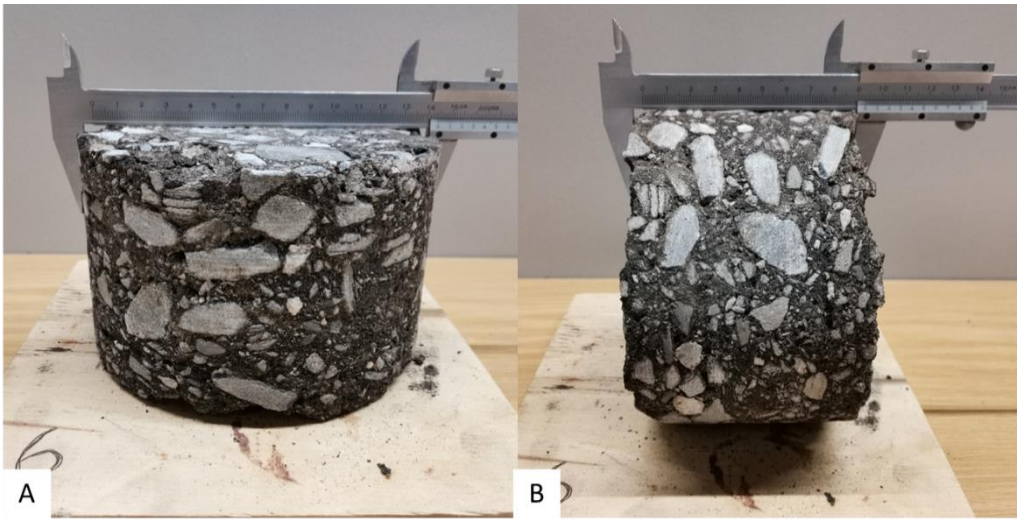

Figure 19 a) Diameter readings taken, and b) height measurements taken for bulk density calculations.

Williams (1969) stated in the Wirtgen laboratory handbook that accelerating the curing process by increasing the temperature is not advisable. For foam or emulsion specimens, the increase in temperature can cause bitumen particles to heat up beyond their respective softening points. This would ultimately lead to changes in the characteristics and behaviour of the stabilised material.

2.4. Once all specimens reach equilibrium, place the specimens in a room or compartment to cool off to a temperature of 25.0 ºC, which is known as room temperature. For this test, the UTM test chamber was used for the cooling period. The UTM has a built-in compressor that is capable of maintaining a constant temperature over a long period. The UTM's chamber was also chosen as it would lead to less variation in temperature if the Specimens had to be moved

2.5. Once room temperature is achieved, measure and calculate the bulk density of each specimen. This is completed by measuring the height of each Specimen at four evenly spaced locations on the Specimen as shown in Figure 19. With the height measurements complete,

the Specimen's diameter should be measured at three different locations on each Specimen. This technique is used to ensure an accurate representation of each Specimen is taken into account during calculations.

2.6. After all, measurements are finalised, determine the mass by weighing each Specimen. Calculate the bulk density by using the equation listed below:

$$BD_{specimen} = \frac{4 \times M_{specimen}}{\pi \times d^2 \times h} \times 10^6$$

Where

$BD_{Specimen}$	|Bulk density of Specimen (kg/m^3),
$M_{Specimen}$	|Mass of Specimen (g),
H	|Average height of the Specimen (mm), and
D	|Average diameter of each Specimen (mm).

3.2.4 ITS Test Procedure

The following section will describe the procedure followed to test each Specimen in the UTM. Firstly, the base plate with accompanying lower loading strip is placed and locked into place on the loading platform. When the lower loading strip is firmly in place, take the specimen and place it on its side onto the lower loading strip. While holding the Specimen steady, take the upper loading strip with the accompanying plate and place it on top of the specimen by sliding it into the vertical frame guides. Ensure that each specimen is centred between the loading plates to ensure

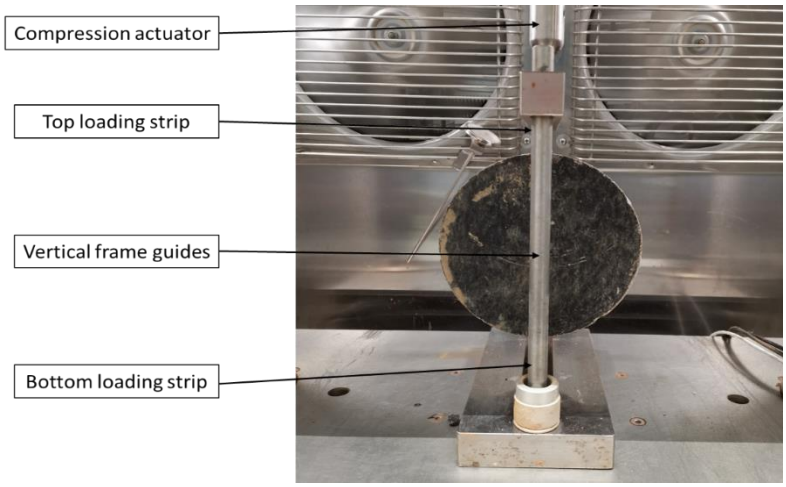

Figure 20 UTM layout for indirect tensile strength testing.

that no eccentric loading is applied during testing. An example of this layout is depicted in Figure 20.

Once the Specimen is securely in place, a seating load of 0.1 kN is applied to the frame and Specimen. Williams, (1969) advises that during the pre-load stage, the frame with accompanying Specimen should be examined for any symmetrical errors. If there are no errors observable, the frame should be loaded at a constant strain rate of 50.8 mm/min without shock. This load should be applied until the specimen fails. If the failure point is reached, loading should be stopped and the maximum load should be recorded to the closest 0.1 kN. The displacement at the breaking point should also be recorded to the closest 0.1 mm. The final reading that is necessary is the Specimen's internal temperature. If the Specimen is not already broken in half, force it open to retrieve the internal temperature to the closest 0.1 ºC. With all the necessary measurements in place, the indirect tensile strength can be calculated by making use of the equation below

$$ITS = \frac{2 \times P}{\pi \times h \times d} \times 10^6$$

Where
ITS |Indirect tensile strength (kPa),
P |Maximum applied load (kN),
h |Average height of the Specimen (mm), and
d |Average diameter of the Specimen (mm).

When all testing is complete, a small sample should be broken off from the Specimen and dried in a drying oven at 110 ºC to determine the moisture content. The sample should be dried out for 24 hours and must be weighed before and after the drying period. The moisture content is then determined according to the method 'A.4' from Williams, (1969) which is displayed below.

$$W_s = \frac{M_{CM} - M_{CD}}{M_{CD} - M_C} \times 100$$

Where
W_s |Moisture content (% of the dry material),
M_{CM} |Mass of the moist material and container (g),
M_{CD} |Mass of the dry material and container (g), and
M_C |Mass of the container (g).

3.3 Monotonic triaxial test

To provide critical performance properties necessary to evaluate a BSM mix design, the shear properties such as cohesion and friction angle are required These properties can be obtained through monotonic triaxial testing. The shear properties that are determined by the monotonic triaxial can be compared with current BSM classification limits to indicate the layer's shear performance properties. BSM mixes can fall between a range of BSM1 to BSM2. BSM1 mixes indicate that a high-quality mix is being used that can withstand high traffic loading whereas the latter (BSM2) would indicate that poor quality material is being used with inadequate shear properties. The better a material's classification, the lengthier the lifespan of the layer.

3.3.1 Testing apparatus

The following parts that are stated below are the testing apparatus used during the monotonic testing. These parts include triaxial cell, rubber bladder, air compressor, water bath, forced-draft drying oven, compression testing machine, digital thermometer, and wooden carrier plate. All of the apparatus will be discussed in depth in Appendix A.

3.3.2 Specimen Preparation

Usually, for research purposes, 10 Specimens should be manufactured that are 150 mm in diameter and 300 mm in height. From these 10 specimens, 8 are tested at dry conditions and the remaining two at wet conditions. Since limited samples were available only dry testing could be achievable.

1. Curing procedure

    1.1. Commonly after Specimens are compacted, they are left overnight in their respective moulds and covered with a moist hessian cloth[6]. Since the core Specimens came from a pre-existing road, this step can be excluded.

[6] Hessian cloths are designed and manufactured to be breathable, thus it is resistant towards condensation. This leads to a reduced risk of Specimens being spoiled due over-saturation cause by condensation.

1.2. Place each Specimen on a carrier plate. Ensure that each Specimen is marked with an identifying marker.

1.3. Before curing can start, measure the following for each Specimen: *a)* Specimen mass, *b)* Specimen height measure at four equally spaced locations, *c)* Specimen diameter measured at four different locations located ad mid-height of the Specimen.

1.4. With these measurements, calculate the bulk density of each Specimen using the equation stated below.

$$BD_{specimen} = \frac{4 \times M_{specimen}}{\pi \times d^2 \times h} \times 10^6$$

Where

$BD_{Specimen}$	|Bulk density of Specimen (kg/m^3),
$M_{Specimen}$	|Mass of Specimen (g),
H	|Average height of the Specimen (mm), and
D	|Average diameter of each Specimen (mm).

1.5. After the calculations are complete, place the Specimens in a forced draft oven at 40 ºC ± 1 ºC. Leave the Specimens in the oven for 8 hours.

1.6. After 8 hours, remove the specimens. Place a plastic bag over each specimen and ensure the plastic bag is sealed to ensure no moisture loss.

1.7. Place the Specimens back in the oven at 40 ºC ± 1 ºC for another 48 hours.

1.8. After 48 hours, remove the Specimens from the oven and fit them with new dry plastic bags. Leave the Specimens at room temperature (25 ºC±2 ºC) for a minimum period of 12 hours to allow for cooling. Before the testing procedure starts, each Specimen should be weighed.

3.3.3 Testing procedure

To start the procedure, place the base of the triaxial cell on top of the fixed reaction base. Ensure that there is sufficient clearance to accommodate the entire length of the triaxial cell. Once the base is in place and fairly centred, the Specimen can be placed onto the middle section of the base

plate. Sufficient precaution must be exercised to not damage any of the corners of the Specimen while positioning it. Once the Specimen is securely in place, the rubber membrane can be fitted over the Specimen. Ensure that the side with the bladder valve is facing towards the outside of the testing machine. Slide the cylindrical frame over the bladder and starts fastening the three bolts holding it in place. Place the balancing weight on top of the Specimen, as it should fit perfectly between the top section of the cylindrical frame.

Ensure that the fixed reaction base is levelled according to the specified compression testing equipment being used. In this case, the fixed reaction base would be set to 0 mm which gives it 80 mm upwards and downwards for movement. Once the reaction base is levelled, the fixed loading ram can be lowered onto the triaxial cell. The loading force should be monitored during this period to ensure that no pre-loading occurs. With the loading ram and fixed reaction base in place, the air compressor can be connected to the rubber membrane to start testing.

To initiate the testing procedure, it should be ensured that the programming language used on the compression testing machine applies a constrain strain force of 3 mm/min. It should also be checked that the measurement tool (i.e. the displacement and load measuring tools) are taking measurements at least every second. The maximum displacement that is allowed by the testing protocol is 18 mm (or 6 % strain). After the maximum strain is reached, the actuator must be programmed to unload the Specimen to the starting length. The pressure within the rubber bladder should also be released to remove it. Once the pressure has been released, unscrew all the bolts holding down the cylindrical cell and remove it. Break open the Specimen directly after removing the cell and record its internal core temperature.

3.3.4 Testing Conditions

For the monotonic test, four different confining pressures will be used. The confining pressures are 50 kPa, 100 kPa, 150 kPa, and 200 kPa. Under normal circumstances, eight Specimens are required for testing. This is to ensure that at each confining pressure at least two tests can be performed. Since only one Specimen is available for testing, all for confining pressure are to be tested on this Specimen. For this procedure to work, a load should be applied to the Specimen with a specific confining pressure.

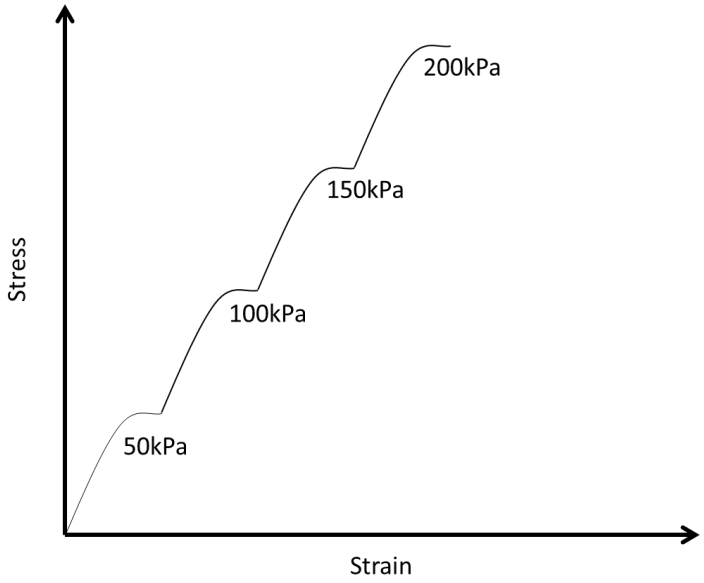

Figure 21 Proposed monotonic testing conditions for Kansanshi.

Once the load reached the maximum point (i.e. where the load starts to plateau), an automatic break detector should be implemented to pause the test. During this pause, the confining pressure can be increased by 50 kPa and the test can continue. This process continues until the breaking point is reached for the 200 kPa confinement pressure. Figure 21 displays the thought process behind this test. It should be noted that the TG2 document by Sabita (2020) specifies that the confining pressures should only include 50 kPa, 100 kPa, and 200 kPa. However, there were only limited specimens available, thus the test procedure was altered slightly to extract more data from the specimens.

To achieve this level of accuracy during testing, a few 'mock' specimens were created according to a BSM2 classification. These Specimens were tested using the above-stated parameters to test the sensitivity of the breaking detector. After numerous tests, it was confirmed that the compression testing machine can detect when there is a change of 2-3 kPa. Thus using this benchmark and dividing by the area of the Specimen, the testing program could be updated to allow for a break detector sensitivity of 0.04 kN.

3.3.5 Data processing

According to (Williams, 1969; Sabita, 2020) the following step and equations are used to calculate the cohesion intercept (C) and internal friction angle (θ) of a specific material.

i. Calculate the bulk density of the Specimen

This step was already completed during the curing process. However, if 10 Specimens are used the below equation should be used to identify and discard any outliers.

$$T_0 = \frac{X_0 - \overline{X_n}}{S_n}$$

Where
T_0 |Value being tested,
X_0 |Bulk density of the Specimen (kg/m^3),
$\bar{x}_n$ |Mean bulk density of the Specimen (kg/m3),
n |Number of specimens, and
S_n |Standard deviation of the Specimen (kg/m^3).

ii. Calculate the applied failure stress

$$\sigma_{a,f} = \frac{4 \times P_{a,f}}{\pi \times d^2} \times 10^6$$

Where
$\sigma_{a,f}$ |Applied failure stress of the Specimen (kPa),
$P_{a,f}$ |Applied failure load of the Specimen (kN), and
d |Diameter of the Specimen (mm),

iii. Determine the total applied stress at failure

The total applied stress at failure can be calculated by adding the applied load to the total deadweight pressure.

$$\sigma_{1,f} = \sigma_{a,f} + \frac{4 \times (M_{TP} + M_{LR})}{\pi \times d^2} \times g \times 10^{-3}$$

Where
$\sigma_{1,f}$ |Total applied stress at the failure of the Specimen (kPa),
$\sigma_{a,f}$ |Applied stress at the failure of Specimen (kPa),
M_{TP} |Mass of the top plate (kg),
M_{LR} |Mass of the loading ram (kg),
d |Diameter of the Specimen (mm), and
g |Standard gravitational acceleration (9.81 m/sec^2).

iv. Determine the linear relationship between total applied stress and confining stress

According to Williams (1969), there is a linear relationship that can be observed between the total applied stress at failure ($\sigma_{1,f}$) and the confinement pressure (σ_3). To determine the values of the linear relationship, a linear regression analysis should be performed on the data to determine the most accurate A and B values as shown in the equation below. The values 'A' and 'B' represent the slope and intercept respectively.

$$\sigma_{1,f} = A \times \sigma_3 + B$$

The linear regression analysis can be applied according to the following steps. Plot the calculated total applied stress over the confinement stress where $\sigma_{1,f}$ is on the Y-axis with σ_3 on the X-axis. Using this data set, assign a best-fit linear trend line to this data. Determine the slope and intercept of the best fit line. According to Mohr-Coulomb's theory, the relationship between the slope and the intercept can be described through the following two equations.

$$A = \frac{1 + \sin(\theta)}{1 - \sin(\theta)} \qquad B = \frac{2 \times C \times \cos(\theta)}{1 - \sin(\theta)}$$

Where
θ |Angle of internal friction (º), and
C |Cohesion (kPa).

Using both equations A and B simultaneously, the internal friction angle and cohesion intercept can be calculated using the equations displayed below.

$$Angle\ of friction = \sin^{-1}\left(\frac{A-1}{A+1}\right)$$

$$Cohesion\ (C) = \sin^{-1}\left(\frac{B \times (1 - \sin\theta)}{2 \times \cos\theta}\right)$$

3.4 Dynamic triaxial test

Pavement structures are designed to transfer the wheel loads of heavy vehicles between the layers, without overstressing the layers. The ability to adequately spread loads to lower layers is dependent on the stiffness of that material. Granular materials have lower stiffness properties than bitumen stabilised materials BSMs i.e. the BSMs have a superior load spreading capability.

Granular material does not conform completely to linear elastic behavioural models. They exhibit elasto-plastic behaviour. In addition, the material is stress-dependent. This would indicate why the stiffness or Resilient Modulus would not be a single value, but rather a varying number as this material is stress-dependent (Jenkins and Rudman, 2019). For these specific reasons, research dynamic triaxial testing is implemented. Dynamic triaxial makes use of varying deviator stresses at constant confining stresses to determine the Resilient Modulus.

For a normal triaxial Specimen, the diameter should be 150 mm and should have a height of 300 mm. If smaller diameter Specimens are used, it is advised to ensure that the Specimen at least retain a ratio of 2:1 for height: diameter. Unfortunately, the pavement depth on the Kanshanshi mine did not meet the 300 mm requirement. For this reason, two Specimens (7 and 8) were identified to be within proximity to each other and also contain the same amount of residual bitumen content. Thus, for this test 2 Specimens, of 143 mm diameter, would be used to perform 1 dynamic triaxial test and 1 monotonic triaxial test.

3.4.1 Difference in Stress Application

The Dynamic Triaxial test is similar to the Monotonic Triaxial test in that stress is applied at a specific confinement pressure to determine a representative shear parameter of the mix. However, there is a difference in terms of how the confinement pressure influences the applied cyclic stress (σ_c) for the Dynamic Triaxial. The difference in the stresses applied between the Monotonic- and Dynamic Triaxial is displayed in Figure 22 below.

It can be observed from Figure 22 that in Dynamic Triaxial Chamber, the specimens' confinement is provided by a rubber membrane and two rubber O-rings.

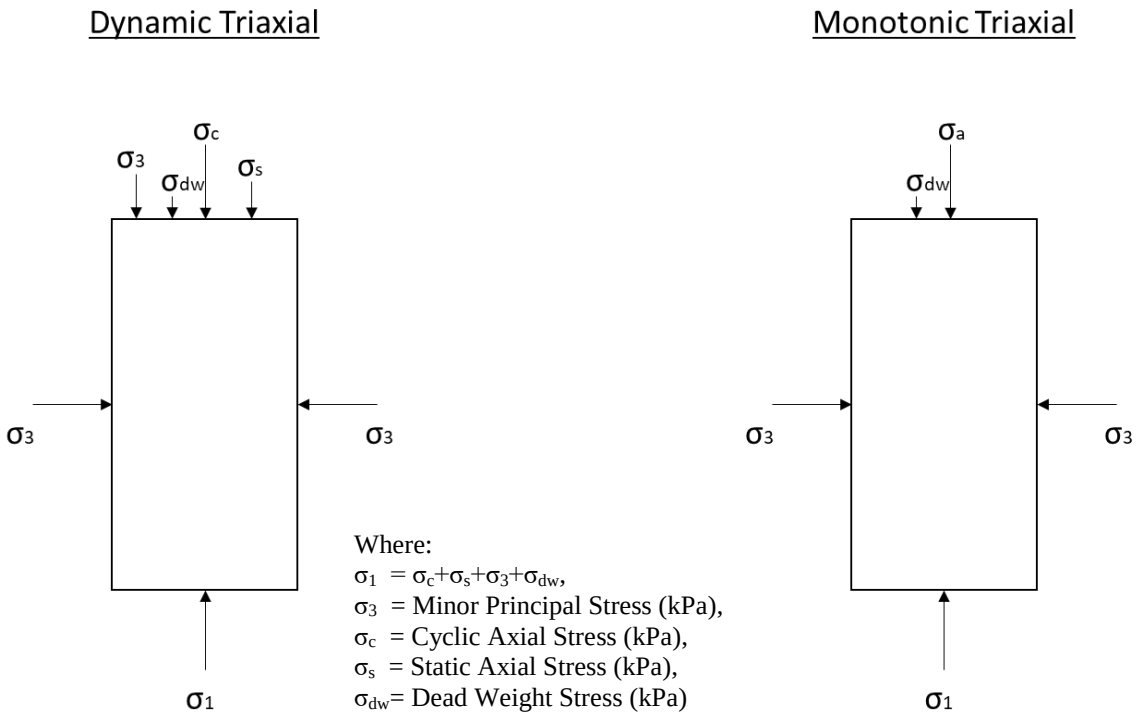

Figure 22 Comparison between the Dynamic- and Monotonic Triaxial Stress Layout (adapted from Jenkins (2000)).

As a result of this confinement stress configuration, the major vertical stress on top of the specimen will also include confinement stresses. However, for the Monotonic Triaxial test, the confinement around the specimen is provided by a rubber bladder and is enclosed in a steel frame. Thus the only stress applied to the specimen is the stress created by the dead weight of the top plate and the stress applied by the actuator.

3.4.2 Testing apparatus

To understand how the test procedure is implemented, it would first be helpful to describe the equipment being used to test the specimens. The setup consists of a compression testing machine, triaxial load frame and Specimen housing, external air pressure regulator, Linear vertical displacement tools (LVDTs) with accompanying brackets, drying oven, carrier plates, and latex membrane.

1. A compression testing machine

According to the TG2 guidelines by (Sabita, 2020), a compression testing machine is required that can apply forces up to 200 kN with an accuracy of ±0.1 kN. The machine should also be able to implement a constant displacement rate of 3 mm/min or rapid variable loading at different sinusoidal frequencies such as 10 Hz. Also, the machine must be able to record displacements in 1-second intervals. The layout of the compression chamber should be such so that the actuator or loading ram is located above the triaxial frame, and the fixed base reacting to the forces must be located at the bottom of the triaxial frame. Between the reaction base and the actuator should also be sufficient space to accommodate the placement and removal of the triaxial frame.

2. Triaxial loading frame

The triaxial loading frame or loading cell is a unit that consists of multiple interconnected parts. The first part is the triaxial base plate as displayed in Figure 23. a). The base plate can be fitted into place on the fixed reaction base via a small hollowed-out section at the bottom of the base. The depth of the hollowed section is just enough to keep the whole triaxial loading frame in place. In the middle of the base plate is a spacer plate that is 152 mm in diameter to allow for the positioning of the Specimens within the loading frame.

Between the spacer plate and the outer edges of the base plate, two cavities have been manufactured to allow for the safe injection and omission of air into the holding area which will be discussed shortly. On the intake cavity, a pressure gauge and two pressure regulating valves are connected of which one is for small changes in air pressure and the other for larger changes in air pressure. This is also to ensure that the confining pressure within the loading frame would stay

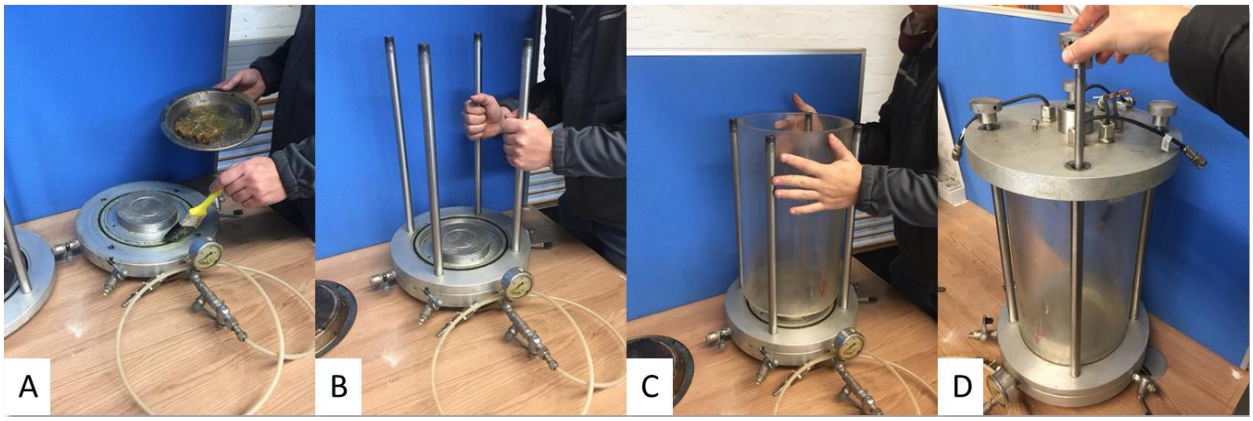

Figure 23 Triaxial loading frame construction.

constant with fairly small fluctuations. On the omitting cavity, only 1 lever valve is connected to ensure that the chamber can be de-pressurised before the loading frame is removed.

On top of the base plate will be fitted another circulate plate as shown in Figure 23. b). This plate, however, only rests on the outer edges of the base plate. This circulate plate also has four openings at the bottom that are spaced out at four 90-degree angles. This is to allow the four hollowed-out guiding rods to connect to this specific plate. With the guiding rods in place, a large diameter Perspex ring can be placed onto the second plate which will act as the bottom seal for the confine-ment chamber as illustrated in Figure 23. c).

Once all the above-stated parts are assembled, the final circular plate can then place on top of the assembled parts. This plate also has four holes at 4 90-degree points to allow the plate to settle onto the Perspex ring. This would form the final seal to create a fully sealed confinement chamber. To keep the top plate from flying off when pressure is injected, another four guiding rods are used. These rods would slip into the cavities of the hollowed-out guiding rods stated above and connect with the bottom base plate.

3. Air compressor

An air compressor unit is required to inflate the confinement chamber to a maximum confinement pressure of 200 kPa ± 2.5 kPa. (Sabita, 2020)also noted that attached to the air compressor should be a pressure gauge that gives the user the ability to adjust the pressure in 1 kPa increments.

4. Carrier Plates

Carrier plates are made from plywood and are used to transport compacted specimens. They can be square or round with a thickness of approximately 15 mm.

5. Drying oven

A continuous forced-draft drying oven that can maintain temperatures of 40±1 ºC. The oven should also be thermos-statically controlled and be able to take at least 240 litres of material.

6. LVDTs

For more accurate displacement readings during testing, three LVDTs will be required. These measuring tools will be placed between the middle third of the sample (in terms of the Specimen's height). To keep these LVDTs in place, two plastic brackets are placed at the top and bottom third individually. Each measuring device is capable of measuring 13 mm in both directions, which results in a 26 mm total displacement measuring distance. These devices are also capable of accurately measuring displacement (stroke) with a tolerance of ±0.001 mm.

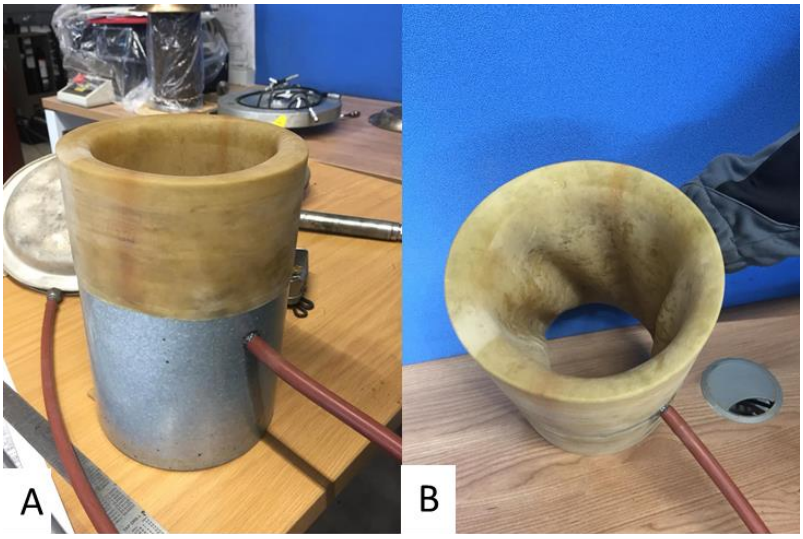

Figure 24 Side (a) and top (b) view of the rubber membrane with positioning ring.

7. Rubber membrane and positioning ring

A rubber membrane is required to cover the Specimen during testing. These membranes are usually made out of latex to allow for stretching. For a fitted membrane, the diameter during manufacturing should be less than the Specimen diameter (152 mm). To install the membrane over the Specimen, a hollow steel ring with a 300 mm height is required. The ring has a hose attached to create a vacuum between the membrane and the ring. This is to allow for the easy installation and removal of the membrane. The rubber membrane with positioning ring is shown in Figure 24

3.4.3 Testing procedure

For the test procedure a few sections will be covered such as measuring and conditioning of the specimens, curing of the specimens, specimen setup, testing conditions, and data assembly/ calculations.

i. Measuring, conditioning and curing

Before any of the Specimens provided can be used for testing, they should be conditioned to the optimum conditions specified for testing. Since all of the Specimens were provided, it is not necessary to cover the Specimens with moist hessian cloths or leave them in any moulds as specified by (Sabita, 2020)t. Two Specimens from Kansanshi were identified for dynamic triaxial testing. Specimen 7 and 8 were located 150 m from each other. According to the information provided by Kanshansi, both of these Specimens also contain the same percentage residual bitumen content (±2.6 %). The method below discusses the test procedure as set out by (Sabita, 2020)

1. Curing

    1.1. Place each Specimen on a carrier plate. Ensure that each carrier plate is labelled.

    1.2. Place the Specimens in a forced-draft drying oven at 40 ºC ±1.0 ºC. Keep the Specimens in the drying oven for 8 hours. Sabita (2020) advise that all Specimens should be no closer than 25 mm from each other to allow for sufficient ventilation.

    1.3. After 8 hours, remove the Specimens from the drying oven and cover them with plastic bags. These bags should fit loosely around the specimens. Ensure that the bags are sealed to prevent moisture loss.

    1.4. Place the covered Specimens back in the oven for 48 hours. The temperature should remain at 40 ºC ±1.0 ºC.

2. Measurements

    2.1. After 48 hours, remove all the specimens. Also, remove the plastic bags from each Specimen.

    2.2. Weigh each Specimen without the carrier plate. Record the mass to the nearest 0.1 gram.

    2.3. Measure the height of each Specimen to the nearest 1 mm. Measure three separate readings at three different locations to take account of any variability.

    2.4. Measure the diameter of the Specimens to the nearest 1 mm. Take this measurement at mid-height of the Specimen at three differently spaced locations.

2.5. Measure the bulk density of each Specimen with the equation below. Only two Specimens are used thus no outliers can be observed.

2.6. Fit dry plastic bags around the specimens. Seal the bags and place the Specimens back on the carrier plates.

2.7. Place the covered Specimens back into the oven at 25 ºC ±1.0 ºC. Leave the Specimen for 12 hours to allow for cooling.

2.8. After 12 hours, remove the Specimens and get rid of the plastic bags. Specimens are now ready for testing.

$$BD_{specimen} = \frac{4 \times M_{specimen}}{\pi \times d^2 \times h} \times 10^6$$

Where

$BD_{Specimen}$	|Bulk density of Specimen (kg/m^3),
$M_{Specimen}$	|Mass of Specimen (g),
H	|Average height of the Specimen (mm), and
D	|Average diameter of each Specimen (mm).

3.4.4 Testing procedure

Since the dynamic triaxial chamber is such an intricate structure, this section will discuss the procedure to assemble it. Afterwards, the test procedure will be discussed. Before starting the assembly procedure of the Dynamic Triaxial Chamber (DTC), find a stable surface on which to assemble. Ensure that the stable surface is located close to the testing chamber, as the completed structure is heavy.

1. Sub-frame assembly

1.1. Firstly, place the DTC's base on the flat surface as shown in Figure 25. a). Ensure that there is enough grease on the rubber seal to prevent any air leaks. Position the assembly close to an edge for easier removal afterwards. With the base plate in place, safely pick up the second 'upper base plate' ring and place it on top of the base plate.

1.2. Once the sub-frame is assembled, place the Specimen in the middle circular plate as indicated in Figure 25. b.

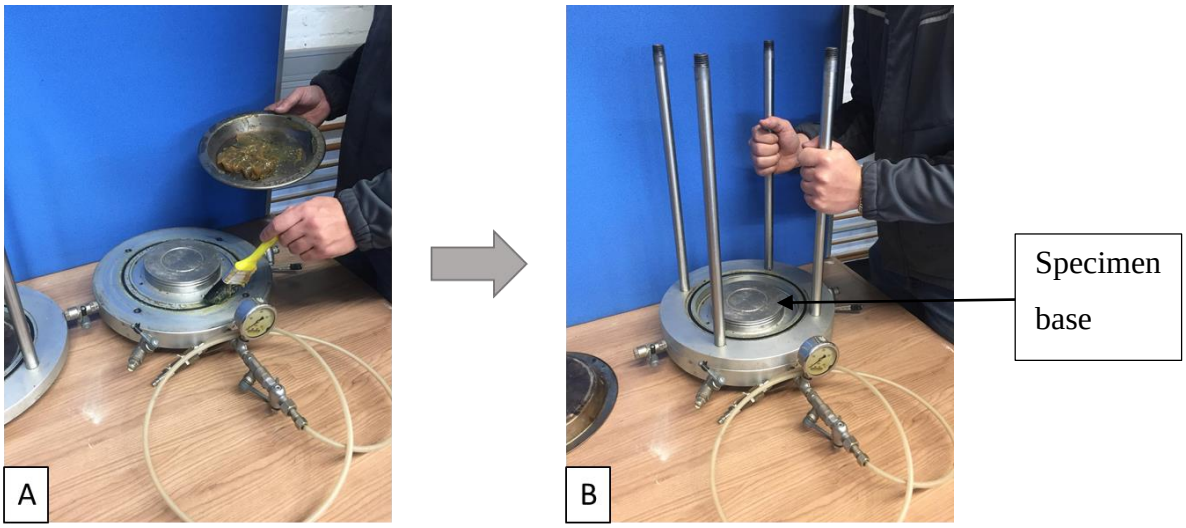

Figure 25 Sub-Frame assembly with a) Base plate and b) upper base plate.

1.3. It should be noted that typical triaxial Specimens are150 mm in diameter and 300 mm in height. The 2:1 height to diameter ratio is considered the standard practice as the H:D ratio has been proven to provide 'true' stress-strain behaviour within the material (Peri, Ibsen and Nordahl Nielsen, 2019). However, the Specimens that were provided from Kanshansi were 143 mm in diameter and between 150-165 mm in height. These Specimens did not comply with the criteria for testing, thus a few alterations had to be made.

1.4. For the dynamic triaxial testing, the two Specimens would be stacked on top of each other. The reason for this modification is due to the theory that, under loading, the friction between two Specimens would be enough to simulate a single Specimen. For this reason, both Specimens were shortened with the diamond blade circular saw to a length of approximately143 mm. Thus the complete Specimen would have a height of 286 mm. The DTC was designed to accommodate 300 mm specimens; thus, a small circular Perspex mould, which is 14 mm thick, was manufactured to fit between the Specimen and the sub-frame. Also, a circular steel plate should be placed on top of the Specimen. The steel plate acts as the load transfer between the actuator rod and the Specimen.

2. Membrane fitment

2.1. Firstly, place the rubber membrane over the circular sheet with an attached vacuum hose as shown in Figure 26. a). Make sure that the membrane is equally distributed over the circular sheet.

2.2. If the membrane fully embraces the circular sheet, start to remove the air via the hose as shown in Figure 26. b). Once all the air is removed, slide the unit over the Specimen to avoid any damage.

2.3. When the membrane reaches the required position, release the pressure from the vacuum hose and allow the membrane to fasten onto the Specimen. Remove the membrane at the top and bottom edges of the circular sheet and slide the circular sheet off of the Specimen.

2.4. Neatly straighten out the membrane at the top and bottom edges of the Specimen by folding it over onto itself. Once all the required parts are covered, place the rubber bands at the top and bottom of the membrane to ensure no air can penetrate through.

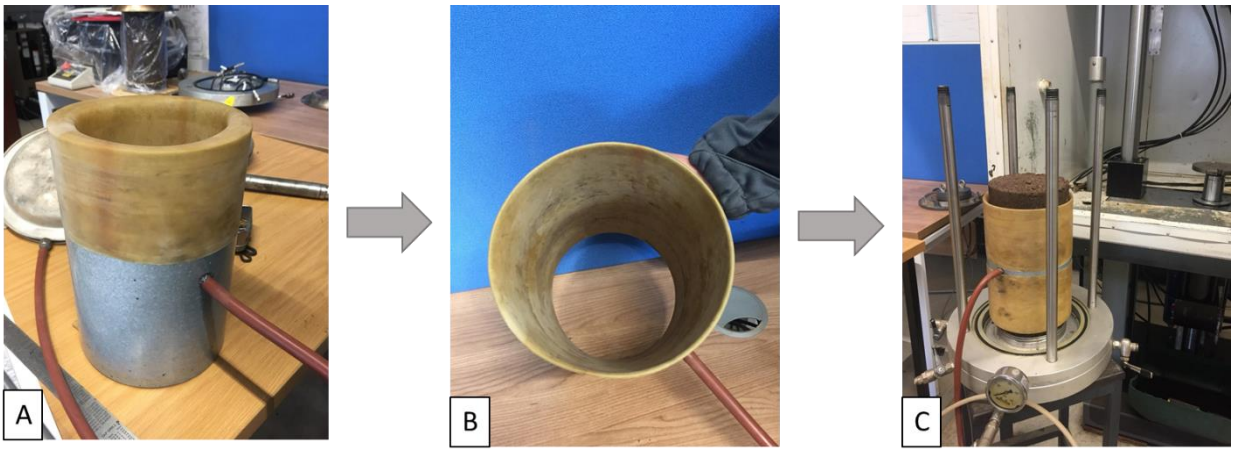

Figure 26 Membrane fitment with a) placing the membrane of the steel sheet, b) creating a vacuum between the membrane and the sheet, and c) placing membrane over the Specimen.

3. LVDT installation

3.1. Install the plastic LVDT holders onto Specimen as shown in Figure 27. c). The plastic rings were manufactured to fit tightly around a 152 mm Specimen. However, the Specimen that was provided is 143 mm in diameter. For this reason, leather strips (±4-6 mm in thickness) were used to fill the gap between the Specimens and the rings.

3.2. Tighten the plastic rings with rubber bands. This step is crucial as it ensures that the plastic rings do not move during loading. This will ultimately result in more accurate readings.

3.3. When the rings are fixed and the LVDTs are installed, as Figure 27.d) displays, place the large Perspex cylinder over the Specimen. Again, ensure that there is sufficient grease between the Perspex and rubber seals, at both the top and bottom of the ring, to ensure no air leakage.

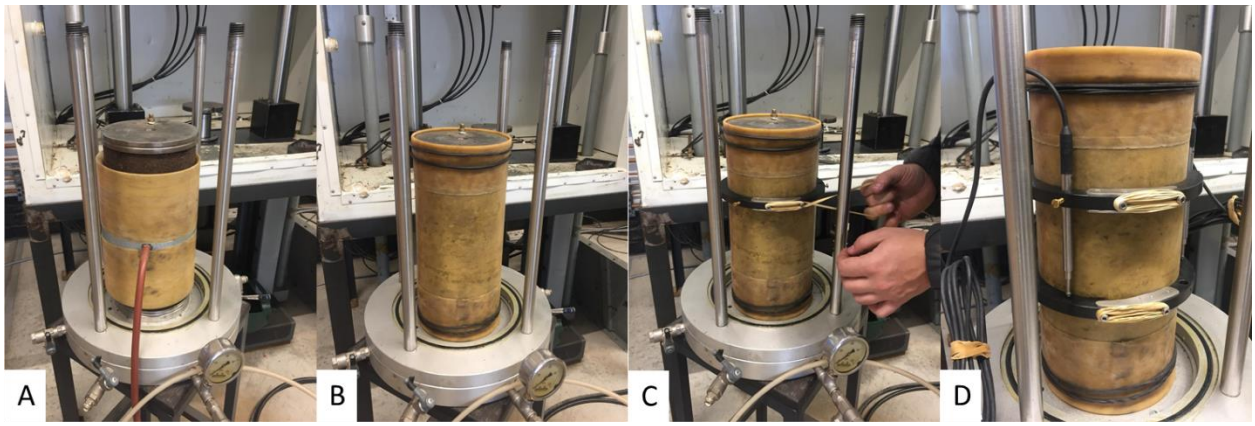

Figure 27 Attaching LVDTs to the Specimen.

3.4. Ensure that all wiring does not overlap the steel plate placed on top of the Specimen. This is to ensure that no wires get damaged by the actuator rod.

3.5. Place the top wire transfer plate on top of the Perspex cylinder. Before positioning the plate, ensure that all the necessary connections between the LVDTs and wire transfer plate are complete. Once all the connections are secured, position the transfer plate tightly on top of the Perspex mould.

3.6. Using the four nuts provided, tighten the wire transfer plate to the DTC using a normal tightening sequence[7].

3.7. Install the four rods that connect the DTC to the bottom base plate using the same tightening sequence as stated above.

3.8. Slightly grease the actuator rod and slide it into the gap in the top frame. The grease is to ensure that the rod can easily move up and down with as little friction as possible. As the DTC setup is now complete, the frame can gently be placed on top of the variable reaction arm of the compression testing machine as shown in Figure 28.

Figure 28 Complete setup of the dynamic triaxial machine.

3.4.5 Testing conditions

To initiate testing procedures, a few preliminary calculations have to be completed to determine the loads that have to be applied to the Specimen. Since the testing conditions are equal to that of

[7] The normal tightening sequence starts by slightly tightening the first bolt, then move directly on the second bolt which is situated 180 degrees away from the first bolt and slightly tighten. After the second bolt, tighten the bolt that can be found 90 degrees to the right, followed by the fourth bolt located 180 degrees from the third bolt(Werner, 2021).

a short term dynamic triaxial test, a constant load will be applied for a certain amount of cycle at a frequency of 10 Hz. This is to ensure the sample does not damage over time due to increased loading, as the Specimens still need to be used to complete monotonic triaxial testing.

Each Specimen will be tested at four different confining pressures (σ^3), namely 50 kPa, 100 kPa, 150 kPa, and 200 kPa. Along with the different confining pressure, each Specimen will be tested at four different Deviator Stress Ratio (DSR), namely 10 %, 20 %, 30 %, and 40 %. This results in 16 different applied loads that have to be calculated for each testing criteria. Normally a mono-

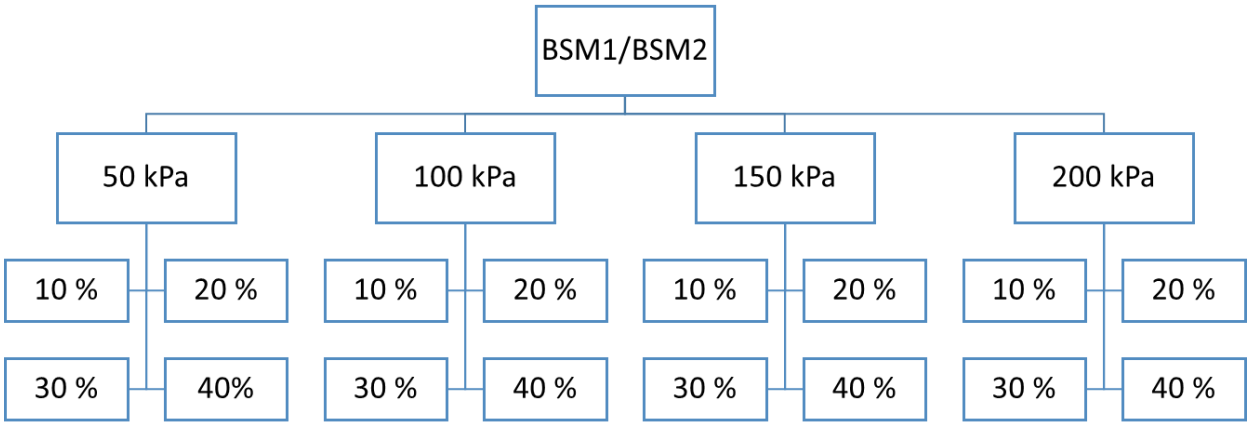

Figure 29 Ultimate stress at failure ($\sigma_{1,f}$) hierarchy.

tonic test has to be done to determine the cohesion intercept (C) and internal friction angle (ϕ) at failure. With these values it is possible to calculate a maximum applied force at failure ($\sigma_{1,f}$), but as there are limited specimens available the dynamic testing will be completed first, followed by the monotonic test.

From the information provided by Kanshanshi mine, it could be deduced that this emulsion treated base (ETB) cores would fall somewhere between the failure classification of a BSM1 and a BSM2 as specified by (Sabita, 2020). This criterion is shown in Table 9 below. Since none of the mine haul roads contained any reclaimed Asphalt, only less than 50 % value was used. Moreover, the cohesion and friction angle values are unknown thus the test will be conducted for both BSM2 classification and BSM1 classification.

Material Class	Percentage reclaimed Asphalt	ITS (kPa)		Triaxial		
		ITS $_{dry}$	ITS $_{wet}$	Cohesion (kPa)	Friction Angle (º)	Retained cohesion (%)
BSM1	<50 %	225	125	250 – 300 (250)	40 – 50 (45)	70 – 85 (75)
	50 – 100 %	225	125	265 – 350 (265)	38 – 45 (38)	75 – 90 (75)
BSM2	<50 %	175	100	200 – 250 (225)	38 – 40 (39)	65 – 75 (70)
	50 – 100 %	175	100	225 – 250 (238)	35 – 40 (37)	70 – 85 (75)

Table 9 Triaxial and ITS criteria for BSM materials (adapted from Sabita (2020)).

Using the above-stated information, the major principal stresses at failure ($\sigma_{1,f}$) at each confining pressure can be calculated for each material class using the equation below. Taking these major principal stresses at failure, the necessary DSR values can be calculated for each material class at each confining pressure.

$$\sigma_{1,f} = \frac{(1 + \sin \emptyset) \times \sigma_3 + 2 \times C \times \cos \emptyset}{(1 - \sin \emptyset)}$$

Where
σ_1 |Major principal stress in the layer (kPa),
σ_3 |Minor principal stress in the layer (kPa),
$\sigma_{1,f}$ |Major principal stress at failure (kPa),
C |Cohesion intercept value of BSM from mix design (kPa), and
ϕ |Friction angle value from BSM mix design (º).

Once all the deviator stresses at failure were calculated for each confining pressure, the respective testing condition DSR stresses can be calculated (i.e. 10 %, 20 %, 30 %, and 40 %). The dynamic triaxial test makes use of a sinusoidal frequency loading pattern, thus it was necessary to calculate the amplitude from trough to peak as shown in the illustration below. The amplitude can be considered as the force between the base force (i.e. respective confining pressure, σ_3) and peak force (i.e. the major principal stress for each DSR, $\sigma_{1,f}$ (%)). Thus the vertically applied stress will vary as the confining stress stays constant as stated by Jenkins and Rudman, (2019).

It is also vital to ensure that the seating load also be taken into account. The seating load is used to stabilise the Specimen and DTC for testing and is usually taken as 0.4 kN. If, during calculations for the amplitudes, the seating load is not taken into consideration; the applied vertical forces will be out of alignment with the rest of the test. This is due to how the MTS compression chamber and accompanying software is calibrated.

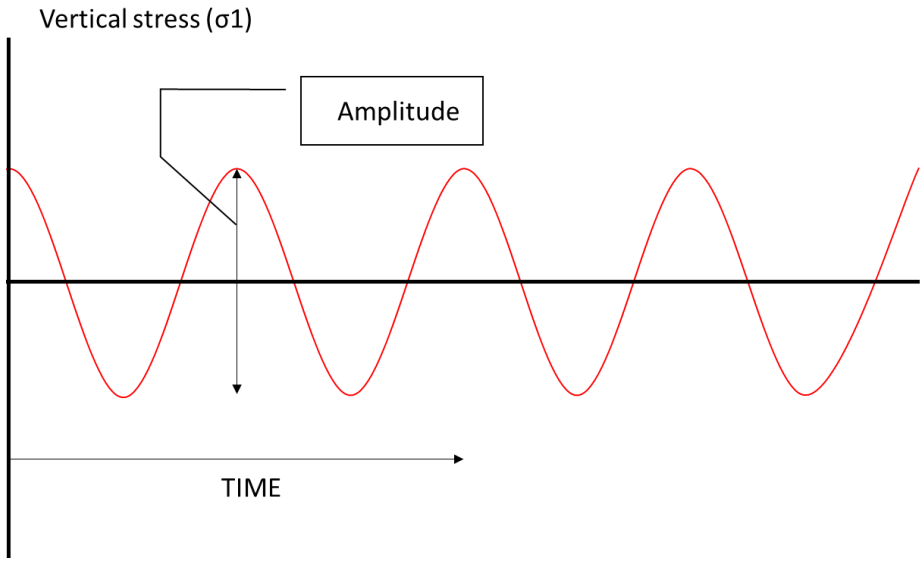

Figure 30 Sinusoidal frequency loading pattern used for dynamic triaxial (adapted from Jenkins and Rudman (2019)).

The MTS software automatically adds the seating load to the base confining pressure loads, but the loading profiles are manually edited and should also be updated separately. As a result, after all the amplitude loads are calculated, the representative seating load (in this case 0.4 kN) should be added and the separate loading profiles should be updated individually. The final input loads for the Dynamic triaxial test are shown in Table 10 below.

Confining Pressure (kPa)	Major Principal Stress at failure (kPa)	Failure Deviator Stress (kPa)	Deviator Stress Ratio (%)	Deviator Stress Ratio Stresses (kPa)	Major Principal Stress s1 for DSR (kPa)	Force of Major Principal Stress (kN)	Seating Load (kN)	Adjusted Force of Major Principal Stress (kN)
50	1302	1252	10	125	175	2.272	0.400	2.672
			20	250	300	4.544		4.944
			30	376	426	6.816		7.216
			40	501	551	9.088		9.488
100	1532	1432	10	143	243	2.598		2.998
			20	286	386	5.197		5.597
			30	430	530	7.796		8.196
			40	573	673	10.395		10.795
150	1762	1612	10	161	311	2.923		3.325
			20	322	472	5.850		6.250
			30	484	634	8.775		9.175
			40	645	795	11.701		12.101
200	1992	1792	10	179	379	3.251		3.651
			20	358	558	6.503		6.903
			30	538	738	9.755		10.155
			40	717	917	13.007		13.407

Table 10 Profile loads for MTS dynamic triaxial testing

3.4.6 Processing data

The main purpose of the dynamic triaxial test is to calculate the Resilient Modulus (Mr) at different confining pressures and compare it with the bulk stresses (θ). With the comparison, it is possible to determine if the load spreading within the layer is adequate or not. For each confining pressure, and at each deviator stress ratio at the respective confining pressure, 100 load cycles were applied. For every 100 cycles, only the last five cycle's data will be used for calculation. It is believed that during the first 95 cycles the Specimen is still stabilizing or settling, thus it would not give accurate and representative results.

Every 5 cycles would result in a set of roughly 2500 data points, due to the MTS taking measurements almost every 0.02 seconds. Each test produces the following test results:

- Axial Force (kN)
- Axial Length (mm)
- Axial Count Cycles (unitless)
- Time (sec), and
- Axial LVDT 1-3 (mm)

For each LVDT sensor, the strain should be calculated using the equation shown below. This equation takes into account the maximum difference in displacement measured over the middle third length of the Specimen. It is believed that in the middle third of a triaxial Specimens the most bulging occurs due to the 2:1 height to diameter ratio. The strain values are calculated for each cycle, resulting in five strain readings for each LVDT sensor per test. With the 5 strain readings, an average strain value can be calculated for each

$$Strain_{LVDT} = \frac{Displacement_{MAX} - Displacement_{min}}{L_{LVDT}}$$

Where

$Strain_{LVDT}$	Strain value for each respective LVDT
$Displacement_{MAX}$	Maximum displacement for respective LVDT,
$Displacement_{IN}$	Minimum displacement for respective LVDT, and
L_{LVDT}	Total length of the LVDT gauge.

With the strain values quantified, the applied cyclic stress can be calculated for each DSR at each confinement pressure. The cyclic stress is needed as the Resilient Modulus is measured by dividing stress by strain. To determine the cyclic stress (σ_{cyclic}), it is necessary to determine the cyclic load (P_{cyclic}) for each cyclic within the 'last five' data set. Each cyclic load can be calculated by subtracting the contact load ($P_{contact}$) from the maximum applied load (P_{max}) observed for each cycle. With both the cyclic load and strain calculated, each LVDT's Resilient Modulus can be determined. To take account of any variability that could exist within the transducer readings, it was decided that 4 average moduli will be calculated for every 5 cycles, namely: {1;2;3}, {1;2}, {1;3}, and {2;3}. Thus if any unusual data is produced, the averages would normalize the data. A summation of the whole procedure is displayed in Figure 31 below. These average resilient moduli are compared to the Resilient Modulus calculated by the actuator displacements. The actuator

measures the displacement over the entire length of the Specimen (i.e. 300 mm) whereas the transducers measure the displacements at the section where most bulging occurs (i.e. middle 100 mm).

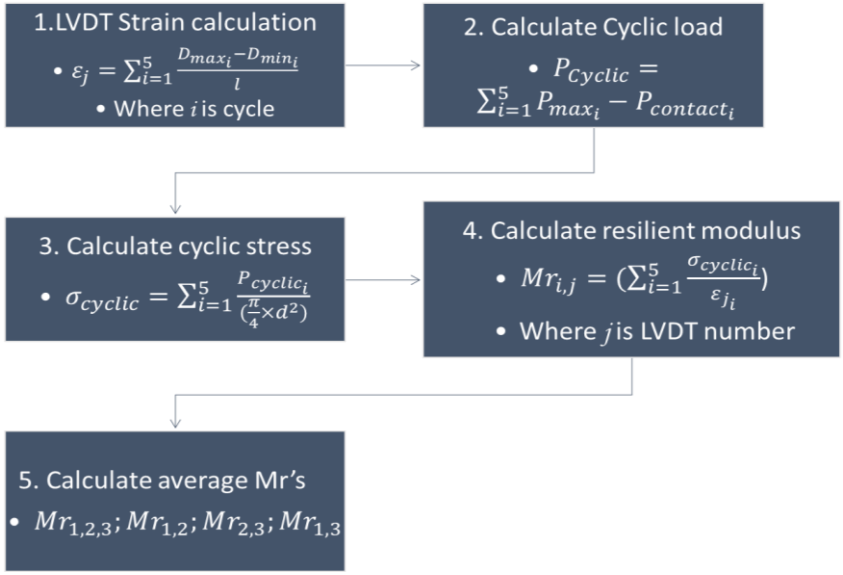

Figure 31 Data processing procedure for Resilient Modulus calculation.

3.4.7 Models for Resilient Modulus

With the processed data it is possible to analyse the different resilient moduli that were determined for various confining pressures at increasing deviator stress ratios. While modelling the data, it will be possible to determine what the stress dependencies will be for Mr. van Niekerk and Huurman (1995) have created a wide variety of models to determine the stress dependencies.

Model Number	Model name	Equation
1	Mr-θ	$Mr=k_1\theta^{k2}$
2	Mr-σ_d-σ_3	$Mr=k_1\sigma_3^{k2}\sigma_d^{k3}$
3	Parabolic Mr-σ_3-σ_d	$Mr=k_1\sigma_3^{k2}(-k_3(\sigma_d/\sigma_{d,f})^2+k_4(\sigma_d/\sigma_{d,f})+k_5$
4	Mr-θ-$\sigma_d/\sigma_{d,f}$	$Mr=k_1\theta^{k2}(1-k_3(\sigma_d/\sigma_{d,f})^{k4})$
5	Mr-σ_3-$\sigma_d/\sigma_{d,f}$	$Mr=k_1\sigma_3^{k2}(1-k_3(\sigma_d/\sigma_{d,f})^{k4})$
6	Mr-σ_3-$\sigma_1/\sigma_{1,f}$	$Mr=k_1\sigma_3^{k2}(1-k_3(\sigma_1/\sigma_{1,f})^{k4})$
7	Mr-θ-$\sigma_1/\sigma_{1,f}$	$Mr=k_1\theta^{k2}(1-k_3(\sigma_1/\sigma_{1,f})^{k4})$

Where

Mr	Resilient Modulus of the layer (MPa),
σ_3	Minor principal stress in the layer (kPa),
σ_1	Major principal stress in the layer (kPa),
σ_d	Deviator stress [σ_1-σ_3] (kPa),
$\sigma_{d,\,f}$	Deviator stress at failure [$\sigma_{1,\,f} - \sigma_3$] (kPa),
$\sigma_{1,\,f}$	Major principal stress at failure (kPa),
θ	Bulk stress [$\sigma_1+\sigma_2+\sigma_3$] (kPa),
k_1, k_3, k_5	Regression coefficients (MPa), and
k_2, k_4	Regression coefficients (unitless).

From the seven models stated above, it is possible to determine which of the factors such as confinement stress, bulk stress, deviator stress ratios or principal stress ratios has the biggest impact on the resilient moduli of the material. Jenkins (2000) explained that Model 6 was created by van Niekerk and Huurman (1995) to take account of the decrease in the Resilient Modulus as the critical value for the $\sigma_1/\sigma_{1,\,f}$ is reached. Models 4, 5, and 7 are also produced in the same manner but consider other variables such as deviator stress ratio or bulk stress. The processed data will be iterated through all the resilient moduli models and compared to determine which model best describes the resilient response of a bitumen emulsion stabilized mine haul road.

However, when trying to plot these models with the raw data, it can be noticed that when fitting a linear regression line would result in an average to very poor correlation coefficient (R^2) value. Using a non-linear regression function combined with an excel solver function, it is possible to normalize or smooth out the data. The method works by getting an average for all the raw Mr data and also an average for all the calculated Mr data using any given model. The difference between these two values is squared and set to a minimum within the solver function to calculate the normalized data. While the solver function is trying to determine the smallest squared difference between the averages, it is iterating through the different regression values to find the 'best fit' values.

3.5 Marvil permeability test

The Marvil permeability test, according to SANS (2012), is a water permeability test that is performed on-site on bituminous material. The water permeability is being tested through the principal of falling head permeameter. SANS (2012) also stated that with the Marvil permeability test, it is possible to determine the interconnectivity of voids in a bituminous material or to what extend the material would display moisture- and oxygen susceptibility. Although not part of the original test procedure, the Marvil permeability test can also be used to comment on the relative compaction of a layer. From the Kanshanshi mine, two Specimens were identified for permeability testing, i.e. Specimen 2 and 4. Both of these Specimen were tested with- and without the thin waterproofing layer on top of the specimens.

3.5.1 Apparatus

This Marvil test apparatus list will include all the standard equipment specified by SANS (2012), but also the modified equipment, explained by Annadale (2012) and Venter (2019), used to perform the Marvil test in a laboratory.

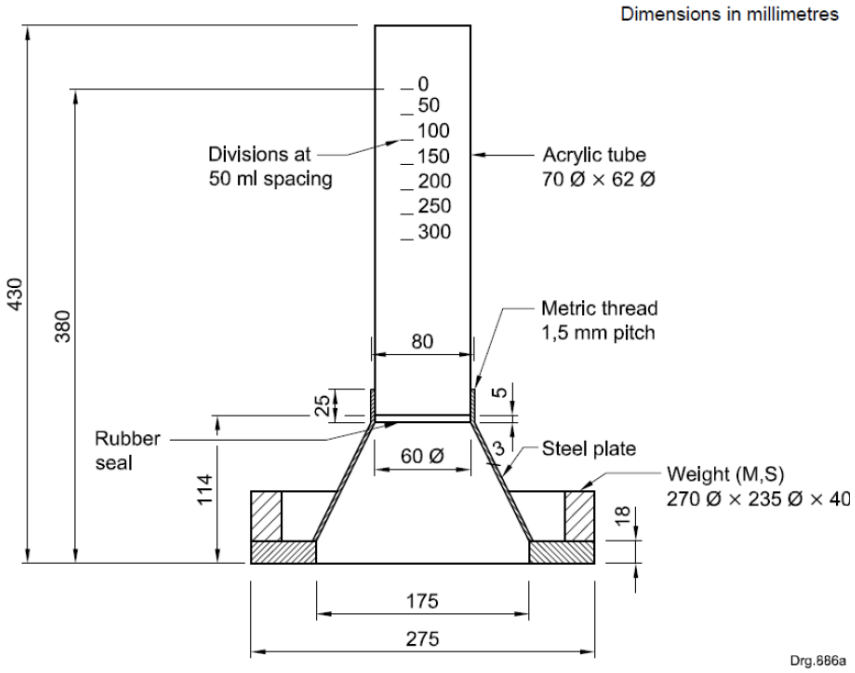

Figure 32 Marvil permeameter (from Venter, 2019)).

1. Marvil Permeameter

The Marvil permeameter consists of a corrosion-resistant steel plate with an outer diameter of 275 mm and an inner diameter of 235 mm. Attached to the steel plate is a corrosion-resistant conical base with a top radius of 60 mm. This is to allow for the installation of the acrylic tube used to observe the volume markings. The acrylic has an outer- and inner diameter of 70 mm and 62 mm respectively. the tube has volume markings inscribed from 0 mm to 600 mm (with 50 mm increments). Figure 32 illustrates the cross-sectional layout of the Marvil permeameter with dimensions included.

2. Adapter plate

The marvil test comes standard with a circular base weight intended to keep the permeameter on the ground. For laboratory use, the circular plate will be used as an adapter plate between the permeameter and silicone mould used to keep the Specimen in place. The circular plate also contains non-corrosive steel and has an outer- and inner diameter of 270 mm and 235 mm respectively. The specifications are also included in Figure 32.

3. Silicone mould

The silicone mould was designed by (Venter, 2019) for cylindrical Specimens to be tested in the laboratory. Previous designs, such as Annadale (2012) and SANS (2012), used a sealing approach on in-situ seals or square seal Specimens. This method worked as the Specimens were always larger than the permeameter's base. The silicone base incorporates the necessary seal to avoid water loss but also allows for the use of a circular Specimen, and Specimens smaller than the permeameter itself. Figure 33 (a) indicates the the design phase of the mould, whereas b indicates the finalied silicone mould.

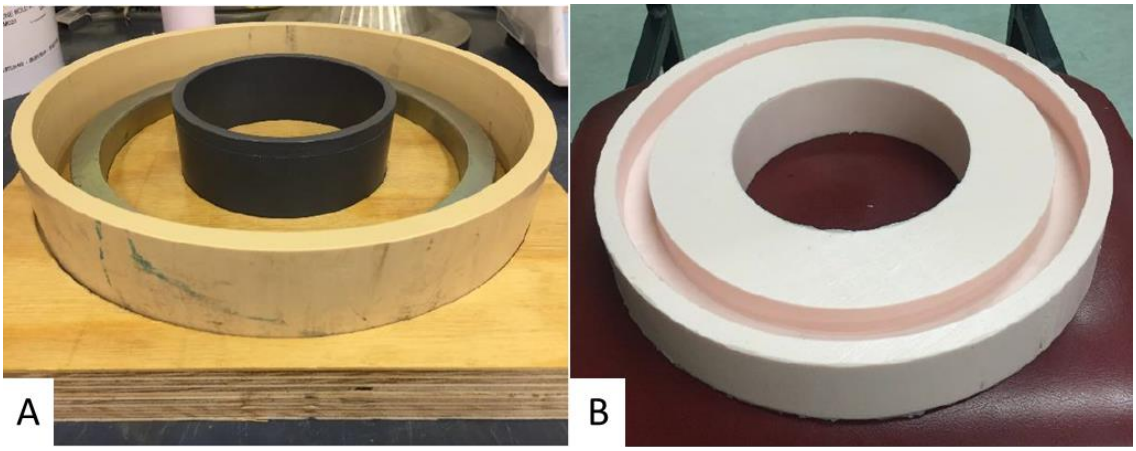

Figure 33 Marvil mould design (a), and final silicone mould (b),

4. Latex membranes

A latex membrane is required to enclose the Specimen to ensure that no moisture is allowed to pass through on the side of the Specimen. It is also to ensure that water only flows through the top of the Specimen. The procedure to create a latex membrane will be discussed in the section below.

5. Rectangular sponge

A piece of square or rectangular sponge is required to balance the Specimen within the silicone mould. Without the reinforcement of the sponge, sagging of the Specimen can occur. This will result in water seeping through on the sides of the Specimen and the silicone mould which would result in inaccurate results. The piece of sponge should be preferably bigger than the cored Specimen.

6. 270 mm diameter steel clamp

According to the updated marvil testing procedure stated by Annadale (2012) and Venter (2019), a circular clamp is required to create a seal between the marvil permeameter and the adapter plate. This is to ensure that no movement occurs between the seal created between the permeameter and the adapter plate.

7. Sealant

An impermeable sealant is required to create a seal between the permeameter and the adapter plate, and also the adapter plate and the silicone mould. The sealant used can vary from all-purpose grease to Bostik power Matic to bentonite clay(Annadale, 2012; SANS, 2012; Venter, 2019).

3.5.2 Latex membrane production

According to the methods used by Annadale (2012) and Venter (2019), to create a latex membrane a PVC pipe that is 75 mm in diameter is submerged in liquid latex. After the entire pipe is covered in liquid latex, the pipe is hung vertically to dry enough until it could be submerged again. The liquid latex is not viscous enough to ensure no movement and thus would result in the formation of an improper membrane. The top sections would be thinner and the bottom sections thicker. This resulted in the creation of a new horizontal membrane machine.

From the photo above, it can be observed that the liquid latex mixture is suspended below the pipe on a round surface. The pipe is connected to a system of gears which allows the pipe to rotate at variable speeds controlled by the variable speed controller. Also, another switch allows the pipe to move in two separate directions, namely forward and backwards, if necessary. With the pipe rotating, the suspended liquid can be raised using the level to provide an even coat on the surface of the pipe. The liquid is lowered again and the latex covered pipe is allowed to dry for some time until the surface is dry. This process is repeated until approximately eight to ten layers of latex are built up onto the pipe.

To remove the membrane from the PVC pipe, a powdery substance is used to cover the surface area of the membrane. This is done to ensure that the membrane does not stick to itself during the removal process. Once the powder is applied, the membrane can be removed by rolling the membrane off the pipe from the right edge. The large membrane can be divided into smaller lengths that can be used to cover individual Specimens.

3.5.3 Test procedure

To start the procedure, find a flat stable surface preferably close to a water source. Otherwise, water will have to be carried towards the Marvil apparatus while filling with water which could result in excessive soaking of the Specimen. Place the top-open ended base structure with the accompanying sponge on the flat surface. With the base structure in place, the Specimen can be prepared for testing. Cover the Specimen with two latex membranes. Ensure that the membrane covers as little as possible of the top surface area of the Specimen to ensure that the test uses as much of the surface area as possible. With the membranes in place, the Specimen can be fitted into the silicone mould. Whilst fitting the mould, ensure that there is little to no disturbance in the placement of the latex membranes.

With the membrane tightly in place within the silicone mould, place the assembled mould on top of the base. With the mould in position, gently press down on the Specimen that is resting on top of the sponge. This is to ensure that a level surface can be achieved and water does not irregularly flow away or towards the Specimen's surface. Fill the outer indentation of the mould with a sufficient amount of grease, while also applying grease to the bottom edge of the adapter plate. Slide the adapter plate into the greased groove. This will result in a tighter seal around the Specimen to ensure no water leakage around the sides. Make sure to remove excess grease with the mould which could result in the contamination of the Specimen. Apply a generous layer of power mastic to the top edge of the adapter plate[8]. Place the Marvil permeameter on top of the layer power mastic and allow it to naturally settle and allow the power mastic to spread of the surface area of the adapter plate's top edge. Apply the steel clamp around the adapter plate and Marvil permeameter and tighten to create an airlock and to ensure that the permeameter does not slide around on the adapter plate.

[8] Previous tests performed by (Venter, 2019) used grease to seal the top edge of the adapter plate. However, during preliminary tests, it was found that the grease sometimes did not provide an adequate seal, thus power mastic was used. Power mastic provides a good water repellent seal while also remaining wet, and also provides more resistance towards upward lift forces cause by the water pressure.

3.5.4 Test conditions

Once the test apparatus has been completely assembled, the test procedure can be commenced. It can be advised that a non-permeable Specimen can be used for the first test. This is to ensure that no water leakage occurs between the membranes or the silicone mould. Once it has been determined that no water leakage occurs, the Specimen can be inserted and the permeameter can be filled up with the water until the '0 ml' mark is reached. This water level should be maintained for the first five minutes of the test. The water level is maintained to ensure that the Specimen is sufficiently saturated before testing commences. For accurate time measurements, a stopwatch was used.

Once the initial 5-minute saturation period has passed, refill the permeameter to the 0 ml mark and reset the timer. During this time no additional water will be added again. Record the time that passes when the water reaches the lower volume indicators on the clear Perspex pipe (i.e. the 50ml, 100 ml, 150ml, etc.) until the water level reaches the 600 ml mark. If the water level does not reach the 600 ml mark before two hours have passed, the test can be suspended as stated by Venter (2019). Other variations of this test method performed by Annadale (2012) only recorded the time it took the permeameter to reach the 300 ml mark. For the alternative test method, the time limit was also set as 2 hours, but only for materials that do not reach the 50 ml mark. If the test method reached the mark after 2 hours, the test was extended for another hour. Since both these methods focused mostly on seals, a new alternative was created between these two methods that would apply to BSM materials. The tests were conducted until the 300 ml mark was reached or until the period of 2 hours was reached.

Once the applicable conditions were met, the test could be finalized and the water could be removed by a drainage pipe or by tilting the permeameter on its side. With all the water removed, the apparatus can be disassembled. Remove the membranes from the Specimen and leave them to dry out. Also, ensure that all necessary surfaces are cleaned and degreased before a new test is conducted.

3.5.5 Calculations

According to (SANS, 2012) there are three categories in which the data can be grouped and processed, namely: low permeability, moderate permeability, and high permeability. If during a test, the permeameter fails to reach the 50 ml mark within two hours, the material is classified as low permeability and no calculations are required. For low permeability materials, the flow can be indicated as < 1L/h.

For moderately permeable materials, the equation below should be used to calculate the flow rate. This equation can be used for any Specimen that passes the 50 ml watermark.

$$P_M = 3.6 \times \frac{V_W}{t}$$

Where
P_M |Marvil permeability rate (litres per hour),
V_W |Volume of water (ml), and
t |Time taken to reach specific volume mark (sec).

Annadale (2012) also stated in his alternative method that the low permeability could be measured to provide some insight into the rate of permeability within a type of material. For this method, a ruler can be used to measure smaller changes in volume between the 50 ml increments. Using the height to volume conversion equation below, the differences in height can be converted into changes in the amount of water. This method can accurately measure the change in water with a ± 3 ml tolerance.

$$V = \frac{\pi \times h \times r^2}{1000}$$

Where
V |Volume of water (ml),
h |Height measurement (mm), and
r |Inner radius of the permeameter tube (mm).

For high permeability materials, the same calculations can be used that determine the flow rate for moderately permeable materials. When all the calculations have been completed, each Specimen can be assigned a permeability classification. The classification table is originally developed by

SANS (2012) but was updated by Annadale (2012) to include two extra classification categories as shown in the table below.

Table 11 Permeability classifications (adapted from Annandale (2012)).

Permeability classification	Water level reached on permeameter
High	150 ml reached after 3 minutes
Moderate	50-150 ml reached after 3 minutes
Low	<50 ml after 3 minutes, but reached 150 ml after 2 hours
Very Low	<50 ml after 3 minutes, but in between 50-150 ml after 2 hours
Impermeable	Between 0-50 ml after 2 hours

3.6 Binder Recovery

After all major testing procedures have been completed, it is necessary to segregate the bitumen from the material. From the divided specimens, it is possible to further analyse the virgin aggregate to determine characterising properties such as grading, etc. This test procedure can also be useful in other aspects, such as analysing the bitumen used within the BSM blend through tests such as the Dynamic Shear Rheometer (DSR), Bending Beam Rheometer (BBR).

Tredoux (2020) and Goosen (2021) defined the three stages applicable to binder recovery which are *a)* Extraction of bitumen from solvent, *b)* removal of aggregate from the solvent mix, and *c)* recovery of bitumen from the solvent mixture. To perform the extraction as stated in *a)* the material is soaked in a mixture of extraction solvents. Once the material has soaked sufficiently, a centrifuge with accompanying sieves are used to segregate the aggregate from the bitumen solvent mixture. For the final step, the bitumen is separated from the solvent mixture through distillation.

3.6.1 Apparatus

This test consists will making use of different machines and thus have different requirements and smaller apparatus. This section will discuss this in-depth and give sufficient background.

1. Plastic buckets

For the binder extraction stated in part *a)*, a minimum of three to four plastic buckets with lids will be required. One bucket is used to soak the Specimen with the desired solvent. The other three buckets are used during the separation phase in the centrifuge machine as the binder-solvent mixture holder. It is stated that the binder-solvent mixture is put through the centrifuge a minimum of three times to ensure all the fines are removed from the solvent mixture(Tredoux, 2020; Goosen, 2021).

2. Grading sieves

To perform the separation of the aggregate and solvent mixture, a collection of sieves (the 10 mm, 2 mm, 0.075 mm, and 0.063 mm) are used to easily separate the material from the binder. During this process, the aggregate can also be rinsed with extra solvent to ensure that most of the bitumen is removed.

3. Solvent

For the extraction solvent, a mixture of Toluene (C_7H_8) and Ethanol (known as C_2H_6O or C_2H_5OH) with a ratio of 15:85 respectively. In previous versions of this test, 100% Toluene was used for the extraction and separation. This was due to the fact the Toluene was a non-corrosive chemical with no severe health threats and could be found readily available. However, previous studies completed by De Jonghe *et al.* (2005) indicated that the pure Toluene tended to cause an explosion due to its volatility. Tredoux (2020) recognized this issue and used Trichloroethylene (C_2HCL_3) as the preferred solvent.

4. Centrifuge

A centrifuge is required to separate the fines from the binder-solvent mixture. This process works by rotating a metal cup at a high angular speed. This procedure imposes a strong outward centrifugal force pushing the solvent out of the metal holder and leaving behind the fine materials. Figure 34 indicates the standard setup for binder extraction with the accompanying sieves.

Figure 34 Centrifuge used for binder extraction.

5. Rotary Evaporator

To recover the bitumen from the solvent mixture, a distil is required. CSIR has identified two methods that can be used for binder recovery, namely: Abson and Rotary Evaporator(Mturi *et al.*, 2015). For this test, only the rotary evaporator was available to perform the test. Figure 35 displays a diagram of the rotary evaporator and well as descriptions indicating the parts. The rotary evaporator operates by heating the bitumen-solvent mixture in an oil bath, which creates vapours. The

vapours condense in the condenser chamber through a decrease in atmospheric pressure, leaving behind the bitumen in the rotating evaporating flask.

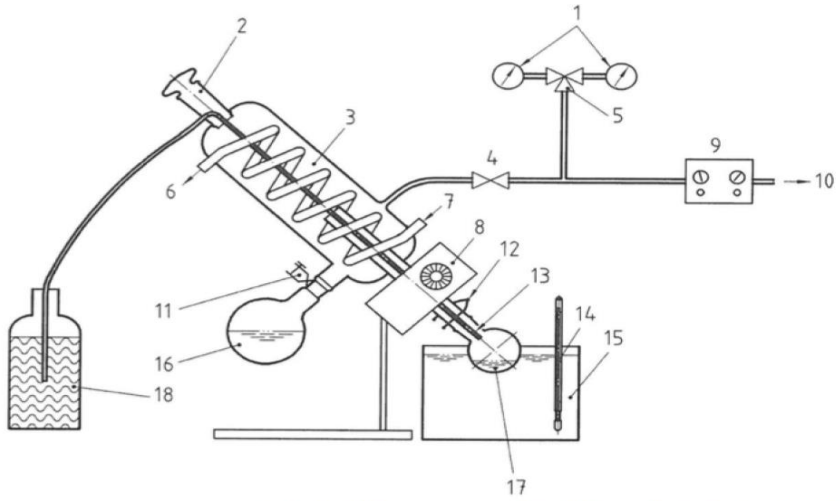

Figure 35 Schematic of the rotary evaporator (adapted from Goosen (2021)).

6. General Safety equipment

Since the binder recovery method makes use of strong chemicals, general health and safety protection wear are required, such as safety goggles, gloves, laboratory coat, and respirator.

7. Forced Draft Drying oven

A continuous forced-draft drying oven that can maintain temperatures of 150±1 ºC. The oven should also be thermostatically controlled and be able to take at least 240 litres of material.

3.6.2 Testing procedure

The following test procedure was completed following the standards stipulated by (SANS 3001 (2011) and EN-12697-3 (2013). Initially, each plastic bucket was weighed to determine its mass. The mass was written on each bucket as this made the procedure easier in terms of weighing specimens. Each Specimen was weighed in their respective plastic bucket and Trichloroethylene solvent was added until the material was completed saturated. SANS 3001 (2011) also specified that

enough solvent should be added to the material to ensure that the mixture has a binder concentration of less than 3 %. The equation stated below can be used to estimate the amount of solvent that should be added to a Specimen.

$$V_S = \frac{M \times S_E}{3}$$

Where
V_S |Volume of solvent that should be added to the material (ml),
M |Mass of the Specimen being used (g), and
S_E |Estimation of the amount of bitumen within the material (%).

The period that each Specimen should soak is dependent on the standard being followed. SANS 3001 (2011) states that a soaking period of 20 to 60 minutes should be followed. During this period the material should be slightly agitated to ensure that the larger stones segregate from the fine- and bituminous material(Goosen, 2021). However, EN-12697-3 (2013) and Tredoux, (2020) insists that 24 hours is used to soak the Specimen to ensure sufficient time for the solvent to remove all the bitumen from the material. Mturi *et al.* (2015) agrees with SANS 3001 (2011) and Goosen (2021) and states the complete process (including soaking, agitation, aggregate separation and binder removal) should not exceed 8 hours. Since the purpose of this test procedure was to extract the virgin aggregate from the bitumen to further analyse, it was deemed acceptable that a 24 hour soaking period was used.

Once the material has soaked for a sufficient amount of time, the extraction process can be initiated. Before the extraction process can be initiated, the material should be agitated once more, since the bitumen tends to harden when split from the aggregate. Start the extraction process by adding small amounts of the solvent- aggregate mixture onto the grading sieves. Add clean solvent using laboratory wash bottles, as shown in Figure 36, and disturb further with hands to ensure that the material is clean for removal. This process can be repeated more than once to ensure that approximately all the bitumen is removed. If the material left behind on each sieve was rinsed, the material can be emptied into a bowl for drying.

Figure 36 a) Agitation and b) washing of the mixture during extraction process.

After all the material has been rinsed and removed from the sieves, the second stage of the extraction process can begin by recycling the bitumen- solvent mixture through the centrifuge to remove any excess fines that may still be trapped within the mixture.

After the mixture has been recycled through the centrifuge approximately 3 times, the solvent can be added to the bitumen extraction plant as shown in Figure 37 below. The apparatus used below is a variant of the rotary evaporator called the Heidolph Laborota 4003. Under normal conditions, the rotary evaporator will spin the flask holding the mixture at 75 revolutions per minute (rpm) in an oil bath with a temperature of 110 ºC. This is to ensure that all the solvent can evaporate without causing the bitumen to bubble which can result in a loss of bitumen. The temperature is also chosen as 110 ºC to prevent the bitumen from artificially ageing. Since the test is only performed to determine the percentage of bitumen, the temperature can be increased to 180 ºC with great caution.

Figure 37 Rotary Evaporator used for binder extraction.

3.6.3 Calculations

For the entire binder recovery procedure, a small calculation process is used to determine the amount of binder that was recovered as well as the percentage loss of total material. The percentage loss of material is calculated to ensure that as little as possible material has been lost due to unforeseen error or negligence. To calculate the percentage loss within the system, the equation below can be used. A percentage of less than 5 % loss was deemed acceptable.

$$L_{\%} = \frac{M_i - [\sum_{n=1}^{3}(M_{k_n} - M_{j_n}) + (B_k - B_j)]}{100}$$

Where

$L_{\%}$ |Percentage loss from start to finish of the recovery cycle (%),
M_i |Mass of the sample before testing (g),
M_k |Mass of the container with the material after drying (g),
M_j |Mass of the container only (g),
n |Number of different containers used,
B_k |Flask with recovered binder weight (g), and
B_j |Flask weight only (g).

However, to calculate the amount of binder that was recovered from the sample, the equation below can be used.

$$B_{\%} = \frac{B_k - B_j}{M_i} \times 100$$

Where
M_i |Mass of the sample before testing (g),
B_k |Flask with recovered binder weight (g), and
B_j |Flask weight only (g).

3.7 Sieve analysis

The dry and wet sieving methods are used for the sieving of aggregates for BSM. The reason is that the P0.075 fraction is extremely important for foamed bitumen and emulsion. According to SANS (2013) with the grading analysis results, it is also possible to determine a material's design equivalent material class. Also, this test procedure determines whether the aggregate conforms to the standards set out for particle size distribution for certain material types. The grading analysis test can also be used to discover different connections between the particle size distributions and the packing of the material (in terms of compaction), the interlocking ability (in terms of densification), and the blending of the material. The testing procedure, as well as the calculations, are discussed in depth in Appendix B.

3.8 Atterberg Limits and Linear shrinkage

The Atterberg limit test is performed to give a good indication of the materials performance characteristics and can also be used to classify a specific material(Asphalt Academy, 2009). The Atterberg limit tests include a plastic limit (PL)- and liquid limit (LL) test. Both of these tests provide a good indication of the plasticity that can be expected within the material. With the PL and LL, the plasticity index (PI) can be calculated using the equation below. With the PI value, it is possible to provide a range of moisture contents at which this material type would remain in a plastic state. Linear shrinkage (LS) is also a good indicator of materials at which it would remain plastic at certain moisture conditions. According to Asphalt Academy (2009), linear shrinkage outweighs

the plasticity index in terms of its ability to accurately represent the materials shear strength performance under the influence of water.

$$PI = LL - PL$$

Where
PI |Plastic Index,
LL |Liquid limit of soil, and
PL |Plastic limit of soil (%).

The liquid –and plastic limit test procedures were followed per the specification set out by the TMH1 document (method A2 and A3).

3.9 Flakiness index

The flakiness index is a test procedure that measures the mass of coarse aggregate that passes a specific slot or slots. These slots have a specified width which is stipulated by its representative fraction size and is displayed in Table 12 below. As seen in the table, each slot width is approximately half of the width of the sieve openings through which the material fraction passed(TMH1, 1989).

Table 12 Slot sizes concerning fraction sizes (adapted from TMH1, 1989).

Size of the fraction to be gauged (Sieve size in mm)		Minimum length of slot (mm)	Width of slot (0.10 mm tolerance)
Passing	Retained		
75	63	150	37.5
63	53	126	31.5
53	37.5	106	26.5
37.5	26.5	75	18.75
26.5	19	53	13.25
19	13.2	38	9.5
13.2	9.5	26.4	6.6
9.5	6.7	19	4.75
6.7	4.75	13.4	3.35

3.9.1 Apparatus

1. Metal gauge

A metal sheet that is approximately 1,6 mm thick is required to be used for the flakiness index gauge. The sheet should include the necessary slots for each fraction included in the test method as indicated in Table 12. It should be specified that the grading fractions refer to the aggregate the passed the specific sieve (on the left) but was retained on the other sieve (right column). The manual method can also be substituted for a flakiness index machine.

2. Balance

A balance is required to weigh the material. The balance should be able to carry a mass of up to 4 kg, but also be accurate to 1 gram.

3. Test sieves

200 mm Test sieves are required to complete the sieving process. These sieves must conform to the standards specified by SABS 197. The required sieves should have openings with the measurements specified in Table 12. TMH1 (1989) declared that the 4.75 mm sieve should be made out of wire mesh.

3.9.2 Test procedure

Before testing can start, all fractions passing the 5 mm sieve and retained on the 75 mm sieve should be discarded as it is not applicable in this test. To use the flakiness gauge, place it over a bucket or any type of holder on which it could rest. Start by passing the material through the biggest slot moving towards the smallest slot. Measure the mass of material that passes each slot and record it to the nearest 1 gram.

With the recorded masses, the flakiness index can be calculated using the equation below

$$FI = \frac{M_{PASSING}}{M_{TOT}} \times 100$$

Where
FI |Flakiness Index (recorded to the nearest 0.1 decimal),
$M_{PASSING}$ |Mass of material passing certain slots (g), and
M_{TOTAL} |Total mass of material (g).

3.10 Aggregate Crushing Value (ACV)

The Aggregate Crushing Value refers to a test that measures the number of fines that are produced when applying a steadily increasing load to an aggregate sample. The sample contains materials that pass the 13.2 mm sieve but is retained on the 9.5 mm sieve. The Specimen is placed under loading within a confined chamber to induce confining pressure(TMH1, 1986). The test apparatus and test procedure is further discussed in Appendix C.

3.11 Dynamic Indirect Tensile Test

The dynamic indirect tensile test works similarly to the dynamic triaxial test such that it produces resilient moduli data that can be used to assess the quality of material and produce input variables for pavement life calculation and evaluation. The values that are produced by the dynamic ITT is also a good indicator of the material's spread-ability in terms of load spreading. However, this test procedure does not focus on major principal stresses enforced on the top and bottom of the Specimen but applies the load indirectly similar to the indirect tensile strength test. Using these tests, variables such as temperature, loading rate, and rest periods can be evaluated as this is a non-destructive test(ASTM D4123, 1995).

3.11.1 Apparatus

This test procedure uses mostly the same equipment as stated in the indirect tensile strength test method, but with some small additions.

1. A compression testing machine

A machine capable of applying a compression force onto a Specimen at certain load pulses. These load pulses should be able to be exerted onto the Specimen over various frequencies, load durations and load levels. This compression machine should also be able to reach a maximum load of at least 30 kN. The machine should also be capable of measuring the displacements accurately to the closest 0.1 mm and applying load to the closest 0.05 kN.

2. ITT load frame

The ITT load frame consists of numerous parts that are linked together. Firstly, to keep the Specimen in place, two loading strips of 19 mm x 20 mm x 220 mm are required. For Specimen's that are 100 mm in diameter, the strips are changed to 12 mm x 20 mm x 220 mm loading strips. The surfaces of these loading strips exposed to the sample are slightly mechanically curved to a radius of 76 mm ± 1 mm. This is to provide a stable surface for the round edges of the specimens, as shown in Figure 38 below. These loading strips move towards each other on vertical frame guides. The vertical frame guides are made from 10 mm Ø mild steel rods that are 175 mm in height and are attached to a mild steel base plate.

The base plate can be shifted to align the Specimen with the Compression machine's loading rod. When looking at the load frame, it can be assumed that the bottom load strip is rigid, whereas the top load strip can move unobstructed vertically to accommodate the loading/displacement of the Specimen. Sabita (2020) also pointed out that there are extras that can be added to the loading frame such as load transfer plates, load cell and automatic data logger.

Figure 38 also illustrates the upper rectangular plate that is used to attach the horizontal LVDTs to the Specimen. The rectangular plate is fastened to the Specimen using screws and rubbers with flat surfaces. These rubbers grip onto the surfaces of the Specimen to ensure no movement of the frame with regards to the Specimen but also ensure that no damage is taken by the Specimen

Figure 38 Dynamic Tensile schematic.

3. Load transfer plate:

A load transfer plate can be added to the top-loading strip, as shown in Figure 38, to ensure that no deformation occurs when the load is being transferred from the compression testing machine to the top of the loading strip. The load transfer plate can be round, square, or a steel ball with a diameter of 19 mm. The dimensions of the load transfer plate should be slightly larger than the Specimen being tested. Sabita (2020) added that a ball bearing should not be used between the load transfer plate and the piston.

4. Drying oven

A continuous forced-draft drying oven that can maintain temperatures of 40±1 ºC. The oven should also be thermos-statically controlled and be able to take at least 240 litres of material.

5. Water bath

A water bath is needed that can hold water with a depth of at least 150 mm. The bath should also have a perforated bottom at a height of 25 mm. The water should stay constant at 25±1 ºC with the assistance of a thermostat controller and a circulation mechanism.

6. Digital thermometer

A digital thermometer was used to measure the internal temperature of the core with an accuracy of ±0.1 ºC.

7. Carrier plates

Carrier plates are made from plywood and are used to transport compacted specimens. They can be square or round with a thickness of approximately 15 mm

3.11.2 Test procedure

To start, each Specimen was individually marked and placed on top of a carrier plate. After being marked, each Specimen was placed inside a forced-draft oven at 40 ºC for 72 hours. After the desired period, the Specimens were weighed to determine any moisture loss. If the mass of each Specimen displayed a difference of more than 10 g, the Specimens were put back into the oven for another 24 hours. This cycle would continue until the Specimens reached a constant mass.

Williams (1969) stated in the Wirtgen laboratory handbook that accelerating the curing process by increasing the temperature is not advisable. For foam or emulsion specimens, the increase in temperature can cause bitumen particles to heat up beyond their respective softening points. This would ultimately lead to changes in the characteristics and behaviour of the stabilized material.

With all the Specimens at equilibrium moisture content after curing, the Specimens should be placed in a room or compartment and allowed to cool off to room temperature (25.0 ºC). For this test, the UTM test chamber was used for the cooling chamber. The UTM has a built-in compressor that is capable of maintaining a constant temperature over a long time. The UTM's chamber was also used as it would lead to less variation in temperature as Specimens would not have to be moved between areas. ASTM D4123 (1995) also mentions that unless the chamber's temperature is monitored or the Specimens temperature is known, the Specimen should stay in the chamber for 24 hours before testing. Once the Specimens have reached room temperature, their bulk densities must be calculated. This can be done by using the equation below.$BD_{specimen} = \frac{4 \times M_{specimen}}{\pi \times d^2 \times h} \times$

$$BD_{specimen} = \frac{4 \times M_{specimen}}{\pi \times d^2 \times h} \times 10^6$$

Where

$BD_{Specimen}$	|Bulk density of Specimen (kg/m^3),
$M_{Specimen}$	|Mass of Specimen (g),
H	|Average height of the Specimen (mm), and
D	|Average diameter of each Specimen (mm).

With all the necessary pre-test calculations have been completed, the Specimen can be placed onto the load frame. Ensure that the Specimen is centred within the load frame both vertically (y-axis), but also horizontally (x-axis) as shown in Figure 39. This is to ensure that the load is spread out evenly throughout the Specimen with no eccentricities. Once the Specimen is centred, tighten the load frame fasteners which holds the Specimen in place. Apply the horizontal measuring frame to the Specimen, ensure that the measuring frame is parallel with the Specimen, but is also placed in the middle of the Specimen. Figure 39 indicates the positions of the Specimen fasteners (which are two on each side of the Specimen) and the LVDTs with accompanying holding frame.

Figure 39 Positioning of the Specimen fasteners as well as the LVDTs and LVDT frame.

Once the Specimen is in place, preconditioning can occur. To precondition the specimens, a non-destructive force should be repeatedly applied to the Specimen in a haversine (or other) waveform. The non-destructive force should be applied until a uniform deformation observation can be made. ASTM D4123 (1995) specified that the loading is typically repeated for 50-200 cycles, depending on the temperature and loading frequency. The force applied in these cycles is usually between 10-50 % of the maximum tensile strength of the Specimen. The maximum tensile strength can be determined by completing a destructive ITS test. ASTM D4123 (1995) also mentions that if no tensile data is available, typical load ranges from 4-35 N/mm thickness of the core Specimens can be used. Since most Specimens that were provided, had irregular thicknesses, this load range series was used.

Since most Specimens displayed irregular surfaces, a conservative 4 N/mm thickness ratio was used. If the Specimen showed good promise, the force was increased by 300 N. During the test procedure, the horizontal and vertical displacement should be measured via LVDTs or vertical actuator displacements. If the vertical displacement exceeds 0.025 mm, the test should be ceased and the applied load should be lowered.

3.11.3 Calculations

During each dynamic tensile test, the average horizontal and vertical deformations that recovered should be observed for five loading cycles. The five cycles are usually taken as the last five cycles because at this point the repeated resilient deformation has stabilized. Furthermore, this meant that the resilient moduli had stabilized. The following set of equations can be used to calculate the resilient moduli (instantaneous and total) and resilient Poisson's ratio (instantaneous and total).

$$E_{RI} = \frac{P(\vartheta_{RI} + 0.27)}{t \times \Delta H_I}$$

$$E_{RT} = \frac{P(\vartheta_{RT} + 0.27)}{t \times \Delta H_T}$$

$$\vartheta_{RI} = \frac{3.59 \times \Delta H_I}{\Delta V_I} - 0.27$$

$$\vartheta_{RT} = \frac{3.59 \times \Delta H_T}{\Delta V_T} - 0.27$$

Where

E_{RI}	Instantaneous Resilient Modulus (MPa),
E_{RT}	Total Resilient Modulus (MPa),
υ_{RI}	Instantaneous Poisson's ratio,
υ_{RT}	Total Poisson's ratio,
t	Thickness of the Specimen (mm),
ΔH_I	Instantaneous recoverable horizontal deformation (mm),

ΔV_I |Instantaneous recoverable vertical deformation (mm),
ΔH_T |Total recoverable horizontal deformation (mm), and
ΔV_T |Total recoverable vertical deformation (mm).

3.12 Chapter Summary

This chapter presents the proposed experimental design used to determine the performance characteristics of bitumen stabilized material for mine haul roads. The first section of the experimental design included test methods used to determine a better understanding of the material's shear properties. These tests procedures include ITS_{dry} and ITS_{wet}, Monotonic Triaxial, Dynamic Triaxial, and Dynamic ITT. All tests were performed following the specifications set out by the TG2 Guidelines from Sabita (2020).

Furthermore, the next section discusses permeability testing. The purpose of the permeability testing is to provide insight into the feasibility of the dust-palliative layer which is applied to the base layer constantly. The Marvil Permeability test is discussed procedure is discussed according to the standards set out by in the SANS 3001 – BT12.

The final section in this chapter provides test procedures to determine the mix composition of the bitumen stabilized base and also provides an understanding of the virgin aggregates classification. In this section, the binder recovery method is discussed which provides results on the residual bitumen content (%) found within the mix design. Furthermore, this section discusses the Sieve analysis method, Atterberg limits and Linear shrinkage, Flakiness index, and ACV test.

4 Results

4.1 Introduction

This chapter provides an overview of the raw data collection through completing the testing procedures set out in chapter 3. Furthermore, this chapter will analyse the data and determine if there are any correlations between the structural capacity of road structures and the corresponding material properties. This chapter will firstly discuss and list the visual inspection results of the specimens provided. Secondly, this chapter will display and discuss all structural capacity results such as ITS, Monotonic- and Dynamic Triaxial, dynamic ITS, etc. Thirdly, this chapter will list the results obtained for the material property testing. With all the above-stated results, models will be created to determine any correlation between material performance and property classification.

4.2 Visual Inspection

Visual inspections were completed on all the mine haul roads independently seeing that all the mine haul road sections consist of different road structures and material characteristics. These mine haul roads also display different geometrical characteristics.

4.2.1 Kansanshi mine

For the Kansanshi mine, a ‘strip’ map was provided of the haul ramp as displayed in Figure 40. This map provided insight into the position of each core with relation to the ramp length (x-axis) and offset (y-axis). This map also provides the date on which each section was completed with the amount (in litres per square meter) of emulsion used. Figure 41 also provides insight into the section cross fall profile of the mine haul ramp. From Figure 40 it can be observed that Specimen 3 and 9 from this ramp already indicates problems. Patching has been reported on this section of the ramp and as seen on the strip map, minor amounts of the emulsion were mixed with the material, when compared to the adjacent sections.

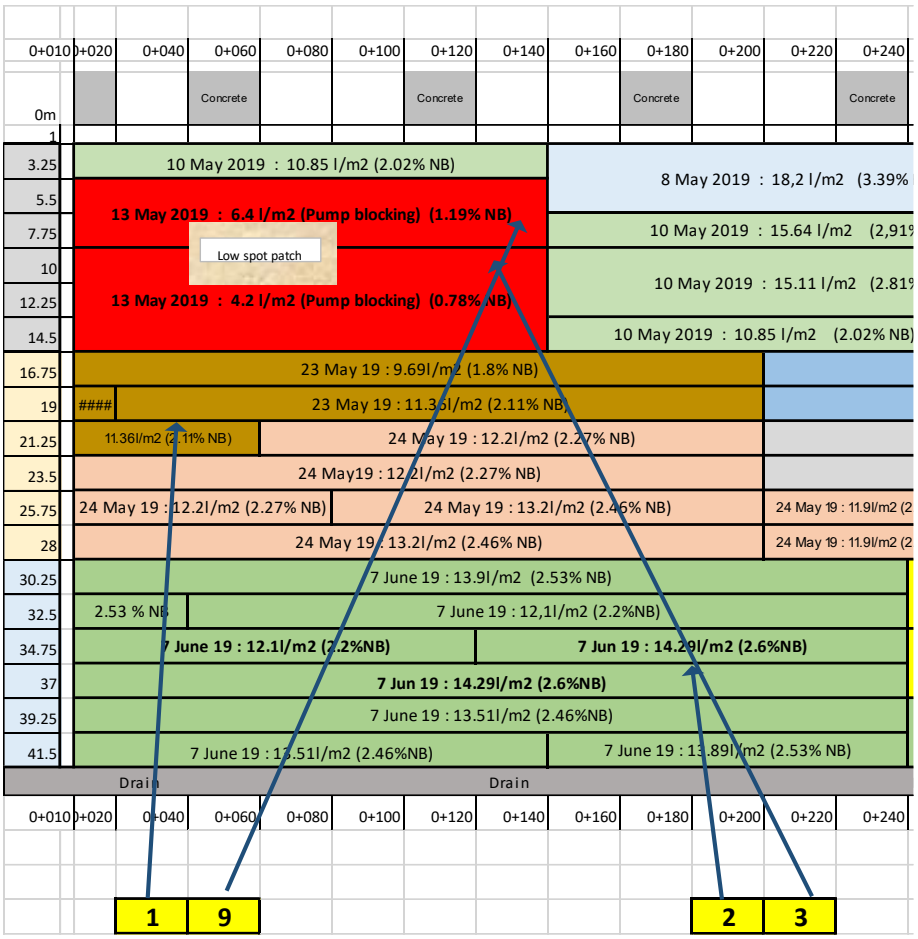

Figure 40 Strip map data for Kansanshi mine.

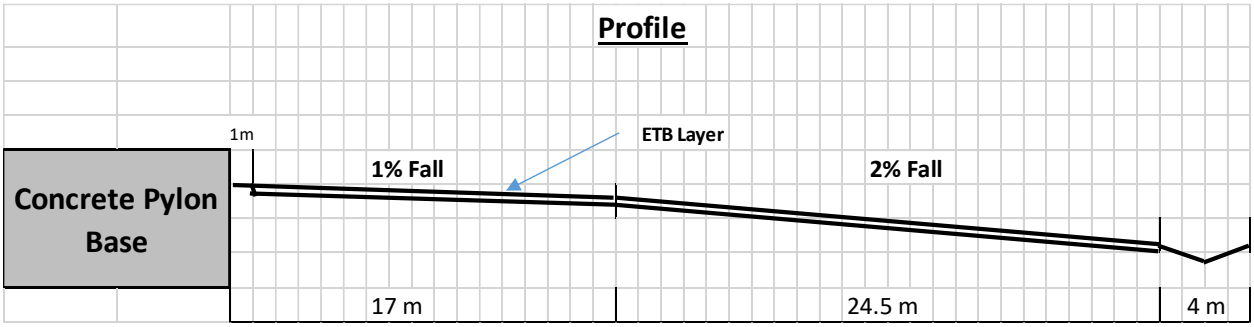

Figure 41 Cross sectional profile of Kansanshi ramp.

The lack of bitumen emulsion can also be observed in Specimen 3 and 9 that were provided. Both Specimens were cracked straight through the middle. Specimen 3 in Figure 42 displays clear signs of dust intrusion on the upper edge of the Specimen. Also, from both specimens, it is clear that there is a lack of binder to create cohesion, which would also result in fatigue cracking and premature failure. From Figure 42 it is also noticeable that a waterproofing layer was sprayed over the ramp. In some cases, the film thickness was measurable and was approximately 4 mm in thickness. This thickness would also vary depending on where each Specimen is located due to the cross falls on the ramp.

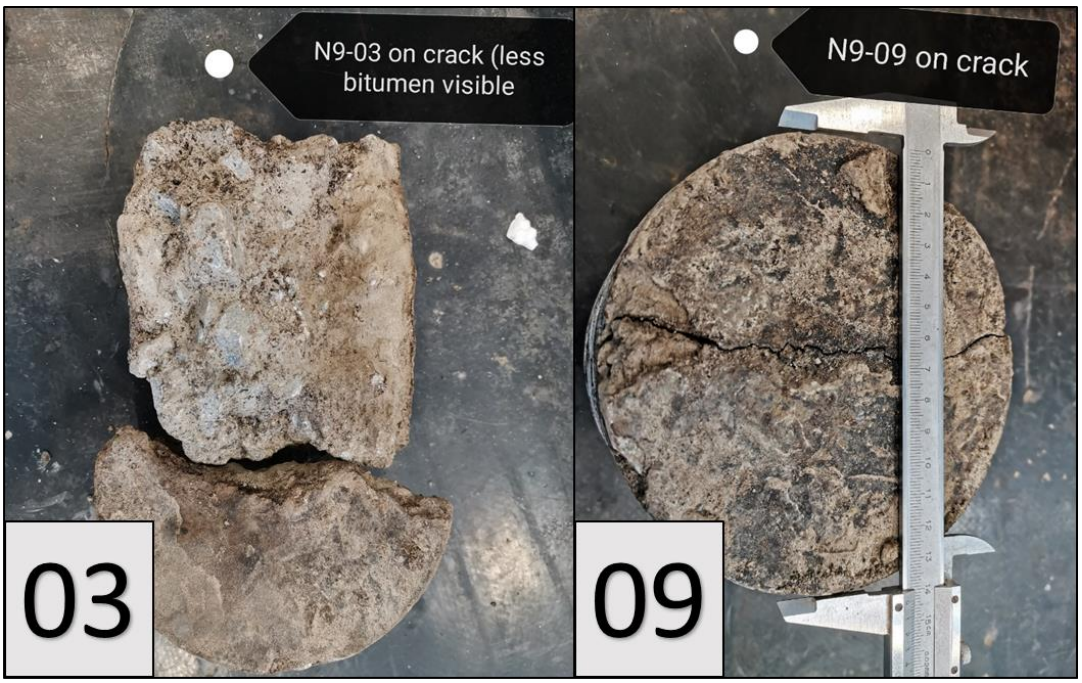

Figure 42 Specimen 3 and 9 core inspection.

Some Specimens also displayed signs of irregular aggregate fraction distributions. From Figure 43 it can be observed larger stones tend to lump at the bottom with smaller aggregate accompanied by fines. Initial assessment of all 9 Specimens from Kansanshi indicated variable layer height. Certain Specimens measured at 165 mm in height where others were measured at 100 mm. The material also seemed to be brittle as the slightest pressure would cause sections to chip off.

Figure 43 Irregular stone distribution in Kansanshi Specimen.

4.2.2 Kalumbila mine

For the Kalumbila ramp, no 'strip' map was provided to indicate which sections were completed on which day and also the amount of emulsion used (as there might be slight variations daily). However, from the information that was provided, as shown in Figure 44 and Figure 45, it is known that the Specimens provided originated from two different haul ramps. Specimen 1 to 4 originated from the East ramp and Specimens 5 to 8 originated from the West ramp. Both ramps have an approximate slope of 9.7 % and cross falls as indicated in Figure 45. According to the specifications provided by Kalumbila, trolley lane 1 (Specimens 1-4) consists of a 75 mm crushed rock layer followed by a 50 mm graded crushed stone layer and finished off with a 75 mm graded treated layer mixed with SS60 emulsion. This results in a layer height of 200 mm. On the 2nd trolley ramp (Specimens 5 to 8), Kalumbila specified that layer consists of 200 mm graded crushed rock where the top 26 mm is G1 and treated with SS60 emulsion.

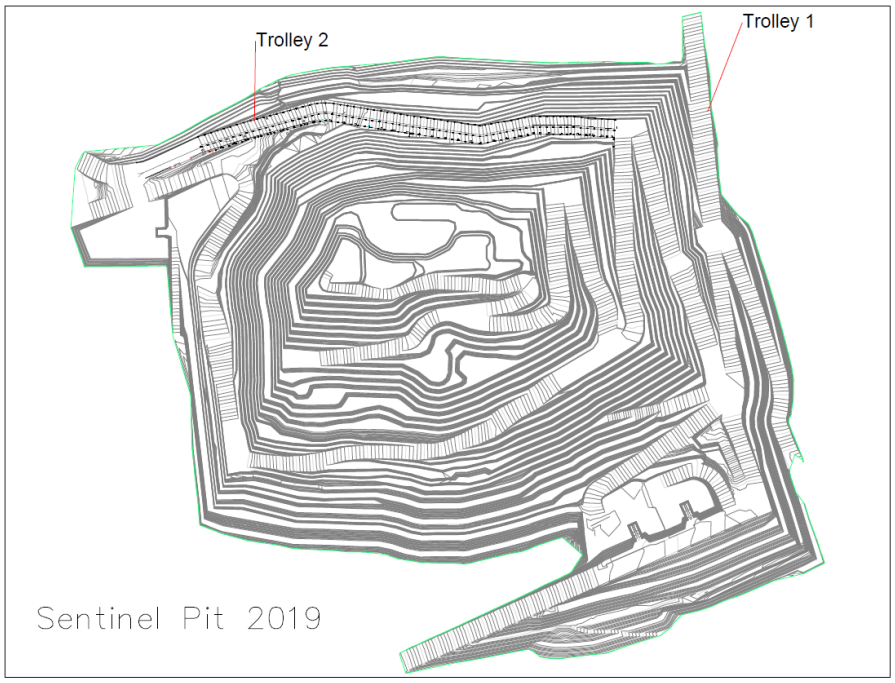

Figure 44 Topographic view of Trolley lane 1 & 2 from Kalumbila mine.

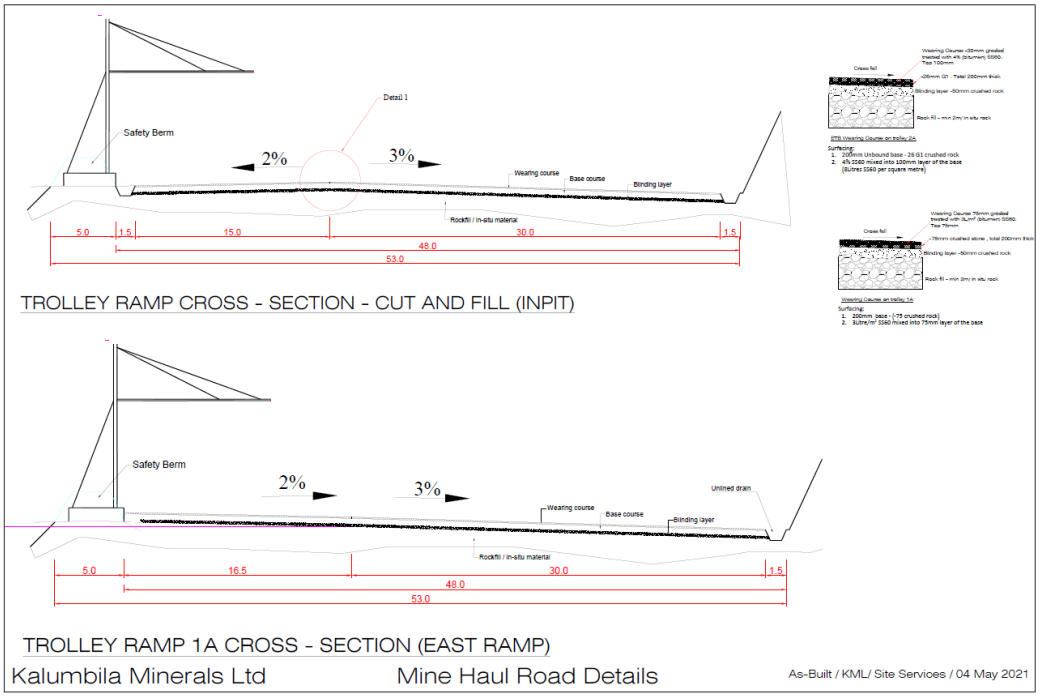

Figure 45 Cross Sectional view of Trolley ramps on Kalumbila mine.

From initial inspection of the specimens, it is apparent that the layer thickness varies significantly. Certain Specimens displayed heights of 39 mm where others displayed heights of 60 mm. Specimen two only had a thickness of 19 mm which would indicate it could be part of the top G1 layer. This was unclear as none of the other Specimens indicates such a small upper layer with a darker discolouration. There were also visible signs of separation between the Waterproofing layer and the base layer in Specimen 4, as seen in Figure 46. This could be due to improper cleaning of the surface before applying layers. This leads to the film bonding to the dust instead of the base layer.

Figure 46 Layer separation observed in Specimen 4 from Kalumbila mine.

From Trolley Lane 2, the Specimen height varied from 25 mm layer thickness to 58 mm layer thickness. Specimens 6 and 8 also displayed observable signs of cracking through the middle of the specimens. As a result of these cracks, those two Specimens could not be tested to determine structural capacity results.

4.3 Indirect Tensile Strength

4.3.1 ITS_{DRY} Kansanshi

For the ITS test procedure, 5 specimens were tested from the Kansanshi mine, of which 3 were dry specimens and 2 wet specimens. For Specimen 1 from Kansanshi, a peak ITS_{dry} of 608.2 kPa was achieved with a maximum displacement of 7.22 mm. For Specimen 5, a peak ITS_{dry} of 360.9 kPa was achieved with an accompanying maximum displacement of 4.99 mm. For the last dry Specimen, number 6, a peak ITS_{dry} of 161.0 kPa was reached with a maximum observed displacement of 6.96 mm. Figure 47 follows the sequence in which Specimens were tested and the respective ITS_{dry} results.

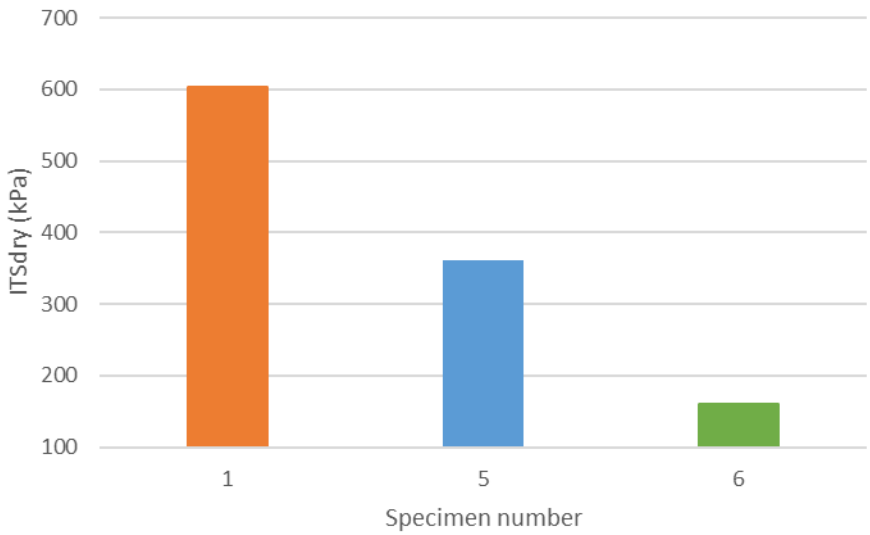

Figure 47 Sequence in which Specimens were broken with respective ITSdry results.

Preliminary observation would indicate that as the length between the position of each core and the base of the ramp increased, a noticeable decrease in indirect strength performance occurred. However, there are a variety of other variables that should also be taken into accounts such as residual bitumen content, Specimen diameter and height, and indirect tensile strength (kPa). Table 13 exhibits the specifications and results obtained for the dry Kansanshi results. It should be noted that the residual bitumen contents stated in Table 13 are those specified by the mine and not the recovered binder percentages which will be discussed further.

Table 13 ITS_{dry} results for Kansanshi.

Specimen number	Diameter (mm)	Height (mm)	Residual bitumen content (%)	Displacement at break (mm)	ITS (kPa)
1	143	91.875	2.11	7.222	602.8
5	143	94.775	2.67	4.996	360.9
6	143	90.375	2.27	6.965	161.0

However, when using the ITS_{dry} over bitumen content plot, as shown in Figure 48, it is clear that there is an error in terms of bitumen content specified in each Specimen. According to normal standards, as specified by (Sabita, 2020), a negative parabolic plot can be expected when comparing residual bitumen content to ITS results. In return, these results would display at which bitumen content would the peak confinement capacity of the base layer occur.

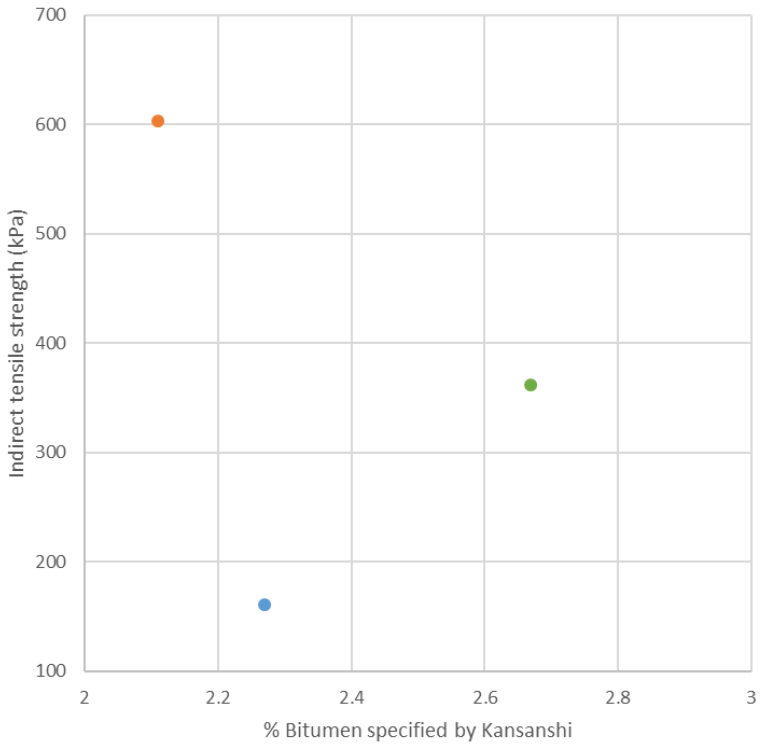

Figure 48 ITS_{dry} results plotted against residual binder content.

If previous studies completed by the mine have determined that the optimum bitumen content should be between approximately 2.3 %, most results should be within a 5 to 10 % standard deviation range of the average. However, when taking 2.11 % (from Specimen 5) as the base, it can be observed that Specimen 1 is 26.5 % larger. Also, Specimen 6 is 7.6 % larger than the base tensile strength. It was also noted that from the internal discolouration caused by the bitumen in the specimens, Specimen 6 (which supposedly had the most bitumen) showed the least amount of discolouration. Also, Specimen 5 (which is supposed to have a bitumen content in the middle of all 3 Specimens) showed the most discolouration indicating that large amounts of bitumen are present.

4.3.2 ITS_{DRY} Kalumbila

For the ITS_{dry} test procedure, 3 specimens were tested from the Kalumbila mine, of which all 3 were dry specimens. For Specimen 1 from Kalumbila, a peak ITS_{dry} of 228 kPa was achieved with a maximum displacement of 5.7 mm. For Specimen 2, a peak ITS_{dry} of 103 kPa was achieved with an accompanying maximum displacement of 3.6 mm. For the last dry Specimen, number 6, a peak ITS_{dry} of 344 kPa was reached with a maximum observed displacement of 7.2 mm. Figure 49 follows the sequence in which Specimens were tested and the respective ITS_{dry} results.

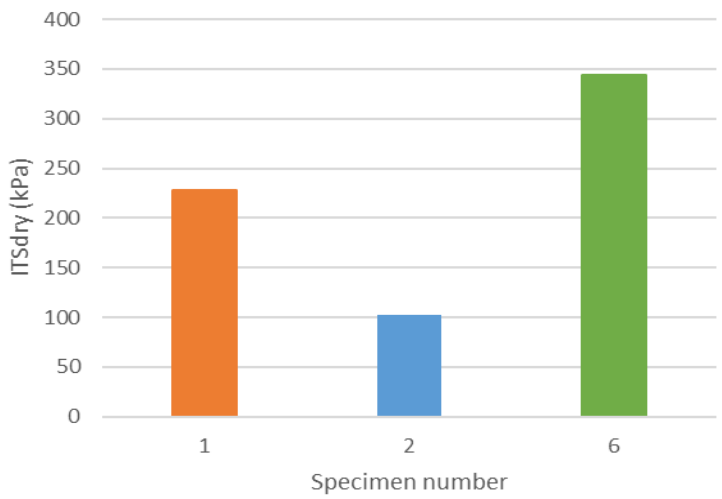

Figure 49 Sequence in which specimens from Kalumbila were tested with respective ITSdry results.

Preliminary observation would indicate that lower ITS_{dry} results are obtained on the East Trolley Ramp as indicated by Specimen 1 and Specimen 2, and higher ITS_{dry} results are obtained on the West Trolley Ramp as indicated by Specimen 6. However, there are a variety of other variables

that should also be taken into accounts such as residual bitumen content, Specimen diameter and height. Table 14 exhibits the specifications and results obtained for the dry Kalumbila results.

Table 14 ITSdry results for Kalumbila.

Specimen number	Diameter (mm)	Height (mm)	Residual bitumen content (%)	Displacement at break (mm)	ITS (kPa)
1	143	65.3	1.25	5.7	228
2	143	58.4	0.97	3.6	103
6	143.5	52.3	1.82	7.2	344

However, when using the ITSdry over bitumen content plot, as shown in Figure 50, it is clear that Indirect tensile strength does increase linearly with respect to the increasing residual bitumen content. According to the TG2 Guidelines, as specified by (Sabita, 2020), a negative parabolic plot can be expected when comparing residual bitumen content to ITS results. This would indicate that the peak ITSdry results has not been reached and further studies into optimum bitumen content would have to be considered.

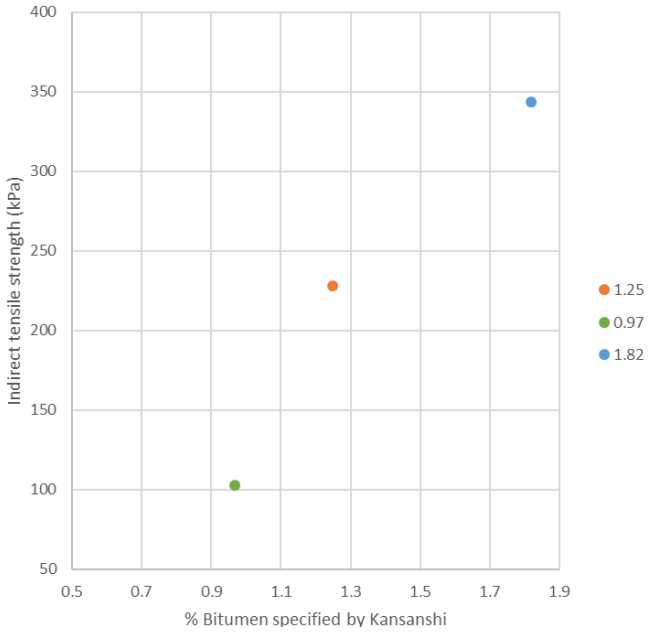

Figure 50 ITSdry results from Kalumbila plotted against residual bitumen content.

4.3.3 ITS_{wet} Results Kansanshi

For Kansanshi mine, testing was completed on 2 specimens to retrieve soaked indirect tensile strength data. Both cores were previously used to complete Marvil permeability testing. Specimen 2 reached a maximum ITS_{wet} of 130.0 kPa with a maximum displacement of 6.24 mm. Specimen 4 reached a maximum ITS_{wet} of 98.0 kN before breaking with an accompanying maximum displacement of 6.1 mm. The results of both wet and dry Specimens can be viewed in Figure 51 below.

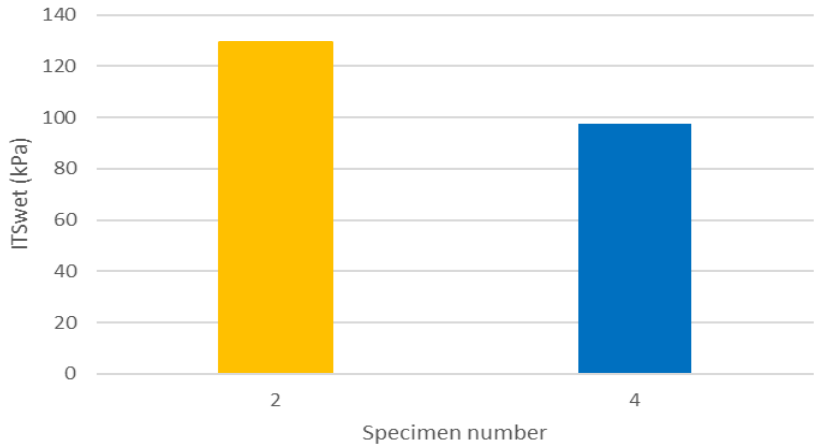

Figure 51 Sequence in which soaked Specimens were tested with respective ITSwet results.

Using these results, the indirect tensile strength for each Specimen can be calculated and plotted against its respective bitumen content specified by Kansanshi.

Table 15 ITS_{wet} results for Kansanshi.

Specimen number	Diameter (mm)	Height (mm)	Residual bitumen content (%)	Displacement at break (mm)	ITS (kPa)
2	143	74	2.60	6.242	129.5
4	143	78	2.39	6.106	97.7

From these results, it can be deduced that there is a linear trend that occurs. As the percentage of residual binder increases, the soaked indirect tensile stress increases as seen in Figure 52. However, as stated in the dry Specimen discussion, some irregularities have been spotted and further analysis was completed. Also, it is visible from Figure 52 that the BSM mix design displays a constant

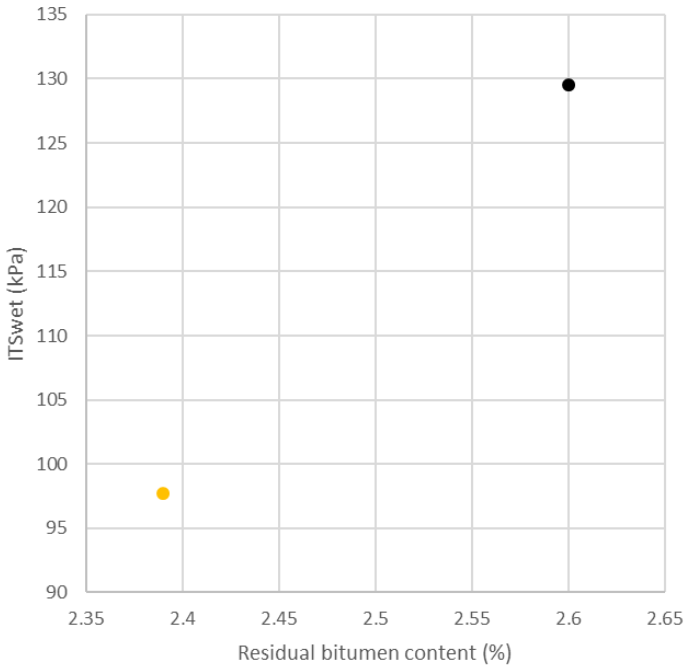

Figure 52 ITSwet results plotted against residual binder content.

increase in ITS_{wet} as the residual binder content increase. Although only two data points are available due to a shortage of test specimens, given historical data presented by Jenkins, Greyling and Collings (2021), the ITS_{wet} results were as expected indicating an increase in tensile strength against an increase in residual binder content under soaked conditions.

4.3.4 Comparisons

4.3.4.1 Kansanshi ITS_{dry}

For the dry specimens from Kansanshi, the results were analyzed and compared to the industry standard results for BSM1 and BSM2 (with less than 50 % RAP) indirect tensile strength results. From Figure 53 it can be observed that Specimen 1 and 5 comply with the standards set out for

BSM1 material classes which are 225 kPa. However, Specimen 6 failed to meet the criteria for BSM1 material classes. Also, Specimen 6 was compared with BSM2 criteria and also failed to meet the required specifications which were 175 kPa.

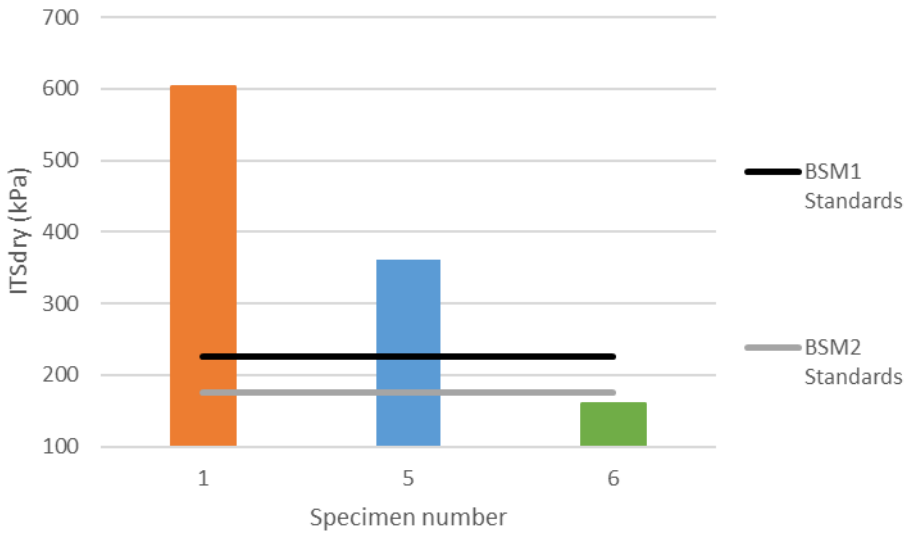

Figure 53 ITS_{dry} results compared to the BSM1 and BSM2 standards.

4.3.4.2 Kalumbila ITS_{dry}

For the dry specimens from Kalumbila, the results were analyzed and compared to the industry standard results for minimum BSM1 and BSM2 (with less than 50 % RAP) indirect tensile strength limits. From Figure 54 it can be observed that Specimen 1 and 6 comply with the standards set out for BSM1 material classes which are 225 kPa. However, Specimen 2 failed to meet the criteria for BSM1 material classes. Also, Specimen 2 was compared with BSM2 criteria and also failed to produce ITS_{dry} values higher than 175 kPa which is the minimum BSM2 ITS limit.

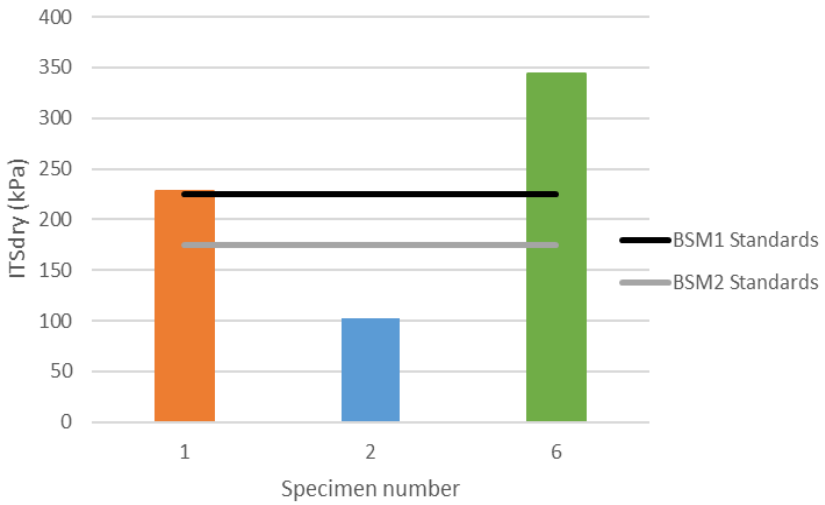

Figure 54 ITSdry results from Kalumbila compared to BSM1 and BSM1 minimum limits.

4.3.4.3 Kansanshi ITS_{wet}

For the ITS_{wet} specimens, the same procedure was followed. Both Specimens were compared to the industry standard ITS values for soaked BSM1 and BSM2 material classes which are 125 and 100 kPa respectively. Specimen 2 barely passes the BSM1 standards by 4 kN as shown in Figure 55. Whereas Specimen 4 failed to meet both BSM1 and BSM2 indirect tensile strength standards. Although limited Specimens were available for testing, from the available Specimens it can be deduced that approximately 33 % of the material will fail to meet BSM2 standards under dry conditions and approximately 50 % of the material will fail to meet BSM2 standards under wet conditions.

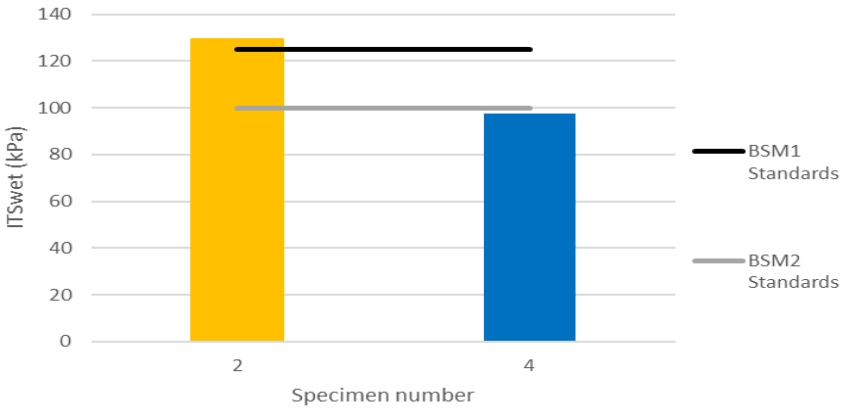

Figure 55 ITSwet results compared to the BSM1 and BSM2 standards.

4.3.5 Stiffness comparison

An unusual occurrence is observed during the loading cycle of the test procedure. Figure 56 indicates the stiffness's that was observed during the three tests. In the figure, Specimen 1 and 5 can be monitored as having the same stiffness. However, the gradient produced by Specimen 6 is considerably lower. The lower gradient indicates that Specimen 6 has a lower stiffness than Specimen 1 and 5. This can be due to several factors such as a lack of compaction or a lack of cohesion and interconnectivity between the particles. It could also be due to an incorrect material grading used. If the amount of fine present within the Specimen was more than required, it could lead to bad packing between the material.

A similar scenario has been observed within the data from the ITS_{wet} specimens. Both Specimens mostly followed the same Stiffness gradient of 0.312 kN/mm. However, after the peak load was reached for both specimens, Specimen 2 displayed a steeper downward gradient than Specimen 4 as shown in Figure 57. Post peak gradients indicate the ductility of the material. In other words, how much a material can plastically deform until failure. In this state, the decreasing breaking rate in Specimen 4 would be favourable as it would result in the layer retaining strength for a slightly longer period. The ductility can be due to several factors such as a lack of compaction, lack of cohesion and interconnectivity between the particles, or due the amount of residual binder present in the material. It could also be due to an incorrect material grading used.

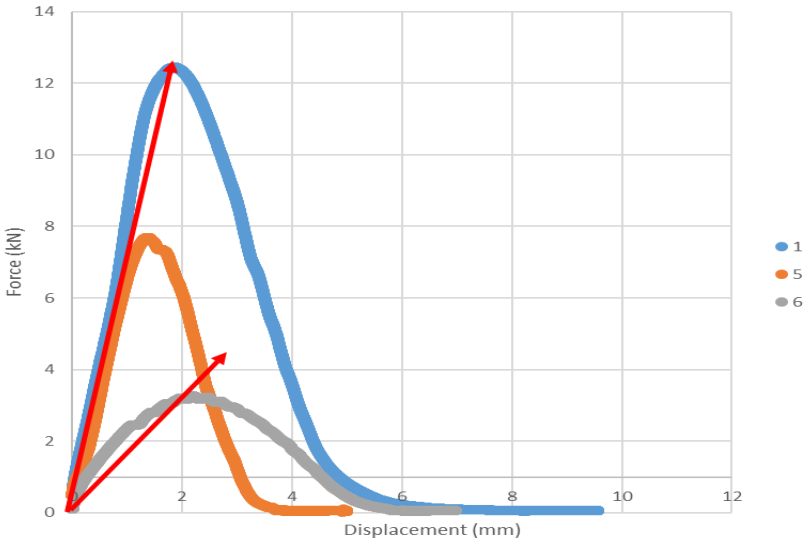

Figure 56 ITSdry rate of break comparison.

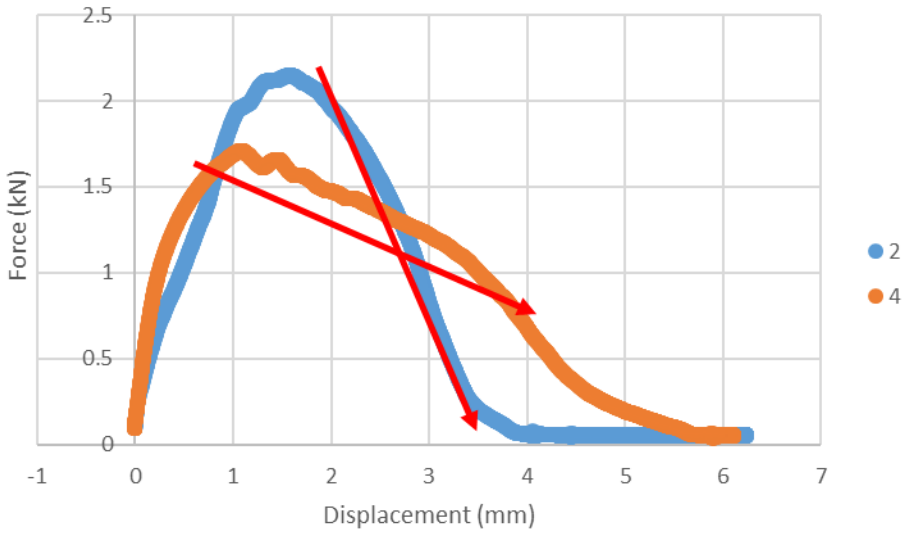

Figure 57 ITSwet rate of break comparison.

4.4 Resilient Modulus Analysis

This section of the results will list and discuss the results obtained for dynamic triaxial testing on the emulsion treated base layer material for Kansanshi. The typical behaviour of granular material stabilized with bitumen emulsion is shown in Figure 58 below. In the figure, the resilient moduli are plotted against the sum of principal stresses (θ). This plot type is used as it gives an indication of the material's stress dependency under repeated loading as discussed more in Section 2.5.3.3. With this data, it is possible to observe the material's response under repeated loading (Mazibuko, 2020).

Figure 58 illustrates that as the confining pressure (σ_3) increases, the resilient moduli (Mr) increases. However, it is noticeable that as the major principal stress (σ_1) increase at each confining pressure, the respective Resilient Modulus decreases. It should be noted that Figure 58 displays the raw triaxial data that must be analyzed further to get rid of abnormalities. To further analyze the results obtained, 7 Resilient Modulus models are plotted and listed. These models are used to describe to what extent the material is stress-dependent. Also, the models can be used in the mechanistic-empirical analysis method to determine the load spreading ability of the base layer.

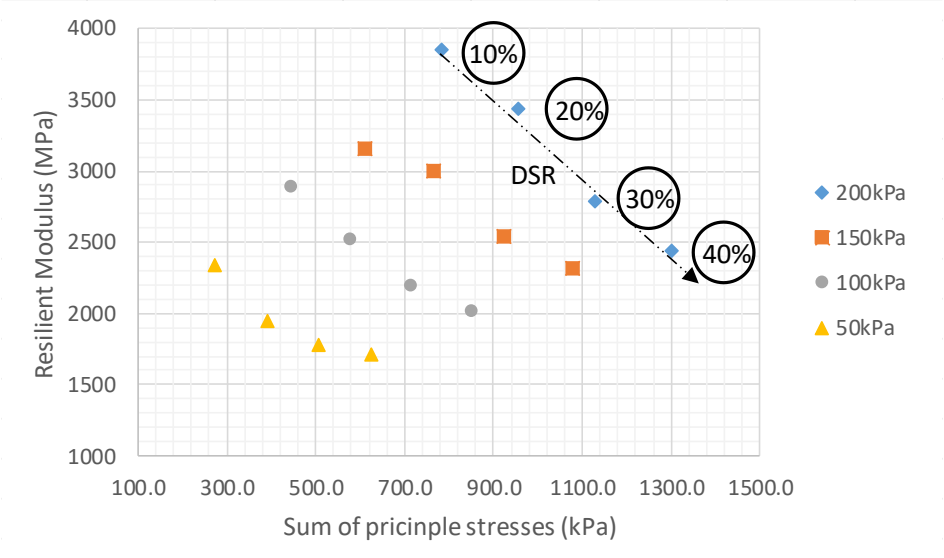

Figure 58 Resilient Modulus data observed plotted against the sum of principal stresses for Kansanshi.

Certain models discussed below observe the relationship between Resilient Modulus and bulk stresses (sum of all principal stresses) while other models focus on the relationship between resilient moduli and confining pressure (σ_3). Other models focus on the effects of the deviator stress ratio (DSR) has on the Resilient Modulus models and also the effects of the principal stress ratios (PSR) on the resilient moduli models. Each model will be analyzed individually by making use of linear regression models as discussed in Section 2.5.3.3 and a coefficient of fit (r^2) will be calculated for each model. Finally, all the correlation coefficients can be compared to determine which models best describe the materials load spreadability.

4.4.1 Mr-θ model

The Mr-θ model ($Mr = k_1\theta^{k2}$) is the most generally used model to describe a material's resilient response under dynamic loading as it is the simplest model available. This model compares the Resilient Modulus with the sum of principal stresses (θ) as depicted in Figure 59. From this model, it can be observed that the parent material with the addition of emulsion is stress-dependent as the Resilient Modulus increase with the increase in bulk stress.

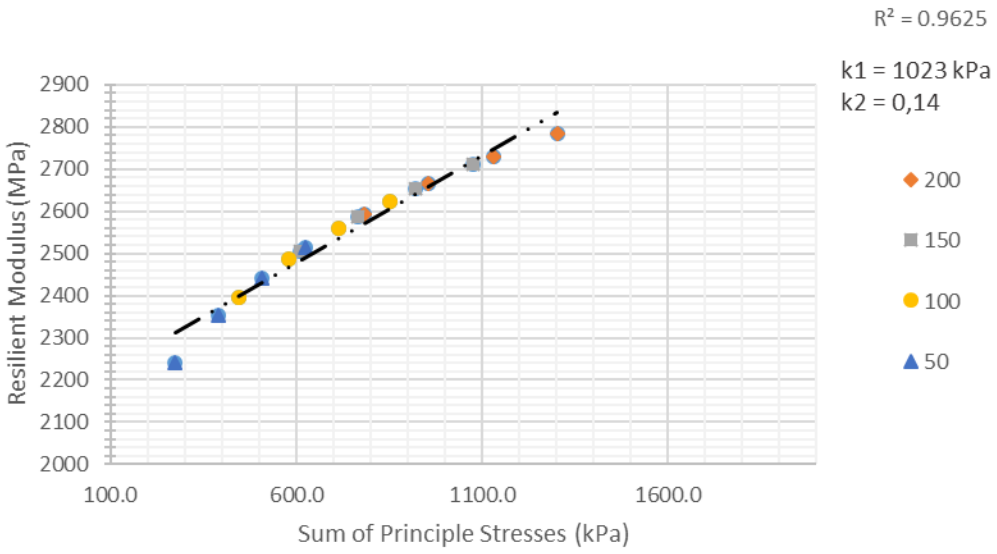

Figure 59 Mr-θ model on linear scale.

However, as stated in the Hitchhikers guide to pavement engineering by Jenkins and Rudman (2019), the results can best be analyzed on a logarithmic scale. This is visible as Figure 60 displays the Mr-θ model for the same results, but with both axes' in a logarithmic scale. The correlation coefficient for the normal model displays a value of 0.9625 which is considered acceptable while

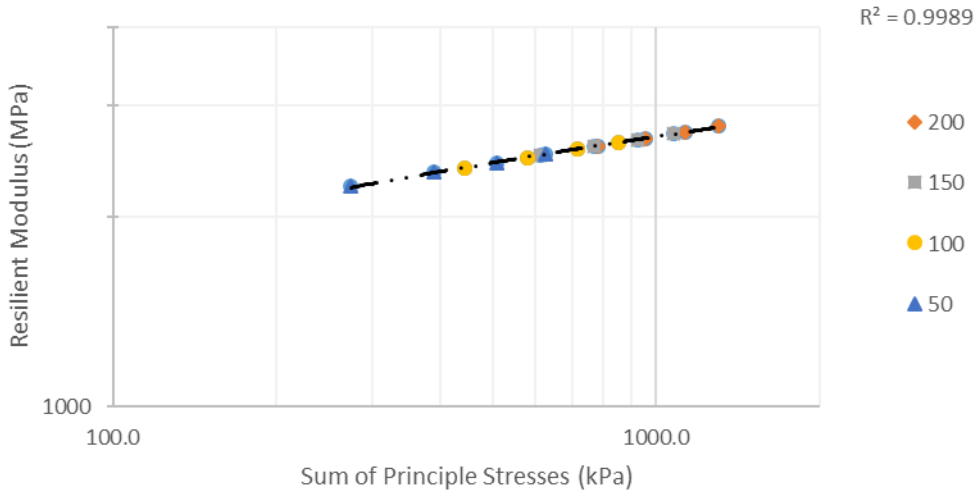

Figure 60 Mr-θ model plotted on a logarithmic scale.

the R^2 for the logarithmic plot is calculated to be 0.9989. The change in R^2 is since the material factor, k_2, exponentially influences the resilient moduli data.

Nonetheless, in both models, the R^2 correlation perfectly describes the stress dependency of the material. With this model, the k_1 and k_2 factors were calculated as 1022.52 kPa and 0.1397 respectively. From the figures, it is also possible to observe that there is a linear trend between the bulk stress and the resilient moduli. As the bulk stress increase, so does the resilient moduli increase.

4.4.2 Mr-σ_3-σ_d model

Similarly, to the Mr-θ plot, the intention of the Mr-σ_3-σ_d model ($Mr = k_1\sigma_3^{k2}\sigma_d^{k3}$) is to provide a relationship between the resilient moduli for the material and the respective confining stresses and deviator stresses. This results in a model in which the confining stress (σ_3) and the deviator stress (σ_d) individually influences the Resilient Modulus.

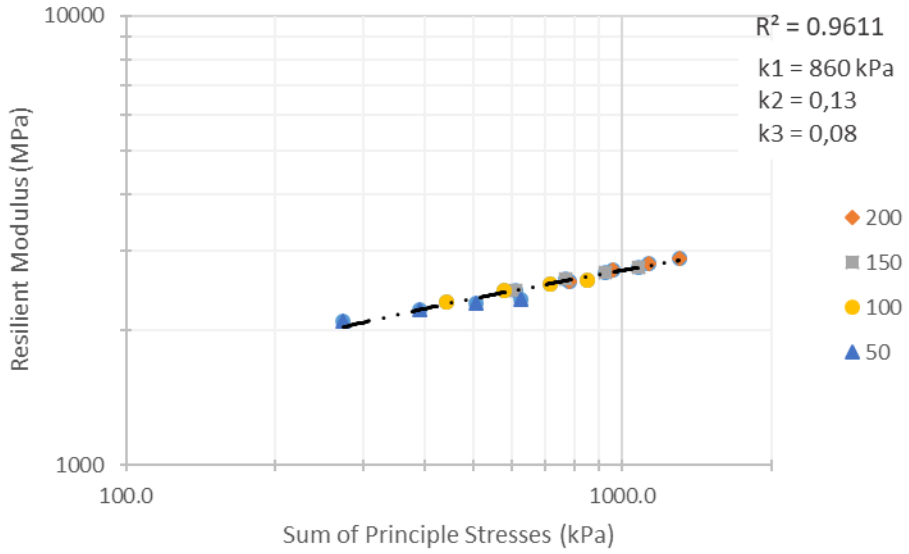

Figure 61 Mr-σ3-σd model for Kansanshi.

From the model above, a correlation coefficient of 0.961 was calculated. This indicates that this model is also a perfect fit for analyzing the data. However, there is a slight difference between the correlation coefficient of the Mr-σ_3-σ_d model and the Mr-θ model. There is a better relationship between the bulk stress and Resilient Modulus than the confining- and deviator stresses and the Resilient Modulus. It should also be noted that the Mr-σ_3-σ_d model does not take into consideration that at high deviator stress ratios there is a reduction in Resilient Modulus. This is called stress

softening. Thus this model only describes stress stiffening which is not applicable for granular materials, as emulsion stabilized material is still considered as granular.

4.4.3 Parabolic Mr-σ_3-σ_d

The parabolic Mr-σ_3-σ_d model ($Mr=k_1\sigma_3^{k2}(-k_3(\sigma_d/\sigma_{d,f})^2+k_4(\sigma_d/\sigma_{d,f}) + k_5)$) also considers the confinement stress as an influencing factor. Additionally, this model takes into consideration the deviator stress ratio due to the resilient moduli decreasing at high stresses as the material reaches maximum loading. It should be noted that in this model the confinement stress and deviator stress ratio is integrated into the model separately. The model has been unable to describe the Resilient Modulus of the emulsion stabilized Specimen as revealed in Figure 62.

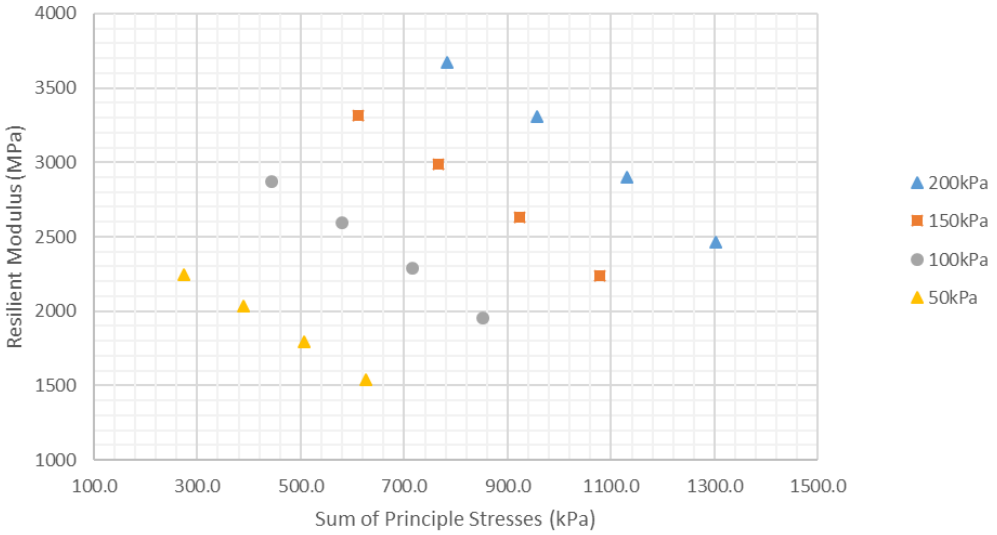

Figure 62 Parabolic Mr-σ3-σd model for Kansanshi.

Numerous iteration of data processing has been implemented to determine whether an error occurred during the data processing. It is clear from Figure 62 that this model cannot adequately describe the Resilient Modulus of this specific material type in terms of the material's confinement stress and deviator stress ratios. However, according to research completed by van Niekerk (2002) constant values were determined for coefficients k3, k4, and k5 which are 2, 3, and 1 respectively. This is due to the parabolic nature in the second part of the model, $Mr = (..)(a.x^2+b.x+c)$. When considering k5 as 1, the second part of the equation converts to 1 for the boundary condition of x

$= \sigma_d/\sigma_{d,f} = \sigma_d = 0$. Thus by optimizing the regression routine, the optimal k3 and k4 coefficients were determined as shown in Figure 63 to be 2 and 3 respectively (van Niekerk, 2002).

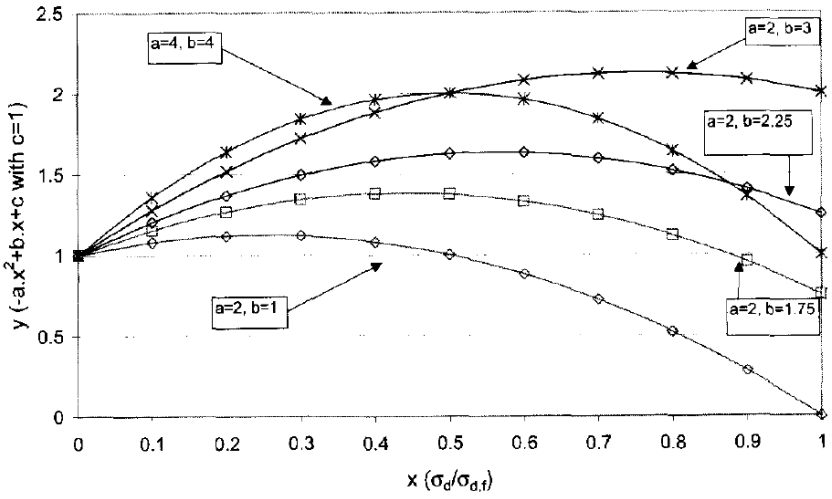

Figure 63 Shape of the parabolic term as a function of coefficients a and b (from van Niekerk (2002)).

Implementing these new variables, a new parabolic Mr-σ_3-σ_d model is created as depicted in Figure 64. This model produced a R^2 of 0.984 which indicates a good fit. The slight increase in resilient modulus at higher bulk stresses provides an indication of stress stiffening occurring when considering the constant k3, k4, and k5 variables.

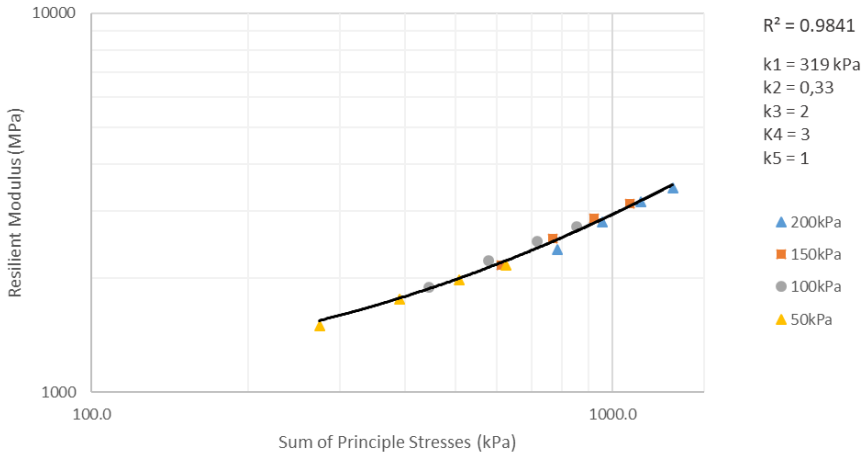

Figure 64 Adapted parabolic Mr-σ3-σd model.

4.4.4 Mr-θ-$\sigma_d/\sigma_{d,f}$ model

The Mr-θ-$\sigma_d/\sigma_{d,f}$ model ($Mr=k_1\theta^{k2}(1-k_3(\sigma_d/\sigma_{d,f})^{k4}$) aims to provide a model which describes the Resilient Modulus in terms of the sum of the material's principal stress and the resulting deviator stress ratio. Both factors are analyzed separately within this model. The Mr-θ-$\sigma_d/\sigma_{d,f}$ model is an alternative to the simple Mr-θ model stated previously. However, in this model, the main factor influencing the Resilient Modulus is not only the sum of principal stresses but also the deviator stress ratio. This indicates that this model considers that there is a linearly increasing pattern between the Resilient Modulus and bulk stresses, but also takes material softening at high stresses into account, where the Resilient Modulus decreases.

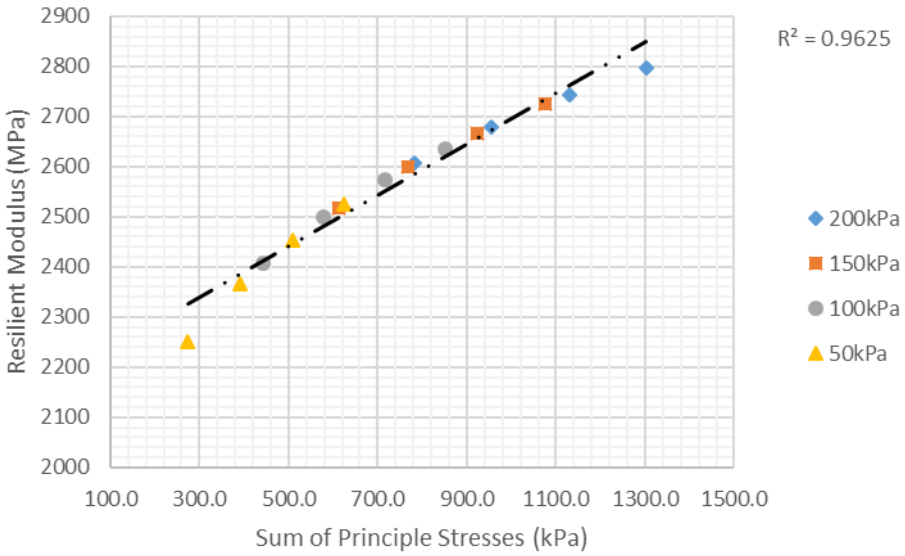

Figure 65 Mr-theta-σd/σd,f model for Kansanshi material.

From Figure 65 it is observable that the correlation coefficient calculated for this model was 0.9625 which indicates that this model perfectly describes the relationship of the material between Resilient Modulus, bulk stresses, and deviator stress ratios. Also, it can be observed that there is a slight deviation in the linear trend as the bulk stresses increase indicating slight material softening.

4.4.5 Mr-σ_3-$\sigma_d/\sigma_{d,f}$ model

Similarly to the previous model, the Mr-σ_3-$\sigma_d/\sigma_{d,f}$ model ($Mr=k_1\sigma_3^{k2}(1-k_3(\sigma_d/\sigma_{d,f})^{k4})$) determines the Resilient Modulus in terms of the confinement stresses and deviator stress ratios observed within the material. In this case, the sum of principal stresses is removed and replaced by the confinement stress as the main influencing factor. Also, this model takes into consideration the decrease in Resilient Modulus that occurs with increasing deviator stress ratios. The goal of this model is to determine if the confinement stress has a noticeable influence on the Resilient Modulus of the material as well as consider how the deviator stress ratio, coupled with the confinement stress, influences the Resilient Modulus.

Figure 66 below indicates that the correlation coefficient calculated for the Mr-σ_3-$\sigma_d/\sigma_{d,f}$ is 0.0502. This value points out that the model does not adequately describe the relationship between the Resilient Modulus and confinement stress and deviator stress ratio.

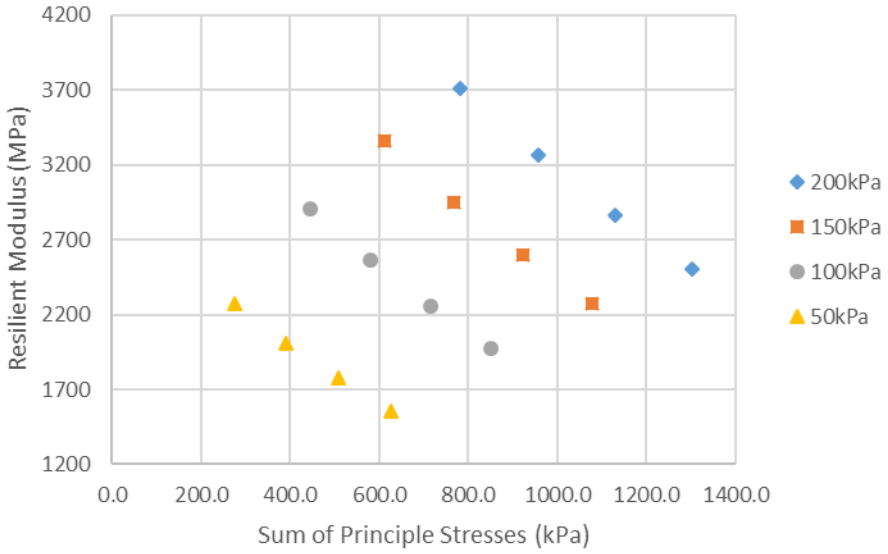

Figure 66 Mr-σ3-σd/σd,f model for Kansanshi.

Also, from this model is can be observed that the bulks stress better correlates to the Resilient Modulus data than the confinement stress. This would indicate resilient moduli of the emulsion stabilized material from Kansanshi is dependent on the sum of principal stresses and not the confinement stresses.

4.4.6 Mr-θ-$\sigma_1/\sigma_{1,f}$ model

The Mr-θ-$\sigma_1/\sigma_{1,f}$ model ($Mr=k_1\theta^{k2}(1-k_3(\sigma_1/\sigma_{1,f})^{k4}$) is similar to the Mr-θ-$\sigma_d/\sigma_{d,f}$ in that it is an alternative model to the base Mr-θ model. This model also considers the sum of principal stresses as the core influencing factor. However, instead of considering how the increasing deviator stress ratio influences the Resilient Modulus, this model considers the principal stress ratio (PSR). This model aims to determine if there is any difference in the Resilient Modulus when considering the PSR instead of the DSR. The results obtained for the Mr-θ-$\sigma_1/\sigma_{1,f}$ model is shown in Figure 67 below. From this picture is can be noted that the correlation coefficient value was calculated to be 0.9625. This correlation indicates that this model is a perfect fit for this material. Also, this correlation indicates that using the principal stress ratio as a contributing factor is just as effective as using the deviator stress ratio.

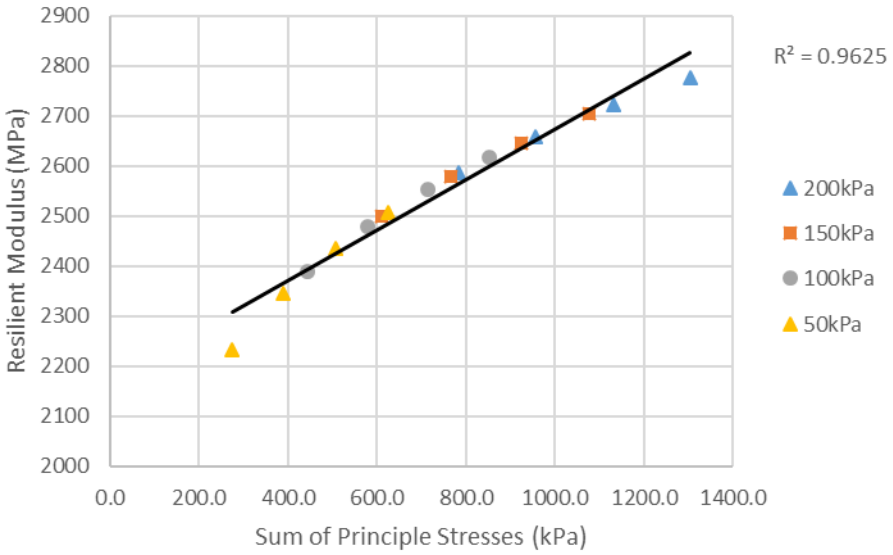

Figure 67 Mr-theta-σ1/σ1,f model for Kansanshi material.

When comparing the correlation coefficient from the Mr-θ-$\sigma_d/\sigma_{d,f}$ model (0.9625) with the correlation coefficient calculated for the Mr-θ-$\sigma_1/\sigma_{1,f}$ model (also 0.9625) it is noticeable that there is no difference in the Resilient Modulus results. This would indicate that either PSR or DSR ratio can be used to take into account the decrease in resilient moduli and high bulk stresses.

4.4.7 Mr-σ_3-$\sigma_1/\sigma_{1,f}$ model

Similarly to the Mr-θ-$\sigma_1/\sigma_{1,f}$ model ($Mr=k_1\sigma_3^{k2}(1-k_3(\sigma_1/\sigma_{1,f})^{k4})$) discussed above, the Mr-σ_3-$\sigma_1/\sigma_{1,f}$ model aims to provide a relationship between the confinement stress, principal stress ratio, and the Resilient Modulus. This model considers confinement stress as the main factor influencing the Resilient Modulus. Also, to take account of the decrease in resilient moduli at high stresses, the principal stress ratio is used to determine if there's any difference between DSR and PSR at higher stresses. Figure 68 below indicates that the correlation coefficient was calculated to be 0.0523. This shows that this model is not able to describe the Resilient Modulus in terms of the confinement stress and principal stress ratios.

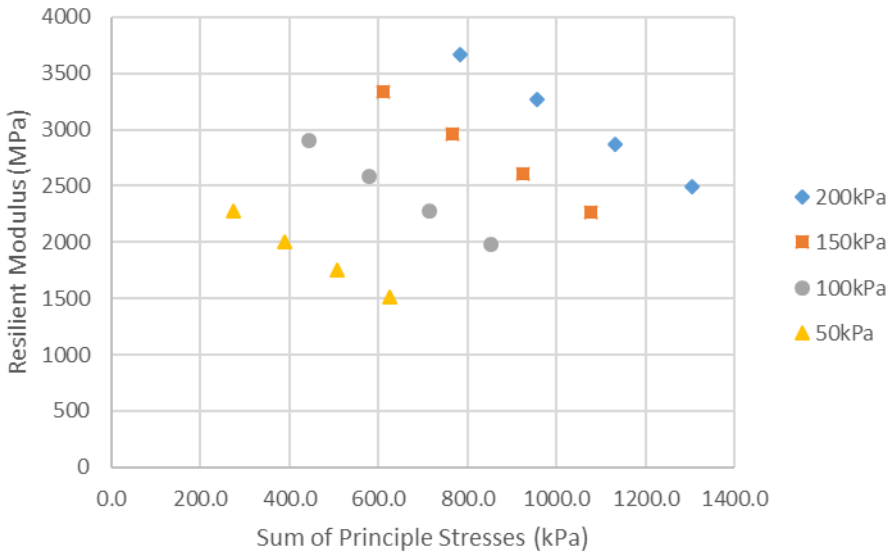

Figure 68 Mr-σ3-σ1/σ1,f model for Kansanshi.

The lack of Resilient Modulus description was also observed from the comparison between the Mr-σ_3-$\sigma_d/\sigma_{d,f}$ model and the Mr-θ-$\sigma_d/\sigma_{d,f}$ model. From all four of these models, it is clear that bulk stress should be used as the principal factor influencing the Resilient Modulus data and not confinement stress. Interestingly, when comparing the R^2 from the Mr-σ_3-$\sigma_d/\sigma_{d,f}$ model with the Mr-

θ-$\sigma_1/\sigma_{1,f}$ model, an increase of 0.021 was observed. Although both models failed to describe the Resilient Modulus, it is interesting to note that the PSR provided better results than the DSR. This would suggest that the PSR provides a slightly better description of what happens to the Resilient Modulus at high bulk stresses.

4.4.8 Summary

The goal of all the above-stated models was to determine which models best describe the resilient response of a BSM-emulsion mix design in terms of bulk stresses. From the simplified models, Mr-θ and Mr-σ_3-σ_d, it can be observed that the bulk stresses or the confinement stresses coupled with deviator stresses can be used to accurately model the resilient response of the base layer. The second iteration of Models considered both the bulk stresses and confinement stresses with additional deviator stress ratios. From these models, it was observed that by combining the deviator stress ratio with confinement stress, the Resilient Modulus of the base layer cannot be accurately represented. While the bulk stress, with complimentary DSR, can adequately describe the base layer's resilient response. For the last set of Models, the bulk stress and confinement stress was combined with the PSR individually. From both these Models, it can be observed the combination of confinement stress and PSR could not create a model that accurately represents the base layers' resilient response. Overall, to determine which model best describes the relationship of BSM-emulsions used on mine haul roads, the correlation coefficient is considered. Ultimately, the best model to describe the base layer is the Mr-θ model with an R^2 of 0.9989 when plotting on a log scale.

4.5 Monotonic triaxial data

Since limited Specimens were available for testing from Kansanshi, the dynamic triaxial test was conducted first, followed by the monotonic triaxial test on the same specimens. The purpose of the monotonic triaxial test procedure is to determine the shear strength properties of the material. These properties include the cohesion intercept and internal friction angle. This can be calculated or observed of the Mohr circles as illustrated in Figure 70. The results of the monotonic triaxial test as shown in Figure 69 below.

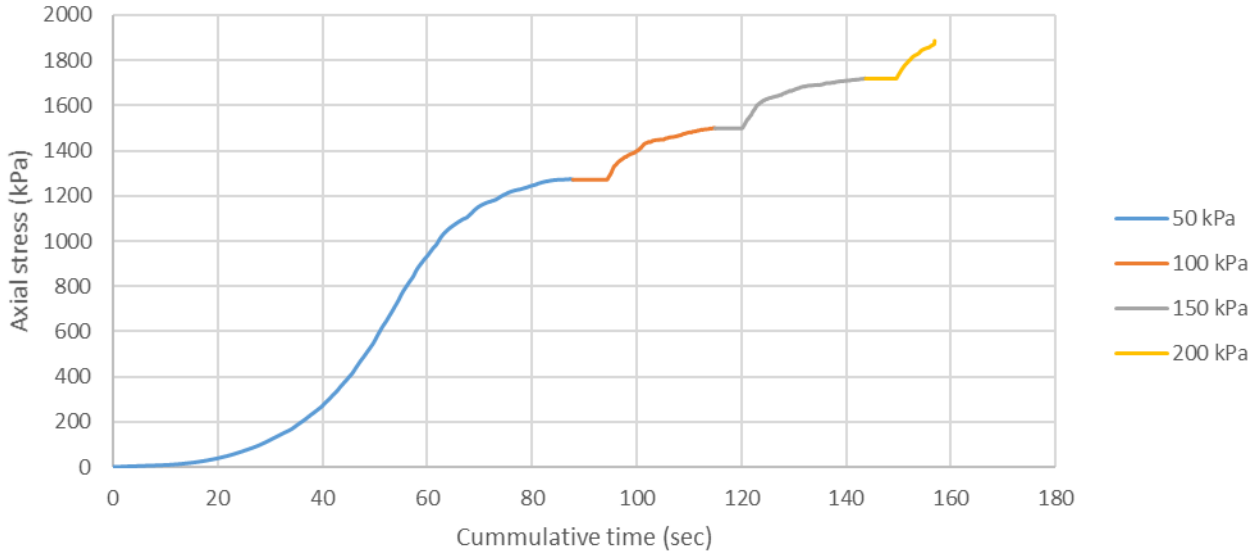

Figure 69 Monotonic triaxial results obtained for Kansanshi ramp.

As seen in Figure 69, the test procedure was stopped at each confining pressure just as the stress started to plateau. Once stopped, the confinement pressure was increased in increments of 50 kPa and the test was continued. From this figure, it is visible that at 50 kPa confinement stress, the Specimen was able to withstand axial stress of 1275 kPa. At 100 kPa, the Specimen was able to withstand axial stress of 1501 kPa. At 150 kPa, the Specimen was able to withstand axial stress of 1720 kPa. Lastly, the Specimen was able to resist axial stress of 1958 kPa at 200 kPa confinement stress.

Using the information from Figure 69, the maximum applied stress with accompanying confining stresses can be used to plot the Mohr circles. From this plot, the cohesion intercept was measured to be 240 kPa with an internal friction angle of 41.6 º. Using the guidelines for BSM material as specified in the TG2 document by (Sabita, 2020), this material and mix can be determined if it complies with the limits according to its cohesion and internal friction angle. According to the guidelines, the Specimen is determined to comply with the limits set out for a BSM2 mix. Conversely, the Specimen is determined to comply with the limits of a BSM1 in terms of its internal friction angle. Ultimately, the material can be classified as a BSM2, although the retained cohesion could not be calculated due to a lack of specimens.

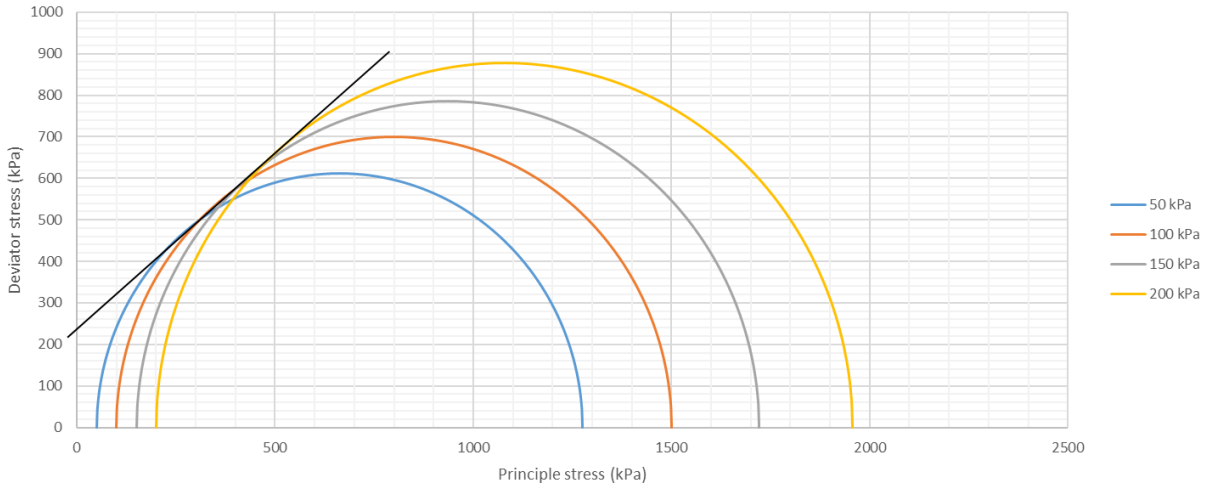

Figure 70 Mohr-Coulomb plot for Kansanshi BSM mix.

Table 16 BSM classification of emulsion Specimen.

	Shear parameter	BSM classification
Cohesion (kPa)	240	BSM2
Internal Friction Angle (º)	41.6	BSM1

4.6 Binder recovery data

For the binder recovery process, the following values were obtained as shown in Table 17. This table specifies the Specimen number as well as the amount (in gram) of bitumen that was recovered from each Specimen. Each resulting percentage of residual bitumen is calculated by dividing the recovered binder by each Specimen's dry weight. For each Specimen, the percentage of material loss during the process is calculated to determine whether the results are credible or not. From the results stated below, an average residual bitumen content of 2.21 % was calculated for the Kansanshi specimens, with a standard deviation of 0.721 %.

Table 17 Binder recovered from Kansanshi and Kalumbila Specimens.

Specimen number	Total Specimen Weight (gr)	Recovered binder (gr)	% Binder	Mass loss during the recovery process (%)
Kansanshi				
1	3134.3	119.19	3.80	1.15
2	2084.6	43.05	2.07	0.89
3	3515.2	51.1	1.45	0.98
4	2293.2	44.69	1.95	0.77
5	3134.0	63.54	2.03	1.42
6	2804.2	83.12	2.96	0.76
7	5107.0	100.84	1.97	1.05
8	4487.0	77.37	1.72	1.06
9	3251.1	63.61	1.96	0.89
Kalumbila				
1	2232.5	27.85	1.25	0.96
4	2248.6	21.72	0.97	1.21
5	1829.3	20.3	1.11	0.96
6	1818.7	33.1	1.82	1.07

Similarly, an average residual bitumen percentage of 1.29 % with a standard deviation of 0.374 %. From this data, it was discovered that there is a 32.6 % variation within the distribution of bitumen

emulsion on the Kansanshi ramp. Correspondingly, it was discovered that there is a 29 % variation within the distribution of bitumen emulsion on both of the Kalumbila ramps. Also, the theoretical residual bitumen content was revealed to be 0.520 % more than the actual average bitumen content that was recovered.

The percentage loss in Table 17 refers back to the discussion in section 3.6.3. This percentage refers to the mass of material (aggregate or binder) that is lost during the test procedure. Each specimen is weighed at the start of the test procedure. Correspondingly, the recovered aggregate and recovered binder is weighed after the test procedure is complete. The difference in mass is calculated and displayed as a percentage. Presently, there are no standards for percentage material loss in binder recovery. However, for internal quality control, a percentage loss which includes all factors such as large aggregate, fines, and binder less than 5 % is deemed acceptable as it would result in 95 % result accuracy. As all specimens displayed mass losses of less than 2 %, which provides an indication that binder recovery results are 98 % accurate.

4.7 Grading analysis

In this section, the grading analysis of each Specimen will be discussed for both Kansanshi and Kalumbila ramps. Table 18 below displays the grading results that were obtained for each Specimen on the Kansanshi Trolley Ramp. The grading results are defined in percentage passing as stipulated in the TG2 document by (Sabita, 2020). From these 4 Specimens, an average grading is calculated which is compared to the industry standard grading limits specified for BSM-emulsion mix designs as shown in Figure 71. From Table 18 it is evident that there are large amounts of fines present within the base layer of Kansanshi. When manufacturing bulk specimens, the material passing the 5 mm sieve is considered fine material. When comparing the results of the grading analysis, the percentage passing the 5 mm sieve ranges between 52 % - 64 %.

Table 18 Grading results obtained for all Kansanshi Specimens.

Sieve size (mm)	Kanshansi 01	Kanshansi 05	Kanshansi 06	Kanshansi 08	Average
50	100%	100%	100%	100%	100%
37.5	100%	100%	100%	100%	100%
28	100%	98%	100%	100%	99%
20	97%	88%	97%	100%	96%
14	91%	76%	87%	86%	85%
10	81%	66%	75%	77%	75%
7.1	72%	59%	65%	68%	66%
5	64%	52%	57%	61%	58%
2	52%	40%	44%	48%	46%
1	46%	35%	38%	41%	40%
0.600	42%	31%	34%	37%	36%
0.425	38%	28%	30%	35%	33%
0.300	34%	24%	25%	31%	29%
0.150	25%	15%	15%	24%	20%
0.075	17%	7%	7%	16%	12%

Upon further inspection of Figure 71, it can be seen that the course material (50 mm to 5 mm) found within the base layer tends to run parallel to the upper limit (fine material) of the BSM-emulsion standard. From the 2 mm sieve downward, the grading can be perceived to be positioned outside the upper limit grading. This indicates that there are excessive fines present within the base layer of the Kansanshi Trolley Ramp. This could lead to the premature failure of the base because the emulsion can not completely disperse within the material. The presence of excess fines would

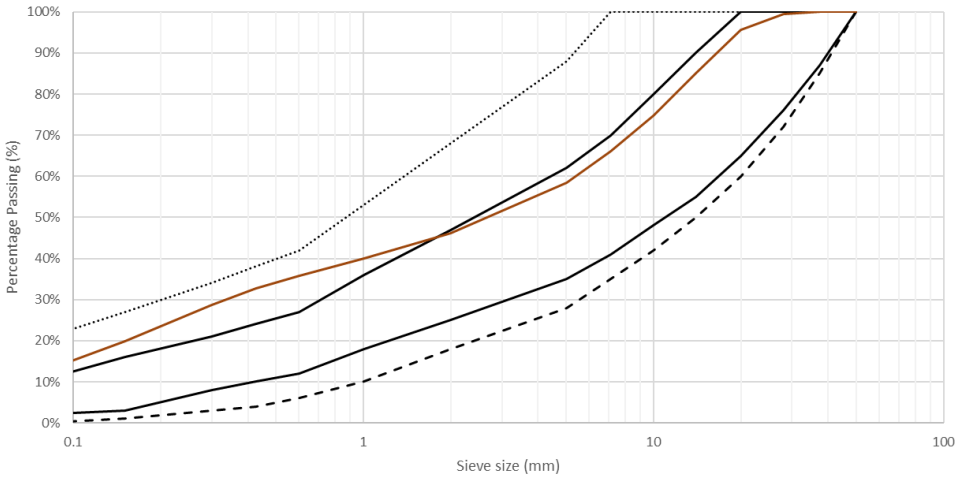

Figure 71 Average calculated grading for Kansanshi compared to BSM-Emulsion grading limits.

cause the emulsion to bond with the fine material causing improper bonds between the emulsion, fines and larger aggregate leading to a lack of cohesion.

Table 19 below displays the grading results that were obtained for each Specimen on the Kalumbila Trolley Ramp. The grading results are defined in percentage passing as stipulated in the TG2 document by (Sabita, 2020). From these 4 specimens, an average calculated grading is compared to the industry standard grading limits specified for BSM-emulsion mix designs as shown in Figure 72. It was observed that the Specimens from Kalumbila displayed a much better particle distribution than those from Kansanshi. When manufacturing bulk samples, the material passing the 5 mm sieve is considered fine material. Comparing the results of the grading analysis, the percentage passing the 5 mm sieve ranges between 47 % - 60 %.

Table 19 Grading results obtained for all Kalumbila Specimens.

Sieve size (mm)	Kalumbila 01	Kalumbila 04	Kalumbila 05	Kalumbila 06	Average
50	100%	100%	100%	100%	100%
37.5	100%	100%	100%	100%	100%
28	100%	100%	100%	100%	100%
20	95%	95%	100%	98%	97%
14	81%	81%	88%	82%	83%
10	67%	69%	77%	73%	71%
7.1	54%	62%	68%	64%	62%
5	47%	55%	60%	56%	54%
2	35%	43%	45%	42%	41%
1	29%	37%	38%	36%	35%
0.600	25%	33%	33%	31%	31%
0.425	22%	29%	30%	28%	28%
0.300	19%	26%	27%	24%	24%
0.150	12%	17%	17%	15%	15%
0.075	6%	10%	9%	7%	8%

When regarding the grading comparison in Figure 72, it is clear that particle size distribution on the Kalumbila ramps better represents an ideal grading (fuller grading) than that of the Kansanshi mine. The coarse section of Kalumbila specimens' grading is closer to the upper BSM limit (fine) than the lower limit (coarse). However, considering the middle grading section from 5 mm upward, the grading curve shifts closer to the ideal grading which should be situated directly in between both upper- and lower limits. The fine fraction, which is material between 0.6 mm and 0.075mm, is observed to lie outside the bounds specified by the upper limit. This indicates that in general over the pavement layer, there is an excess of fine material (between the 1 mm and 0.150 mm fractions) which can cause premature failure of the layer.

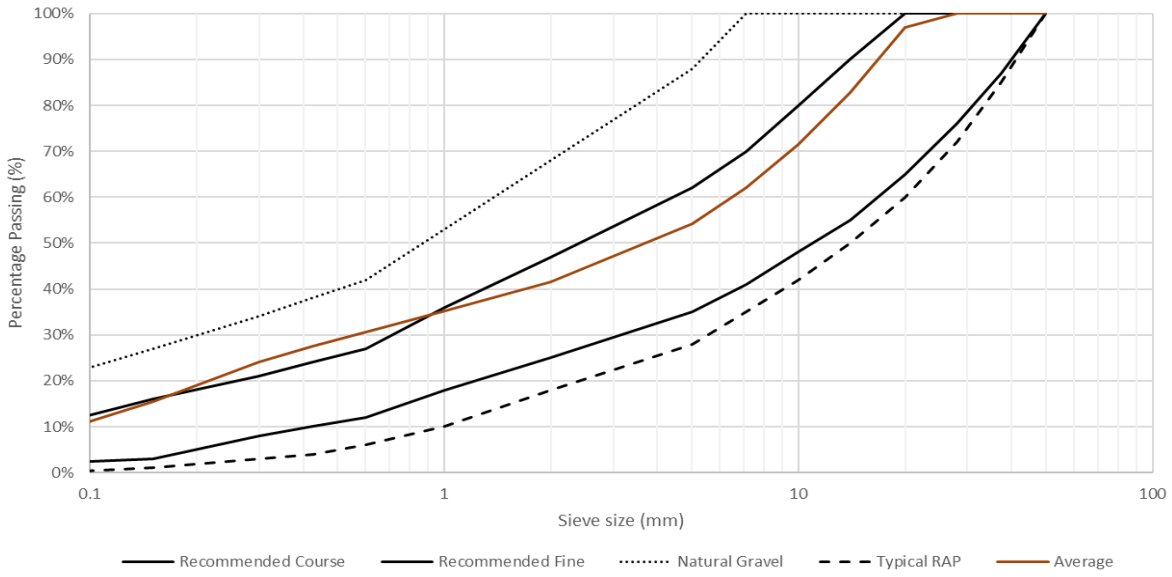

Figure 72 Average grading from Kalumbila compared to the upper- and lower limits specified for BSM-emulsions.

In the presence of large amounts of fines, the emulsion will tend to stick to the fines. As a result, bitumen stabilized materials are reliant on the sand skeleton structure (2.0 mm to 0.075 mm fractions) for the material performance (Wirtgen GmbH, 2012). The current grading envelope of Kalumbila indicates that there will be a lack of cohesion within the BSM mix design as a result of the high fines content. Also, an increase in the fine content will results in a higher demand for bitumen emulsion content resulting in higher production costs. Overall the grading analysis displays that the Kalumbila Trolley Ramps display the most favorable grading as there are less fines present.

4.8 Marvil permeability

For the Marvil permeability test, two Specimens from both Kansanshi and Kalumbila were conditioned for testing. Each Specimen was tested for permeability with the waterproofing layer on top. After each test, the specimens were air-dried and the waterproofing layer removed for further testing. Figure 73 describes the permeability rate that was observed over time. A logarithmic scale was used over the time axis, as it was discovered that there was an exponential decrease in flow rate over time. From Figure 73 it is visible that there is still a steady rate of flow through the Specimen even with the addition of the waterproofing layer sprayed on top. This could be due to micro-cracks that formed on the surface and outer edges of the Specimen allowing water to flow through easier. However, when comparing the gradients of flow for both with and without waterproofing, it was observed that there is a steeper flow rate observed for the Specimen without the waterproofing layer.

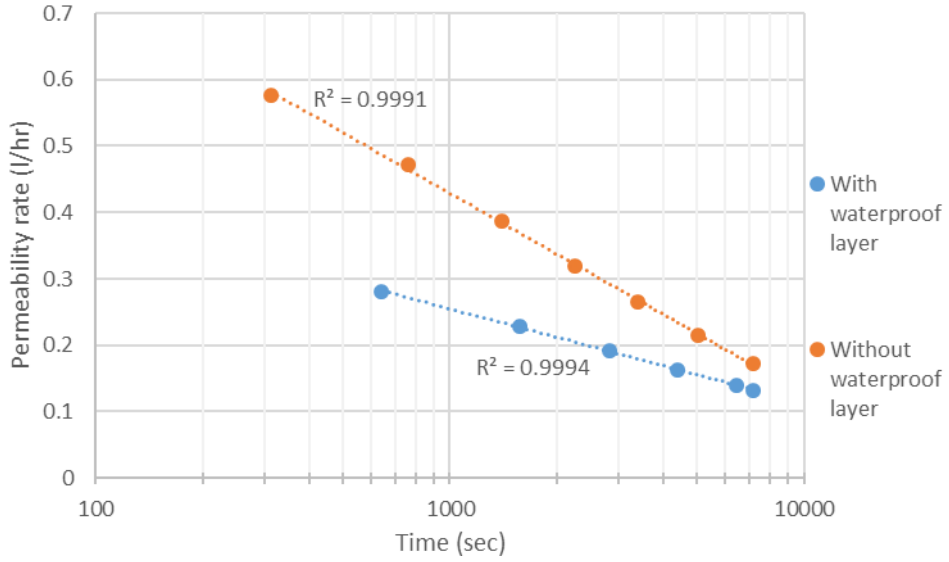

Figure 73 Permeability results of Specimen 2 from Kansanshi.

The results that were observed of Specimen 4 from Kansanshi are shown in Figure 74. Permeability testing was conducted on the Specimen with and without the waterproofing layer present. The Specimen was allowed to air-dry before the removal of the waterproof layer. From Figure 74 it is

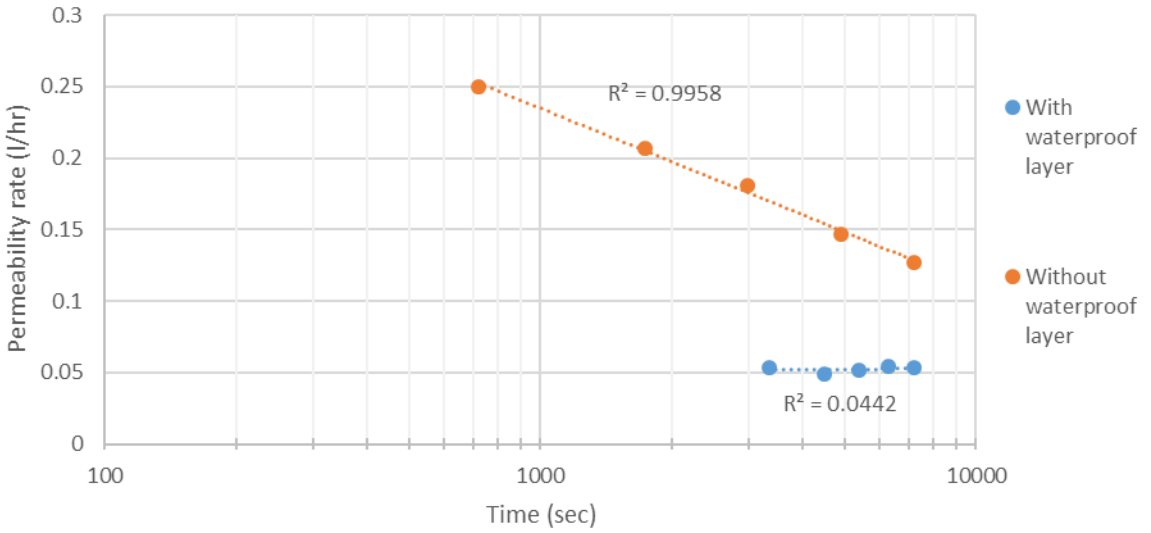

Figure 74 Permeability results observed of Specimen 4 from Kansanshi.

visible that with the addition of the waterproofing layer, almost no water penetrated through the Specimen with a constant rate of 0.05 litres/hour. This indicates that the Specimen remained mostly waterproof. After the removal of the waterproofing layer, a much steeper rate of flow was noted for the Specimen.

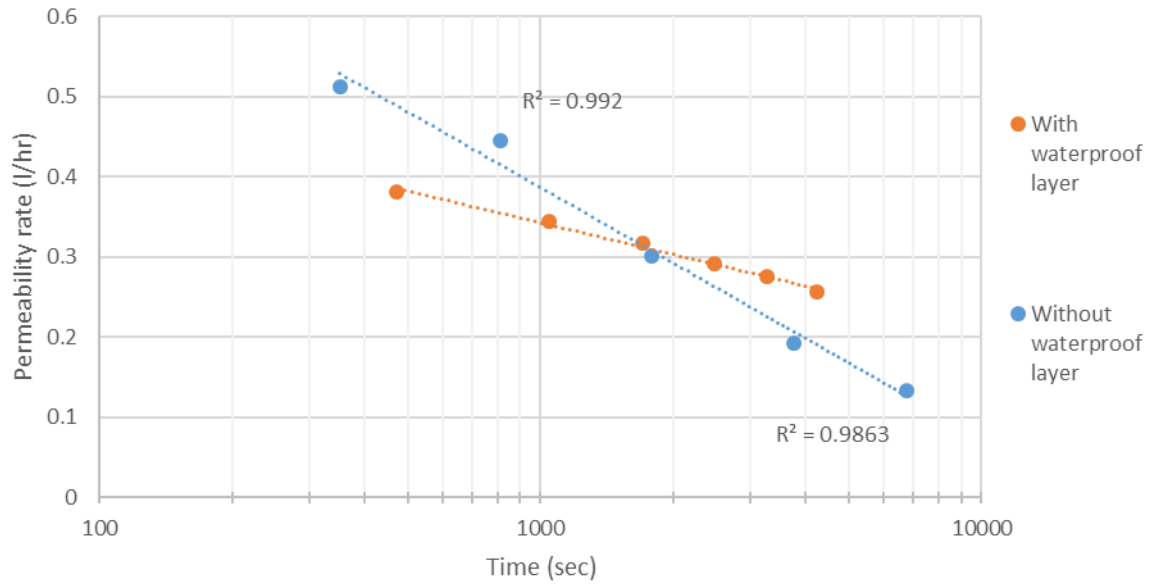

Figure 75 Permeability results plotted against time for Specimen 1 from Kalumbila.

For Specimen 1 from Kalumbila, the permeability results are displayed in Figure 75. The results indicate the permeability flow rate at 50 ml intervals. From this figure, it is visible that there is still a steady rate of flow through the Specimen even with the addition of the waterproofing layer sprayed on top. This could be due to micro-cracks that formed on the surface and outer edges of the Specimen allowing water to flow through easier. However, when comparing the gradients of flow for both with and without waterproofing, it was observed that there is a steeper flow rate observed for the Specimen without the waterproofing layer.

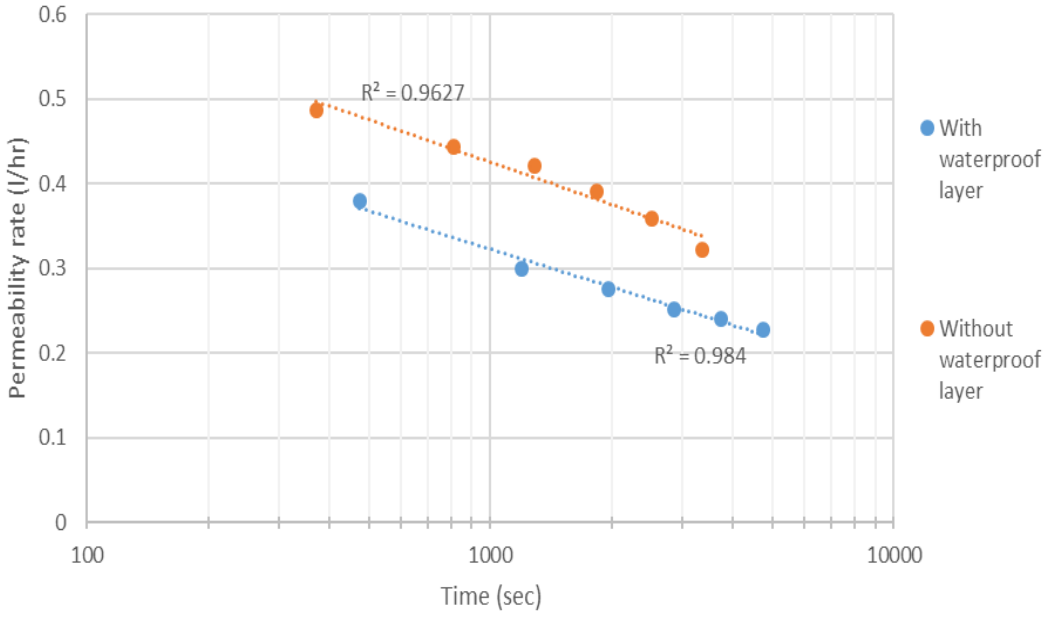

Figure 76 Permeability results for Specimen 3 for Kalumbila.

The results obtained for the last Specimen, 3 from Kalumbila, are shown in Figure 76 below. . From this figure it is visible that there is still a steady rate of flow through the Specimen even with the addition of the waterproofing layer sprayed on top. This could be due to micro-cracks that formed on the surface and outer edges of the Specimen allowing water to flow through easier. However, when comparing the gradients of flow for both with and without waterproofing, it was observed that for this Specimen the flow gradients were mostly identical. There is only a slight increase in flow gradient observed in the Specimen without the waterproofing layer.

When comparing the results obtained for all the Specimen with- and without the waterproofing layer, it was discovered that there is a similar trend between the majority of the specimens. In Figure 77 below it can be observed that 75 % of Specimens with the waterproofing layer are within the standard deviation of the average (indicated with the blue line). The same trend was observed for the majority of the Specimen with the top layer removed (average indicated by the yellow line). In both situations, Specimen 4 from Kansanshi displayed results that are significantly below the averages indicating the section performed exceptionally good.

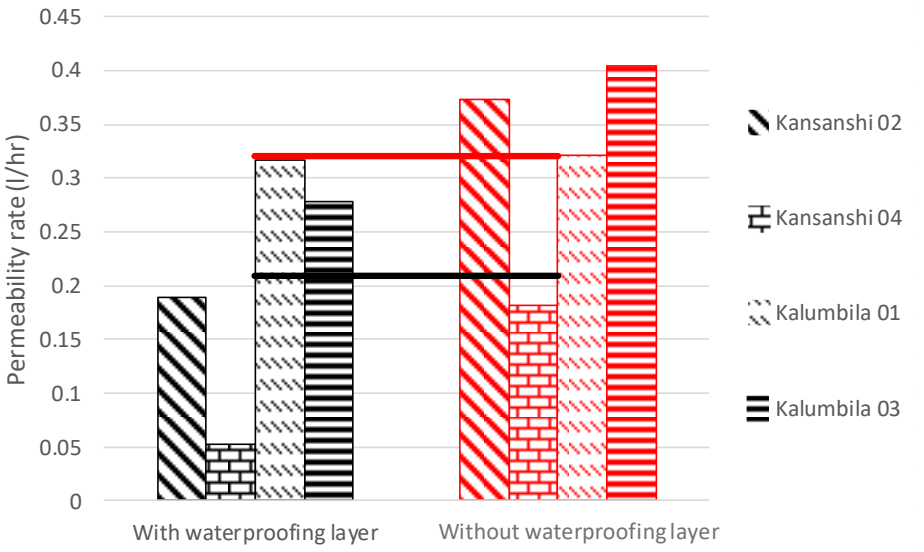

Figure 77 Comparison between waterproofing layer and non-waterproofing layer for both Mine Haul Roads.

Also, from Figure 77 it is clear that the dust palliative layer does protect the BSM base layer in terms of water intrusion. Less water intrusion into the BSM base layer would result in a stronger base layer, as water would lead to a decrease in shear strength.

4.9 Atterberg limits and linear shrinkage

Atterberg limits tests were performed on both Kansanshi and Kalumbila specimens. However, during the test procedures, it was determined that all Specimens were non-plastic. A plastic limit value could not even be obtained or calculated as the material already failed during the condition-ing taps. This indicates that in both mines, the material is cohesionless. It is unsure whether the

trichloroethylene from the binder recovery method could have impacted the cohesion of the material or if the material is just generally cohesionless. No untreated Specimens were available to test the hypothesis. For the linear shrinkage test, the material displayed no evidence of shrinkage occurring. According to the SAPEM document by South African National Road Agency Limited (2014), if the material showed signs of less than 0.5 % linear shrinkage, the material can be considered as non-plastic. This according to the Atterberg limits and linear shrinkage test, the material of both Kansanshi and Kalumbila can be considered as non-plastic.

4.10 Flakiness index results

This section will discuss the results obtained for the flakiness test procedure completed following the specification set out by TMH1 (1989). The flakiness results that were observed are tabulated in Table 20 below. A representative Specimen with a mass of approximately 1.3 kg was used to complete this test. The flakiness index was calculated for each fraction as indicated on the right-hand side of this table. From these results, it was discovered that the larger aggregate fraction, bigger than 26.5 mm particle size, had a flakiness index of 2.7. On the other hand, the particle fractions between 26.5 mm and 13.2 mm displayed flakiness indices between 18.6 and 30.0. The fraction of material between 10 mm and 5 mm displayed flakiness results of 14.4 and 10.2 respectively.

Table 20 Flakiness index results.

Size of the fraction to be gauged (Sieve size in mm)		Minimum length of slot (mm)	Width of slot (0.10 mm tolerance)	Mass passing	Flakiness Index
Passing	Retained				
37.5	26.5	75	18.75	35.5	2.7
26.5	19	53	13.25	390.6	30.0
19	13.2	38	9.5	284.1	21.8
13.2	9.5	26.4	6.6	242.2	18.6
9.5	6.7	19	4.75	191.4	14.7
6.7	4.75	13.4	3.35	133.1	10.2

According to a study completed by Barksdale and Itani (1989), it was found that shape and texture affect material density. Material density will ultimately influence the materials capability of resisting deformation under repeated loading (Resilient Modulus). Barksdale and Itani, (1989) further specified that large aggregate with smooth surfaces and round corners, which are also cubic, will lead to a reduction in the material packing capability which results in a lower density. Nataatmadja and Tan (2001) supported this statement and found that aggregates with flakier surfaces would result in lower Resilient Modulus values. This occurred due to the flakier aggregate breaking under repeated loading. Mishra (2020) specified that for base layer stabilized with bitumen, an ideal flakiness index value of 15 or less should be considered.

Considering the results obtained and correlating with the information mentioned, the higher flakiness indices provides an indication that the in-situ material can lead to higher compaction thus resulting in higher resistance to deformation under repeated loading. This is justified by the high Resilient modulus values determined in Section 4.4 as well as the high Monotonic Triaxial results discussed in Section 4.5. However, considering the large impact of repeated loading caused by Mine Haul Trucks, the high flakiness indices also provides insight into the high concentration of fines observed on both Kansanshi- and Kalumbila Trolley Ramps as large impacts loads can lead to the flakiness material breaking and creating more fines. The increase in fines can lead to a lack of cohesion resulting in the premature failure of the BSM-Base layers. Thus it is clear that not only should material grading be considered during the BSM mix design procedure, but also the flakiness indices of the material as there is a direct correlation between the high flakiness indices and the high concentration of fines within both Trolley Ramps.

4.11 Aggregate Crushing Value (ACV)

This section will list and discuss the results obtained for the ACV test procedure. A representative sample from both Kansanshi and Kalumbila was used for testing. The representative Specimen contained material from the upper particle size (50 mm to 5 mm) to determine what effect loading has on the larger aggregate. For the Kansanshi mine, a sample with a mass of 3.063 kg was used. The results obtained are tabulated in Table 21 below. From these results, it was discovered that 827 grams of material were produced after crushing. This results in an ACV of 27 % which is considered fairly high.

Table 21 ACV test results for Kansanshi.

Kansanshi	
Sieve Size (mm)	Mass Passing (gram)
14	1162
10	628
5	446
2	827

For the Kalumbila material, each particle size was weighed before- and after the test was completed. From this data, it was possible to identify at which particle size the biggest percentage change occurs. The results for the Kalumbila ACV test are shown in Table 22 below. Similarly, to the Kansanshi material, the massing passing the 2 mm sieve was recorded at 902.1 gram which results in an ACV of 28 %.

Table 22 ACV results for Kalumbila.

Sieve size (mm)	Mass before (gr)	Mass after (gr)	Difference (%)
20	236.1	118.7	50%
14	1016.4	447.2	56%
10	830.6	523.3	37%
7.1	683	425.5	38%
5	551	387.9	30%
2	N.A	475.5	ACV
Pan	N.A	902.1	28%

From Table 22, it is also evident that the coarser material (20 mm and 14 mm) display the most amount of change within their fractions, at 50 % and 56 % respectively. The smaller coarse fraction displays a rate of change between 30 – 37 %. From this, it can be deduced that, over time, the coarse material within the base layer will break down into smaller fractions. This is already visible within the grading analysis results as shown in Figure 71 and Figure 72.

4.12 Dynamic Indirect Tensile Test

This section discusses the results obtained for the Dynamic ITT procedure completed on Kalumbila specimens. Only 1 Specimen was tested from Kalumbila, as no other Specimens were left to perform structural testing on. The Specimen was tested at 4 different dynamic loads, namely: 300 N, 400 N, 600 N, and 900 N. A conservative choice was made and the loads were chosen according to the lowest ITS_{dry} value for Kalumbila (2.2 kN).

A breakdown of the load selections is shown in Figure 78 below. The results that were obtained are tabulated in Table 23 below. From this table, it can be observed that at lower loads, the highest resilient moduli were recorded. Also, at the higher loads, lower resilient moduli were recorded.

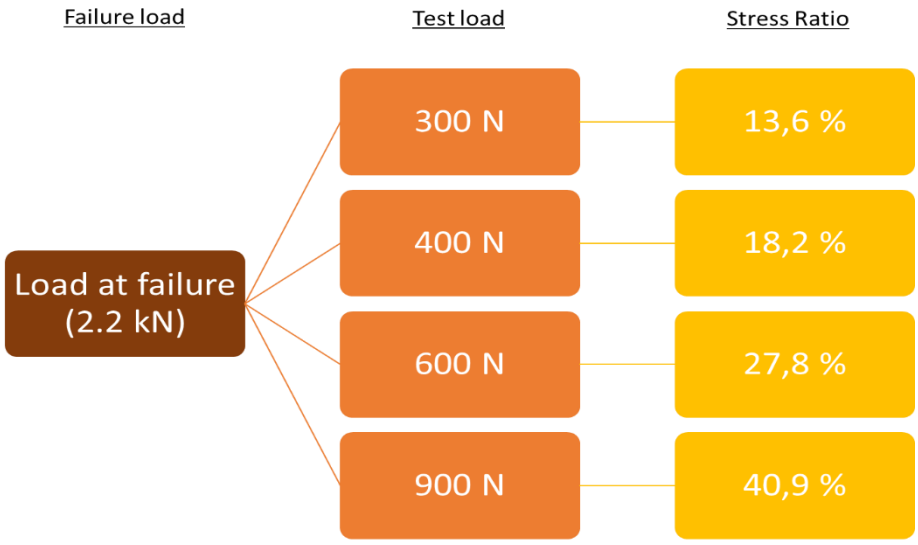

Figure 78 Stress ratios chosen for Indirect Tensile Test.

Table 23 Results obtained of dynamic indirect tensile testing.

	Resilient Modulus at each pulse (MPa)					
Loads (N)	Pulse1	Pulse2	Pulse3	Pulse4	Pulse5	Average
300	7721	8456	6838	7519	7855	7678
400	7317	6719	7326	6159	6626	6830
600	5527	5389	5725	5761	5434	5567
900	4858	4870	4829	4878	4713	4830

From Figure 79 it was also discovered that the decrease in Resilient Modulus followed a logarithmic pattern as the applied load increased. Both a linear, exponential, and logarithmic trend line was fitted to the data. The logarithmic data provided the best correlation coefficient which was 0.9867. This indicates that a logarithmic plot best describes the relationship between applied indirect tensile strength and Resilient Modulus.

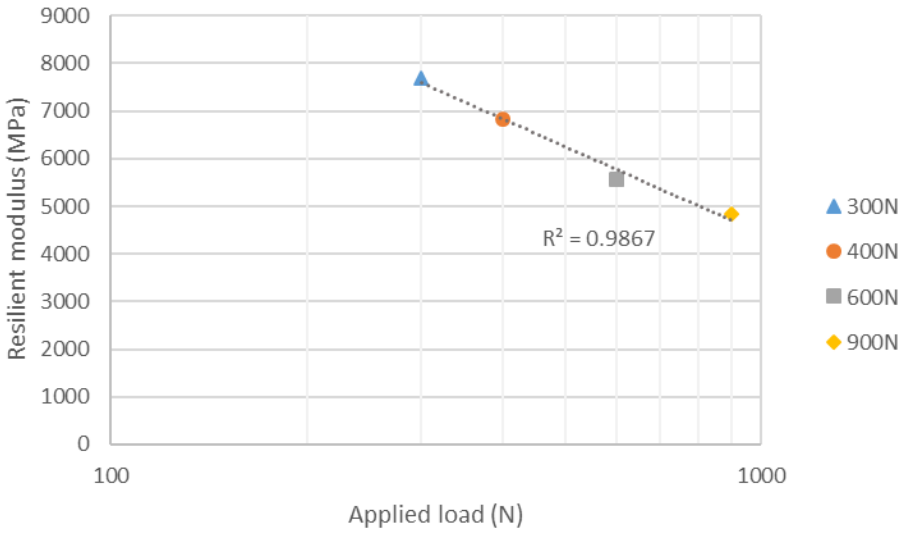

Figure 79 Average Resilient Modulus plotted against applied load.

The overall purpose of the ITT is to evaluate the relative quality of the material and to generate input values for pavement life analysis. This test can also be used to test the effects of temperature, loading rate, and rest periods (ASTM D4123, 1995). However, as only 1 specimen was available for testing, insufficient data is available to produce viable results for those aspects. With the results shown in Figure 79 some insight can still be provided into the expected life span of the BSM mix design. Considering the DSR discussed in Section 2.5.3.2, it is visible that as the load increase closer to the maximum allowed load, the measured Resilient Modulus decreases. This would indicate that with an increase in load, the overall pavement structure will be able to withstand less loading and lead to a shorter lifespan. Also, it is interesting to note that there is a logarithmic correlation between the increase in load and decrease in resilient modulus. The correlation would point out that the resilient modulus exponentially decreases as the applied load increases.

5 Pavement life analysis

5.1 Introduction

This section will aim to provide insight into the structural capacity of the BSM-emulsion base layer. To calculate the structural capacity, the Stress-Strain calculator provided by Rubicon solutions is implemented. With the analyzing tool, the Resilient Modulus can be back-calculated for the base layer, with assumed subbase moduli values. The back-calculated Resilient Modulus will be plotted against the failure envelopes calculated for each material type, and a comparison will be drawn to determine how close the current Pavement Structure is to reaching the failure envelope. These results will provide insight into the long term load spreading potential of the base layer.

5.2 Kansanshi Ramp

For the Kansanshi ramp, it is known that the base layer consists of a 200 mm layer, of which 150 mm is treated with emulsion and the other 50 mm is a granular material. The base layer is placed on top of a subbase layer of compacted rock, which is approximately 2 m in depth. Unfortunately, there is insufficient knowledge available for this layer, in terms of material type and shear failure properties etc. Thus a sensitivity analysis is considered to determine the Resilient Modulus of the base layer. The subbase layer is split into four sections, a 250 mm layer followed by another 250 mm layer, followed by a 500 mm layer, and finally, a 1000 mm layer which is also considered semi-infinite. The layout of the Pavement Structure is displayed in Figure 80 below.

From Figure 80, the three subbase iteration structures are also visible. In each iteration, the first two layers of the subbase will have Resilient Modulus values that will change. But, in all 3 iterations, the first layer of the subbase is considered as a design equivalent G5 material, the second layer is considered as a design equivalent G6, followed by the third layer is considered as a design equivalent G5 and the last layer is also considered as a design equivalent G5.

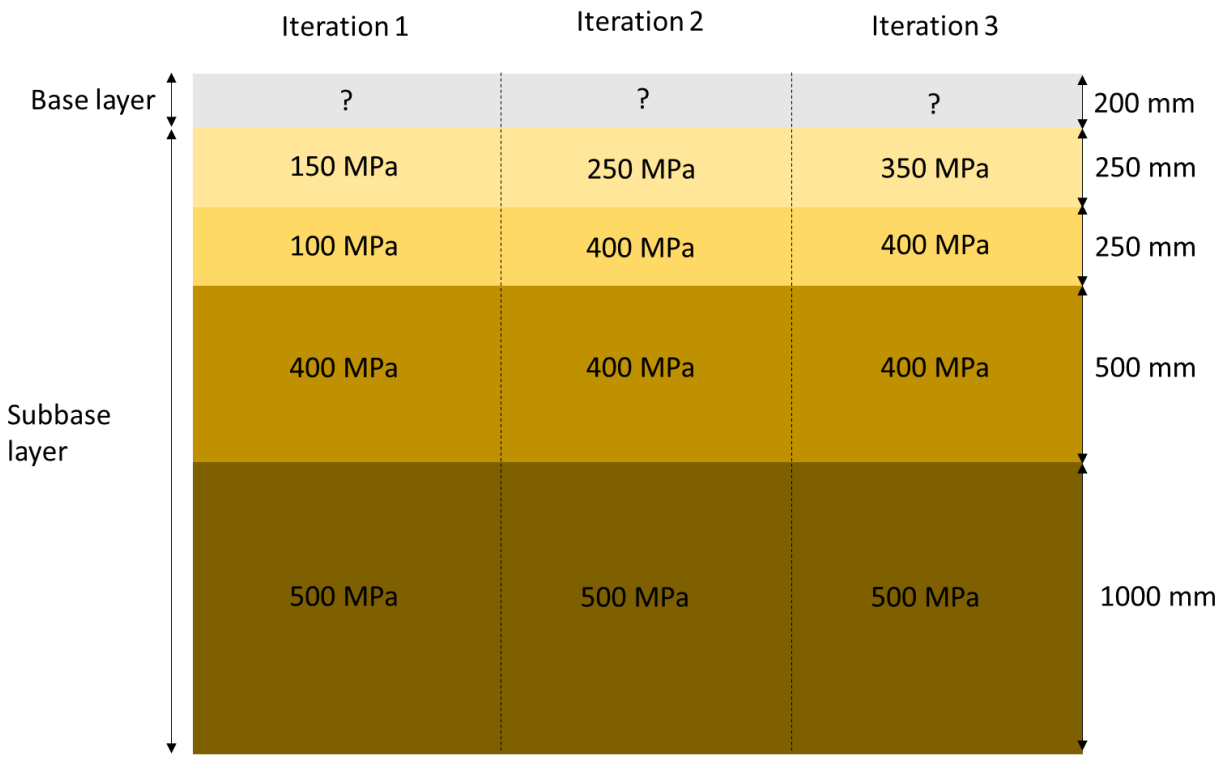

Figure 80 Base and Subbase layer configurations for Pavement analysis for Kansanshi.

For the initial setup of the Stress-Strain calculator, the base layers' Resilient Modulus was chosen as 2552 MPa. The value was calculated from the dynamic triaxial data that was gathered. To back-calculate the Resilient Modulus, the Mr-θ-$\sigma_d/\sigma_{d,f}$ model data was used. The constants k1-k4 were taken from Section 4.4.4 from the Mr-θ-$\sigma_d/\sigma_{d,f}$ model as it best describes the relationship between the Resilient modulus and Bulk Stresses. The following values were used within the spreadsheet as tabulated in Table 24 below. For this model, the input tire pressure was chosen as 700 kPa and the applied load used in the model was 500 kN as the Stress-Strain model does not consider loads bigger than 500 kN.

Table 24 Variables used for Resilient Modulus back calculations.

Resilient Modulus model variables			
K1 = 1022.52	K2 = 0.14	K3 = -0.005	K4 = -0.06
C=240 kPa		θ = 42 °	
Equation			
$Mr=k_1\theta^{k2}(1-k_3(\sigma_d/\sigma_{d,f})^{k4})$			

5.2.1 Results

For the first pavement structure, the base layers' Resilient Modulus was calculated to be 2784 MPa with a percentage difference of 0.05 %. The Major Principal Stress (σ_1) is 689.4 kPa and the Minor Principal Stress (σ_3) is 270.1 kPa. For the second pavement structure, the base layers' Resilient Modulus was calculated to be 2818 MPa with a percentage difference of 0.03 %. The Major- and Minor Principal Stresses for the second Pavement Structure are 697.9 kPa and 321.8 kPa respectively. For the third pavement structure, the base layers' Resilient Modulus was calculated to be 2816 MPa with a percentage difference of 0.14 %. For the final pavement structure, the Major- and Minor Principal Stresses are 688.3 kPa and 323.0 kPa respectively. The Mohr-Coulomb plot is shown in Figure 81 below for each pavement structure.

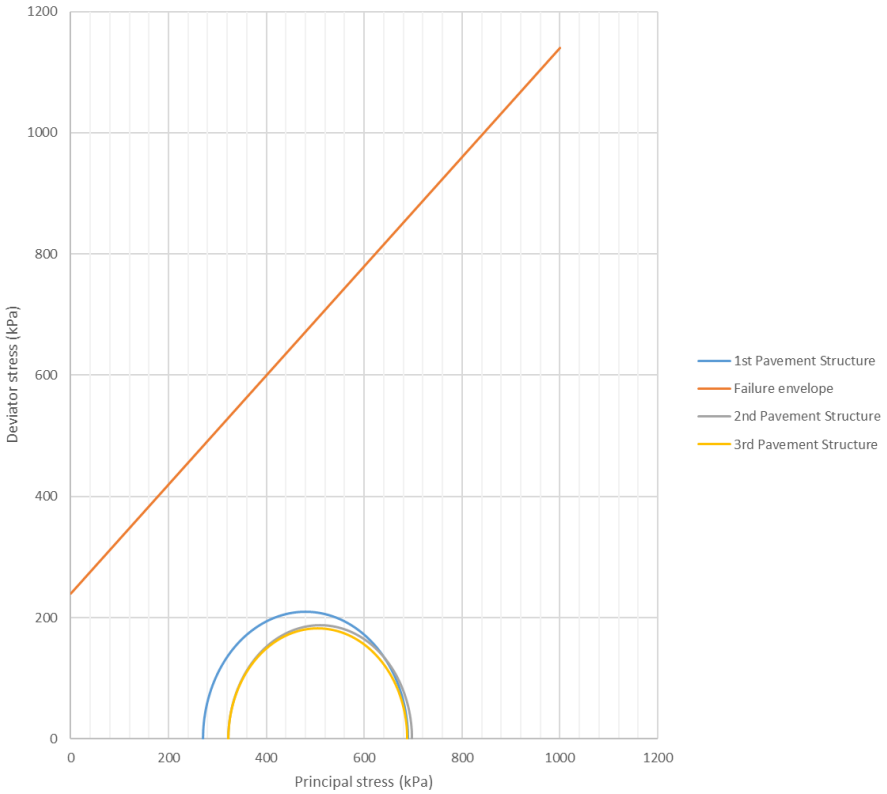

Figure 81 Major and minor principal stresses' Mohr-Coulomb plot for Kansanshi.

It can be observed from the figure above that Pavement Structure1 yields the largest deviator stress at 419.2 kPa. Pavement Structures 2 and 3 only yield deviator stresses of 376.1 kPa and 365.4 kPa

respectively. According to these results, Pavement Structure1 will be analyzed further for the deviator stress ratio. The DSR is calculated by dividing the deviator stress (σ_d) through the deviator stress at failure ($\sigma_{d,f}$). To calculate the deviator stress at failure, subtract the confining stress (σ_3) from the major principal stress at failure ($\sigma_{1,f}$). The major principal stress at failure can be calculated using the equation mentioned in section 3.3.5.

With the equation above, the major principal stress at failure is 2440.5 kPa. With confining stress of 270.1 kPa, the deviator stress ratio at failure can be calculated as 2170.5 kPa. Using the equation below, the DSR (in percentage) is calculated as 19.3 %. The difference between Pavement Structures 1's deviator stress and deviator stress at failure is displayed in Figure 82.

$$DSR = \frac{\sigma_d}{\sigma_{d,f}} \times 100$$

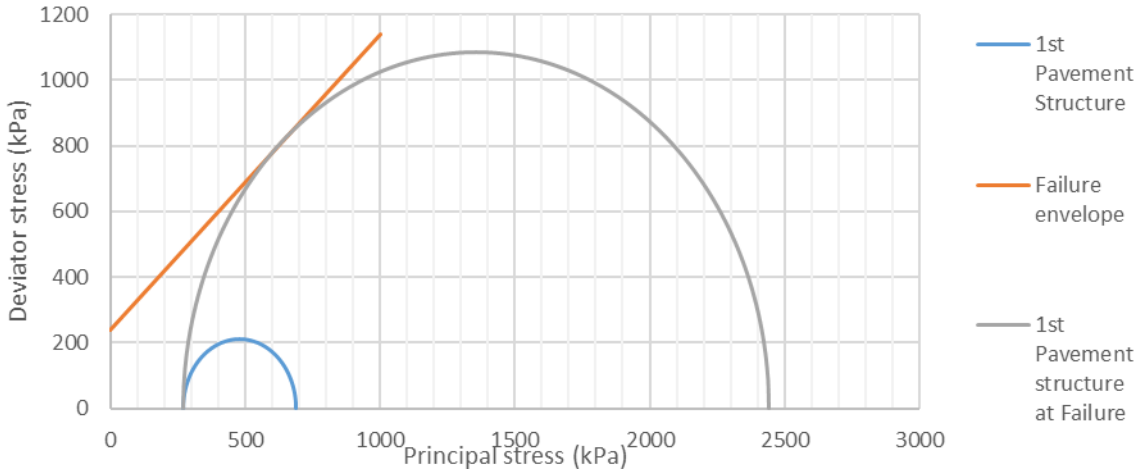

Figure 82 Pavement Structure1 compared to Pavement Structure1 at failure for Kansanshi.

To assess if the DSR is good or not, certain criteria has to be stipulated. According to the relationship between DSR and Pavement Life, Table 25 lists the typical Million Equivalent Standard Axles (MESAs) with respective DSRs. The pavement life values were calculated using the following values, cohesion of 250 kPa, friction angle of 40 °, retained cohesion of 70 %, and MDD of 100 %.

The Stellenbosch transfer function from the TG2 Guidelines by Sabita (2020) was used to determine expected load repetitions against given DSR ratios. The equation from Sabita (2020) is shown below.

$$\log N = A - 57.286(DSR)^3 + 0.0009159(P_{MDD} \times RetC)$$

Where
N |Number of axle repetitions to reach a set rut depth,
A |Reliability Coefficient linked to Road Category,
DSR |Deviator Stress Ratio (as a fraction),
P_{MDD} |BSM Dry Density (expressed as a percentage of MDD), and
RetC |Retained Cohesion (%).

Table 25 Categories to classify Pavement Life in terms of DSR.

Category	DSR (%)	MESAs (x10^6)
Very Poor	31-35	0.5-3.2
Poor	28-31	3.2-10.0
Moderate	21-28	10.0-50.0
Good	<21	50.0+

With this information in mind, the DSR for the Kansanshi ramp is calculated as 19.3 %. This DSR value indicates that the base layer displays good long term spreading potential. This DSR value also indicates that the base layer will be able to withstand high loading for 50+ MESAs without showing signs of structural damage. It should be noted that the DSR can increase slightly if mine haul trucks with carrying capacities of more than 400 Tons are considered. However, the analysis software only allows for wheel loads of up to 500 kN.

5.3 Kalumbila

For the Kalumbila ramps, two different base layer structures exist. The East Trolley Lane base layer consists of 200 mm G1 material with a maximum stone size of 26 mm. The top 100 mm of this layer is treated with SS60 emulsion. The West Trolley Lane base layer consists of a 200 mm layer of crushed stone with a maximum particle size of 75 mm. The top 75 mm of this layer is stabilized with SS60 emulsion. For both ramps, the subbase structure remains the same as specified in Figure 80. For both Trolley Ramps, the same testing conditions will be adhered to as specified in Figure 80 as well.

1. East Trolley Lane

For the east Trolley lane, the base layers' design life is determined according to the different sub-base moduli that are specified in Figure 80. Also, since the Specimens provided were too small for triaxial testing, the shear properties for the East Trolley Lane is assumed to be the same as those retrieved from the Kansanshi triaxial testing. The initial Resilient Modulus of the base layer is

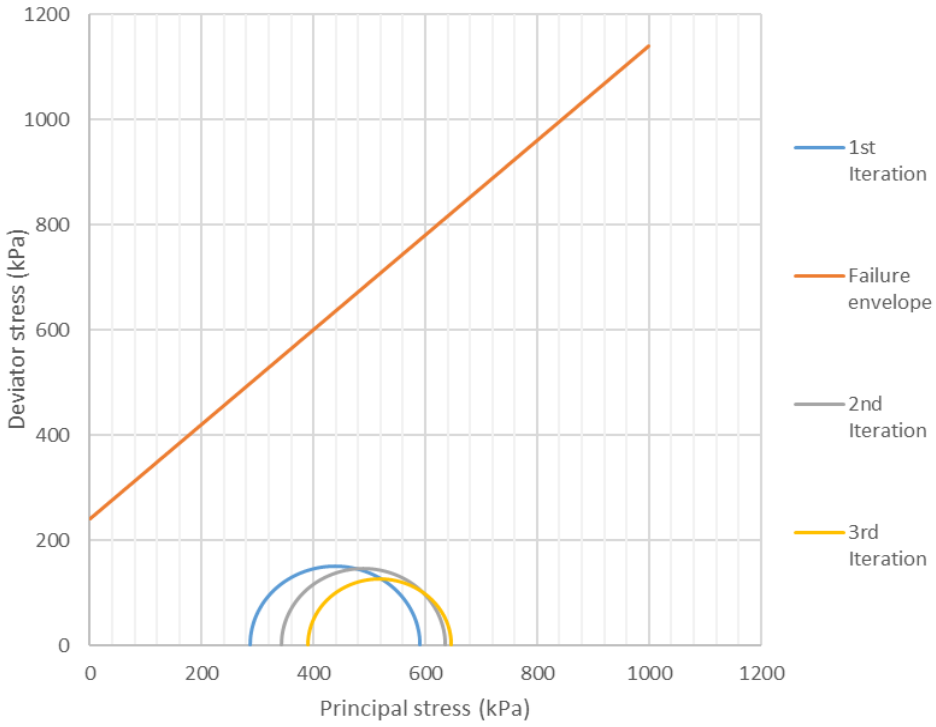

Figure 83 Mohr-Coulomb plot for each Pavement Structure from Kalumbila.

chosen as 6226 MPa. This value was calculated as the average indirect tensile modulus from the dynamic ITT procedure. With these conditions, the following results were obtained and are displayed in Figure 83.

For the first Pavement Structure iteration, the base layers' Resilient Modulus was calculated to be 2707 MPa with a percentage difference of 2.10 %. The Major Principal Stress (σ1) is 590.3 kPa and the Minor Principal Stress (σ3) is 278.2 kPa. For the second pavement structure, the base layers' Resilient Modulus was calculated to be 2773 MPa with a percentage difference of 1.42 %. The Major- and Minor Principal Stresses for the second Pavement Structure are 635.9 kPa and 343.1 kPa respectively. For the third pavement structure, the base layers' Resilient Modulus was calculated to be 2808 MPa with a percentage difference of 1.24 %. For the final Pavement Structure, the Major- and Minor Principal Stresses are 645.2 kPa and 390.9 kPa respectively.

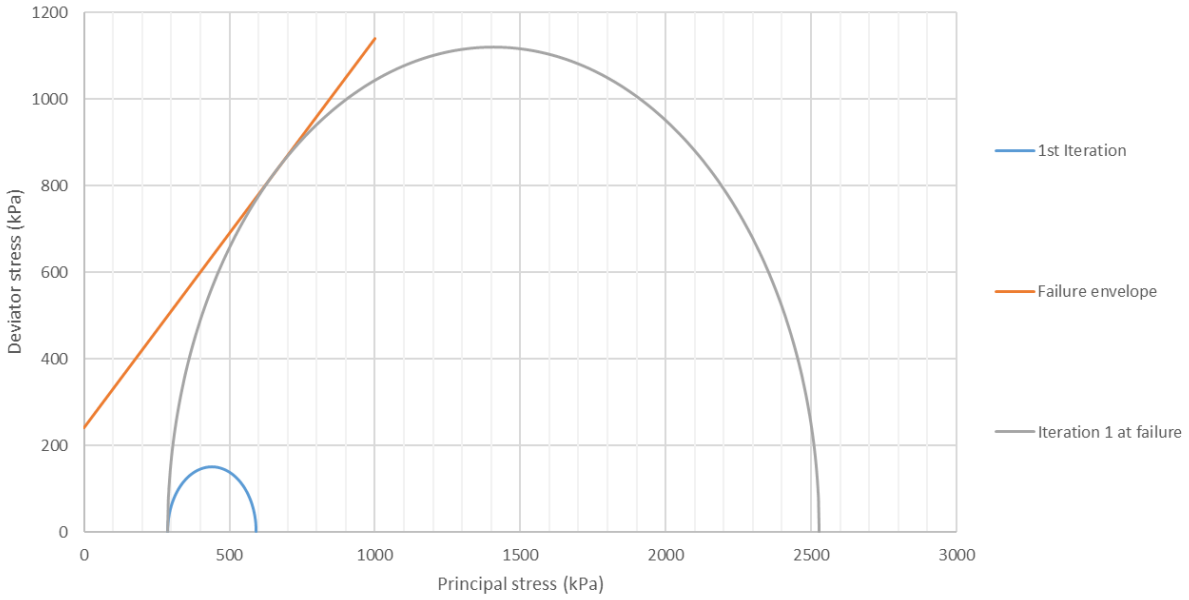

Figure 84 Deviator stress for Kalumbila iteration 1 compared to the deviator stress at failure.

From the values stated and as visible in the Mohr-Coulomb plot, the first Pavement Structure results in the biggest deviator stress in the base layer. To calculate the DSR for the Kalumbila ramps, the same equations are used as stated in the Kansanshi section.

Figure 84 above displays the comparison between the deviator stress (σ_d) calculated for the 1st Pavement Structure of Kalumbila versus the deviator stress at failure ($\sigma_{d,f}$). From this figure alone it is clear that the base layers' load spreading potential is remarkable. The DSR was calculated to be 13.5 %. This would place the base layers' performance within the 0-29 % DSR bracket. With these results, it can be stated that the layer can adequately spread the load through the subbase structure. Also, this base layer will be able to perform for several years before showing any signs of structural damage.

5.4 Conclusion

In this chapter, the load spreading potential for both the Kansanshi and Kalumbila Trolley Ramps were calculated. Several assumptions had to be made for both Subbase Layers' Resilient Modulus. However, to determine the sensitivity of these values, three different iterations were tested. Overall, on both ramps, the DSR fell between the ranges of 11-19 %. The low Deviator Stress Ratio indicates a combination of the Base Layers' good shear properties and resistance to permanent deformation as well as a well-balanced Pavement. The balanced Pavement results in good distribution of stresses provided by the pavement structure that carries extremely heavy mine traffic loads.

6 Conclusions and Recommendations

The purpose of this study was to determine the performance characteristics of bitumen emulsion stabilized material used for mine haul roads. To achieve these goals, a 5 phase process was followed.

- Phase 1: Determine the structural performance of both mine haul roads. This phase included all the destructive testing such as monotonic- and dynamic triaxial, ITS testing, and Dynamic ITT;
- Phase 2: Determine the permeability of the BSM layer with –and without the addition of a waterproofing layer;
- Phase 3: Identify the composition of the BSM-emulsion mixes, including the residual bitumen content;
- Phase 4: Determine the aggregate material properties through standard laboratory testing such as sieve analysis, Atterberg limits, Flakiness index, and Aggregate Crushing Value;
- Phase 5: Pavement Structure analysis in terms of DSR and Stress-Strain Resilient Modulus models.

Structural performance outcome:

- Initial ITS test results from Kansanshi indicate that with increasing residual bitumen content a noticeable increase in indirect tensile strength occurs. Also, with the soaked ITS results, higher strength values are observed at the higher residual bitumen contents.
- It is noticeable, however, that overall the ITS results are lower than expected with some specimens not even meeting the design criteria for a BSM2. It can be speculated that these cores had sustained previous structural damage due to the coring process, however further testing should be conducted to determine whether these values are outliers. Other reasons for the low ITS values can be due to the flakiness and Grading of the material. High flakiness material produces more fines under loading and the current grading already displays large quantities of fine material.

- For the monotonic triaxial testing, the mix design performed excellently with a cohesion of 240 kPa and a friction angle of 41.8 º. With these values, the mix design meets the criteria of a BSM1 material.
- For research purposes, the same specimens were tested again to determine how the material would perform after initial failure had occurred. Surprisingly, the material only dropped to a cohesion of 225 kPa with a friction angle of approximately 38 º.
- Dynamic triaxial data indicates that the material mix performs well under repeated loading, with an average Resilient Modulus of 2552 MPa.

- From the several models used to model the Resilient Modulus, it became clear that Models using confining pressure (σ_3) as the main variable are unable to accurately represent the data.

Permeability outcome:

- Permeability testing on the Kansanshi Specimens indicates that the material is quite permeable with- and without the waterproofing layer. However, there is a noticeable difference in permeability with the addition of a waterproofing layer. This would indicate that the waterproofing layer does work to some extent.

- Permeability testing on the Kalumbila Specimens indicates similar results to the Kansanshi specimens. Again, the material is quite permeable even with the addition of the waterproofing layer. However, there is still a noticeable difference in the permeability rate with the dust palliative added, thus indicating that the spray layer does work to a certain extent.

BSM composition outcome:

- From the binder recovery process, it is possible to determine the residual bitumen content (%) for each Trolley Ramp. For the Kansanshi Trolley Ramp, an average residual bitumen content of 2.2 % is calculated with a standard deviation between the specimens of 0.7%. These values indicate that there is some variability observed in the base layer.

- The binder recovery process on the Kalumbila Trolley Ramp results in an average residual binder content is 1.3 % with a standard deviation of 0.4 %. From these values, it is visible

that Kalumbila implemented less bitumen in their base layer. This would correlate with the lower ITS_{dry} values as well.

Material characterization outcome:

- For the material characterization, a full sieve analysis was conducted on each specimen for both Kansanshi and Kalumbila. For both Mines, the overall grading performs well with the coarser section of the grading fitting close to the upper limit (fine) of the grading specifications for BSM-emulsion mix designs.
- It is observed in both the Kalumbila and Kansanshi Trolley Ramps that the fractions between the 2.0 mm sieve and 0.075 mm contains excess fine material. This is also correlated with the low ITS_{dry} values.
- From the Atterberg limit test, the material for both Kansanshi and Kalumbila is determined to be non-plastic with linear shrinkage of less than 0.5%.
- The Flakiness Index tests values range between 18.6 to 30 between all the fractions. A typical flakiness index value for BSMs would be 15 or less and any value above would have a negative effect on the resistance to repeated loading.
- The ACV test determined that both Kansanshi and Kalumbila trolley ramps, under 400 kN of loading, produce approximately 28 % fines. Further analysis on the Kalumbila material also displays which fractions (from 20 mm to 5 mm) display the largest change in fraction mass between the 20 mm sieve fraction and the 14 mm sieve fraction.

Recommendations:

- For future studies, more Specimens can be tested to provide a good level of confidence in the results obtained. Currently, most specimens are used for multiple tests such as the monotonic and dynamic triaxial.
- Virgin in-situ aggregate can also be tested to create a viable mix design based on the current specifications to confirm whether a better mix design is possible or if the level of service is adequate for the current base layer.

- Further monotonic triaxial testing can also be conducted on soaked Specimens to determine what the retained cohesion of the current mix would be to obtain all three variables needed to classify the material according to BSM standards.

- To provide further permeability results regarding the BSM-Layers, High Pressure Permeability (HPP) testing can be conducted to determine the permeability of the Base Layer under constant pressure.

- The incorporation of BSM material in the Base Layer of mine haul roads does provide promising performance results indicating that the incorporation of BSM material provides better strength properties than conventional untreated materials such as G2 quality material.

- Also, the stress distribution between the 200 mm emulsion treated base layers and 2 m Subbase structures indicate that the pavement structures are well balanced and will provide adequate long term durability.

- The base layer thickness for both Kansanshi and Kalumbila Trolley Lanes yields adequate performance results as the DSR value range between 11-19 %. The low DSR values indicate that the base layers will be able to carry approximately 50+ MESAs.

Bibliography

Adams, T. (2020) *Dust suppression in haul mining roads - a historical perspective*. Available at: https://globalroadtechnology.com/global-road-technology-dust-suppression-in-haul-mining-roads/.

Annadale, W. (2012) *Permeability of Surfacing Seals*. University of Stellenbosch.

Anochie-Boateng, J., Paige-Green, P. and Mgangira, M. (2009) 'Evaluation of Test Methods for Estimating Resilient Modulus of Pavement Geomaterials', *Proceedings of the 28th Southern African Trannsport Conference (SATC 2009)*, (July), p. 254.

Asphalt Academy (2009) *Technical Guideline: Bitumen Stabilised Materials*.

ASTM D4123 (1995) 'Standard Test Method for Indirect Tension Test for Resilient Modulus of Bituminous', *Annual Book of American Society for Testing materiasl ASTM Standards*, 82(Reapproved), pp. 2–5.

Barksdale, R. D. and Itani, S. Y. (1989) 'Influence of aggregate shape on Base behavior', *Transportation Research Record*, (1227), pp. 173–182.

Bradshaw, L. C. (1960) *Paint Technology*, *24*.

Chemoran (2016) 'AFM: Amphoteric emulsion specifications'. Colas, p. 2. Available at: https://www.colas.ie/uploads/datasheets/AFM.pdf.

Committee for State Road Authorities (1990) *TRH20: The structural design, construction and maintenance of unpaved roads, Technical Recomendations for Highways*. Department of Transport.

Committee of Transport Officials (COTO) (2016) *MANUAL FOR VISUAL ASSESSMENT OF ROAD PAVEMENTS Par t E: Unpaved Roads*. Edited by Roads Coordinating Body (RCB), Committe of Transport Officials (COTO), and Road Asset Management Systems (RAMS) Subcommittee. The South African National Roads Agency SOC Limited.

Dal Ben, M. and Jenkins, K. J. (2014) 'Performance of cold recycling materials with foamed bitumen and increasing percentage of reclaimed asphalt pavement', *Road Materials and Pavement*

Design, 15(2), pp. 348–371. doi: 10.1080/14680629.2013.872051.

Ebels, L.-J. and Jenkins, K. J. (2007) 'Mix design of bitumen stabilised materials: Best practice and considerations for classification', *Proceedings of the 9th Conference on …*, (September), pp. 213–232. Available at: http://www.researchgate.net/profile/Lucas_Jan_Ebels/publication/268395132_MIX_DESIGN_OF_BITUMEN_STABILISED_MATERIALS_BEST_PRACTICE_AND_CONSIDERATIONS_FOR_CLASSIFICATION/links/5536290f0cf268fd001612a7.pdf.

EN-12697-3 (2013) *Bituminous Mixtures - Test Methods for Hot Mix Asphalt - Part 3: Bitumen Recovery: Rotary Evaporator*.

Ferry, A. G. (1986) *Unsealed roads: a manual of repair and maintenance for pavements.* RRU Techni. Wellington, New Zealand: National Roads Board.

Goosen, E. S. (2021) *Modelling of Surfacing Seal Binder Ageing and Rheology*. Univeristy of Stellenbosch.

Heath, W. and Robinson, R. (1980) *Review of published research into the formation of corrugations on unpaved roads.* Department of Environment, Dept of Transport, Crowthorne.

Holleran, G. (2009) 'Effect of storage and handling on high binder emulsions.' Available at: http://www.slurry.com/index.php/magazine-articles/163-effect-ofstorage-%0Aand-handling-on-high-binder-emulsions.html.

James, A. (2006) 'Overview of asphalt emulsion.', *Transportation research circular*, (August), pp. 1–15.

James, A. and Zhou, Q. (2012) 'Modified Bitumens Derived From Particle Stabilized Emulsions', (June 2012), pp. 13–15.

Jenkins, K. J. (2000) *MIX DESIGN CONSIDERATIONS FOR COLD AND HALF-WARM*. University of Stellenbosch.

Jenkins, K. J. and Collings, D. C. (2017) 'Mix design of bitumen-stabilised materials–South Africa and abroad', *Road Materials and Pavement Design*, 18(2), pp. 331–349. doi:

10.1080/14680629.2016.1213511.

Jenkins, K. J., Greyling, A. H. and Collings, D. . (2021) 'Bitumen Stabilization of Base Layers for Pavement Rehabilitation reaches Greater Heights', in *International Airfields and Highway Pavements Conference, ASCE*.

Jenkins, K. J. and Rudman, C. E. (2019) *Hitchhikers Guide to Pavement Engineering*. University of Stellenbosch.

De Jonghe, A. C. . *et al.* (2005) *Onderzoek naar de compatibiliteit van bindmiddelen bij gebruik van asfaltpuingranulaat.*

Kashaya, A. A. (2013) *Surface Run-off Behaviour of Bitumen Emulsions used for the construction of seals*. University of Stellenbosch.

Kazemi Esfeh, H., Ghanavati, B. and Shojaei Arani, R. (2010) 'The factors affecting on bitumen emulsion properties', *ICCCE 2010 - 2010 International Conference on Chemistry and Chemical Engineering, Proceedings*, (Iccce), pp. 55–59. doi: 10.1109/ICCCENG.2010.5560360.

Kennedy, T. W. and Hudson, W. R. (1968) 'Application of the Indirect Tensile Test To Stabilized Materials', *Highway Research Board*, (235), pp. 36–48. Available at: http://onlinepubs.trb.org/Onlinepubs/hrr/1968/235/235-004.pdf.

Kitchell, A., Kuchar, B. and Viqueira Rios, R. (2021) 'Unpaved Road Standards for Caribbean and Pacific Islands', *Prepared for the NOAA Restoration Center and Coral Reef Conservation Program*, pp. 1–71.

Long, F. and Theyse, H. (2004) 'Mechanistic-Empirical Structural Design Models for Foamed and Emulsified Bitumen Treated Materials', *Proceedings of the 8th Conference on Asphalt Pavements for Southern Africa (CAPSA'04)*, (September), p. 102.

Manolis, S. (2010) 'Asphalt Emulsion Manufacturing 101', in *Niagara Falls: 2010 Asphalt Emulsion Manufacturing Association, Asphalt emulsion technologies workshop*. Available at: http://www.aema.org/index.php?option=com_docman&task=doc_view&gid=401&Ite%0Amid=46.

Mazibuko, N. mandy A. (2020) *Potential for Recycled Concrete Aggregate Stabilisation with Bitumen Emulsion and Foamed Bitumen . by*. University of Stellenbosch.

Meyer, M. D. (1999) 'Bitumen emulsion', *Akzonobel Surface Chemistry*, p. 31. Available at: https://sc.akzonobel.com/en/asphalt/Documents/AN_Asphalt_Emulsion_TB_eng.pdf.

Mishra, G. (2020) *Flakiness Index and Elongation Index Test on Coarse Aggregates*. Available at: https://theconstructor.org/transportation/shape-tests-on-aggregates/1397/.

Mturi, G. *et al.* (2015) 'A Review Towards a National Bitumen Extraction-Recovery Method.'

Muller, J. (2011) *Bitumen Emulsions*.

Muller, J., Sadler, D. and Van Zyl, G. . (2012) 'Bitumen emulsions in sprayed seals: experience and current best practice in South Africa', *ISAET (International Symposium on Asphalt Emulsion Technology*.

Mulusa, W. K. (2009) *Development of a Simple Triaxial Test for Characterising Bitumen Stabilised Materials, University of Stellenbosch*. University of Stellenbosch.

Nataatmadja, A. and Tan, Y. L. (2001) 'Resilient response of recycled concrete road aggregates', *Journal of Transportation Engineering*, 127(5), pp. 450–453. doi: 10.1061/(ASCE)0733-947X(2001)127:5(450).

National Resources Conservation Services (2007) 'Natural Resources Conservation Service (NRCS) soils', *Choice Reviews Online*, 44(02), p. 44. doi: 10.5860/choice.44-0917.

Needham, D. (1996) *Developments in bitumen emulsion mixtures for roads*. University of Nottingham.

van Niekerk, A. A. (2002) *Mechanical Behaviour and Performance of Granular Bases and Sub-bases in Pavements*. Delft University of Technology.

van Niekerk, A. A. and Huurman, M. (1995) *Establishing Complex Behaviour of Unbound Road Building Materials from Simple Material Testing*. Delft University of Technology, Netherlands.

Paige-Green, P. (1989) 'The influence of geotechnical properties on the performance of gravel

wearing course materials', *UPSpace*, (2017), p. 1:296. Available at: https://repository.up.ac.za/handle/2263/63129.

Peri, E., Ibsen, L. B. and Nordahl Nielsen, B. (2019) 'Influence of sample slenderness and boundary conditions in triaxial test – A review', *E3S Web of Conferences*, 92, pp. 1–6. doi: 10.1051/e3sconf/20199202009.

Redelius, P. and Walter, J. (2005) *Bitumen emulsions*. 6th edn, *Emulsions and Emulsion Stability, Second Edition*. 6th edn. Shell International Petroleum Company Ltd. doi: 10.1201/9781420028089.ch11.

Sabita (2011) 'Manual 30: A guide to the selection of bituminous binders for road construction'. South Africa: Sabita, pp. 1–47.

Sabita (2014) *TG1: Technical Guideline, Dictionary Geotechnical Engineering/Wörterbuch GeoTechnik*. Edited by H. Herrmann and H. Bucksch. Sabita. doi: 10.1007/978-3-642-41714-6_200286.

Sabita (2020) *TG2 : Bitumen Stabilised Materials Southern African Bitumen Association (Sabita)*. Edited by D. Collings et al.

SANS (2012) *SANS 3001-BT12 : 2012 SOUTH AFRICAN NATIONAL STANDARD Civil engineering test methods Part BT12 : Determination of the in situ permeability of a bituminous surfacing (Marvil test)*. Edited by SABS Standards Division.

SANS (2013) *SANS 3001-GR1:2013. Civil engineering test methods. Part GR1: Wet preparation and particle size analysis*. 1.2. SABS Standards Division.

SANS 3001 (2011) *Part AS20: Determining of the Soluble Binder Content and Particle Size Analysis of an Asphalt mix, South African National Standard*.

Schwitzer, M. K. (1972) *Chemistry and Industry*, *21*.

Semugaza, G. (2016) *Comparative Shrinkage Properties of Pavement Materials Including Recycled Concrete Aggregates With and Without Cement Stabilisation*. University of Stellenbosch.

South African National Road Agency Limited (2014) *Chapter 4 Standards*. Second. SANRAL SOC LTD.

Suleiman, M. (2006) *TO CONVERT BITUMEN POWDER TO BITUMEN EMULSION*. University College of Engineering & Technology Malaysia.

Thompson, R. J. and Visser, A. T. (2006) 'Selection and maintenance of mine haul road wearing course materials', *Institution of Mining and Metallurgy. Transactions. Section A: Mining Technology*, 115(4), pp. 140–153. doi: 10.1179/174328606X155138.

TMH1 (1986) 'Method B1: Aggregate Crushing Value'. South Africa, pp. 118–120.

TMH1 (1989) 'Method B3T: Flakiness index', pp. 3–5.

Tredoux, C. (2020) *Rheological Performance of Seals in South Africa Based on Binder Ageing Considerations*. University of Stellenbosch. Available at: https://scholar.sun.ac.za.

Venter, C. (2019) *Asphalt Permeability and Moisture Damage, Notes and Queries*. University of Stellenbosch.

Werner, S. (2021) *Flange Bolt-Up - Torque Tightening, Preload, Torque procedures, Torque Sequence, Torque Wrenches, Preparation Flange Bolt-Up*. Available at: http://www.wermac.org/flanges/flanges_torque-tightening_torque-wrenches.html.

Williams, R. E. O. (1969) 'Laboratory Handbook', *Bmj*, 1(5638), pp. 239–239. doi: 10.1136/bmj.1.5638.239-c.

Wirtgen GmbH (2012) *Cold Recycling Technology*. Wirtgen.

Appendix A

1. ITS Test Apparatus

1.1. A compression testing machine

A machine capable of applying a compression force onto a Specimen at a constant strain rate of 50.8 mm per minute. This compression machine should also be able to reach a maximum load of at least 30 kN. The machine should also be capable of measuring the displacements accurately to the closest 0.1 mm and applying load to the closest 0.05 kN.

1.2. ITS load frame

The ITS load frame consists of numerous parts that are linked together. Firstly, to keep the Specimen in place, two loading strips of 19 mm x 20 mm x 220 mm are required. For Specimen's that are 100 mm in diameter, the strips are changed to 12 mm x 20 mm x 220 mm loading strips. The surfaces of these loading strips exposed to the sample are slightly mechanically curved to a radius of 76 mm ± 1 mm. These loading strips move towards each other on vertical frame guides. The vertical frame guides are made from 10 mm Ø mild steel rods that are 175 mm in height and are attached to a mild steel base plate. The base plate can be shifted to align the Specimen with the Compression machine's loading rod.

When looking at the load frame, it can be understood that the bottom load strip is rigid, whereas the top load strip can move unobstructed vertically to accommodate the loading of the Specimen. Sabita (2020) also pointed out that there are extras that can be added to the loading frame such as load transfer plates, load cell and automatic data logger.

1.3. Load transfer plate

A load transfer plate can be added to the top-loading strip to ensure that no deformation occurs when the load is being transferred from the compression testing machine to the top of the loading strip. The load transfer plate can be round, square, or a steel ball with a diameter of 19 mm. The dimensions of the load transfer plate should be slightly larger than the Specimen being tested. Asphalt Academy (2009) added that a ball bearing should not be used between the load transfer plate and the piston.

1.4. Drying oven

A continuous forced-draft drying oven that can maintain temperatures of 40±1 ºC. The oven should also be thermos-statically controlled and be able to take at least 240 litres of material.

1.5. Water bath

A water bath is needed that can hold water with a depth of at least 150 mm. The bath should also have a perforated bottom at a height of 25 mm. The water should stay constant at 25±1 ºC with the assistance of a thermostat controller and a circulation mechanism.

1.6. Digital thermometer

A digital thermometer was used to measure the internal temperature of the core with an accuracy of ±0.1 ºC.

1.7. Carrier plates

Carrier plates are made from plywood and are used to transport the compacted specimens. They can be square or round with a thickness of approximately 15 mm.

2. Monotonic Triaxial Test Apparatus

2.1. Triaxial cell

The triaxial cell is used to confine the Specimen with the accompanying bladder during loading, thus acting as a confinement chamber. The cell consists of a circular base plate. The base plate has flat bottom unlike the dynamic triaxial. This allows for easier alignment of the completed triaxial cell with the fixed actuator. Also, the consistent load is applied to the Specimen creating friction between the base plate and the fixed reaction arm, keeping the Specimen in place. A hollowed-out cylindrical frame is bolted onto the base plate. This circular frame should have sufficient dimensions to accommodate a 152 mm circular sample with a height of 300 mm and also an inflatable rubber bladder. On top of the cylindrical frame, another hollow plate is fixed which would house the balancing plate.

2.2. Rubber bladder

According to Williams (1969), the rubber bladder used to apply the confining pressure to the Specimen must have an inner diameter of 160 mm ± 5.0 mm. The bladder should also be 300 mm in height. It should be noted that the pressure applied to the bladder should never exceed 250 kPa as the triaxial cell is only designed to withstand a maximum pressure of around 250 kPa.

2.3. Air compressor

An air compressor unit is required to inflate the confinement chamber to a maximum confinement pressure of 200 kPa ± 2.5 kPa. Asphalt Academy (2009) and Williams (1969)also noted that attached to the air compressor should be a pressure gauge that gives the user the ability to adjust the pressure in 1 kPa increments.

2.4. Water bath

A water bath is needed that can hold water with a depth of at least 350 mm. The bath should also have a perforated bottom at a height of 25 mm. The water should stay constant at 25±1 ºC with the assistance of a thermostat controller and a circulation mechanism.

2.5. Force-drafted drying oven

A continuous forced-draft drying oven that can maintain temperatures of 40±1 ºC. The oven should also be thermostatically controlled and be able to take at least 240 litres of material.

2.6. Compression testing machine

A compression testing machine is required that can apply up to 200 kN of force onto the triaxial cell with an accuracy of ±0.1 kN. The machine should have enough clearance to seat the assembled triaxial cell. The machine should also be expected to apply the vertical force at a constant rate of 3mm/min. While applying these constantly increasing loads, the machine should also be able to gather data of the vertical force applied and vertical displacement with an accuracy of 0.05 kN and 0.05mm respectively. Williams (1969) and Asphalt Academy (2009) also described that the geometric layout of the machine should consist of a moving actuator which is situated above the triaxial cell and a fixed reaction base on which the triaxial cell rests.

2.7. Carrier plates

Carrier plates are made from plywood and are used to transport the compacted Specimens. They can be square or round with a thickness of approximately 15 mm.

2.8. Digital thermometer

A digital thermometer was used to measure the internal temperature of the core with an accuracy of ±0.1 ºC.

Appendix B

Test procedure

For the grading analysis, each Specimen previously recovered is tested apart. Seeing as the grading analysis does not focus on the determination of the plasticity index, each Specimen was washed with water over the 0.075 mm sieve to remove most 'Pan' fines. Each Specimen was emptied into a steel pan and dried in a forced-draft oven at 110 ºC for 24 hours. This is to ensure that all material is moisture-free to allow fines to move easier between the finer sieves. The dry weight of each Specimen is observed and tabulated.

From here, the Specimens are riffled through the grading sieves to determine the masses retained in each fraction. Since the stone used within the Specimens are in-situ material from the mines, and the visual study identified some aggregates that were larger than stone sizes specified for emulsion stabilized material, all the sieves were used. The sieve sizes were: 50-, 37.5-, 28-, 20-, 14-, 10-, 7.1-, 5-, 2-, 1-, 0.6-, 0.425-, 0.3-, 0.15-, 0.075 mm, and the pan. Figure 85 below displays the 16 sieves that were used to determine the particle size distribution.

After the material has been vibrating for a while, each sieve is cleaned and removed individually. The aggregate retained in each sieve is weighed and tabulated. Using this information, the percentage passing each sieve can be calculated using the equation below.

$$P_{\%_n} = 100 - \left(\frac{M_{ret}}{M_{tot}} \times 100\right)$$

Where
$P_{\%}$ |Percentage passing respective sieve (%),
n |Referring to the sieve size (mm),
M_{ret} |Mass of aggregate retained on respective sieve (g), and
M_{tot} |Total dry mass of Specimen (g).

With this data, it is also possible to calculate the grading modulus of each material blend using the equation below. Semugaza (2016) defined grading modulus as the indicator for the quality of material that is used within the pavement structure. A grading modulus of more than 2 would indicate

that a material is coarsely graded and would be of good quality. Similarly, a grading modulus smaller than 2 would indicate that a material is of poor quality due to the abundance of finely grained material(South African National Road Agency Limited, 2014).

$$GM = \frac{P_{2.00mm} + P_{0.425mm} + P_{0.075mm}}{100}$$

Where

GM |Grading modulus (%),
n |Referring to the sieve size (mm),
M_{ret} |Mass of aggregate retained on respective sieve (g), and
M_{tot} |Total dry mass of Specimen (g).

Figure 85 Grading sieves used in accordance with SANS 3310-1,2 stand-

Using Table 26 below, a graph can be created to display the minimum and maximum ranges applicable for emulsion or foam mixes. Each Specimens grading result can be plotted within this graph to establish which grading fractions are correct and which fall outside of the allowable boundaries.

Table 26 Lower and upper limits for BSM grading characteristics (from Sabita (2020)).

Sieve Size (mm)	Percentage passing each sieve (%)			
	Target grading for BSM Emulsions		Target grading for BSM Foam	
	Lower Limit	Upper Limit	Lower Limit	Upper limit
50	100	100	100	100
37.5	87	100	87	100
28	76	100	76	100
20	65	100	65	100
14	55	100	55	100
10	47	89	48	89
7.1	40	78	41	78
5	34	68	35	68
2	22	48	25	48
1	15	37	18	37
0.600	11	30	12	30
0.425	9	26	10	26
0.300	7	22	8	22
0.150	5	15	3	15
0.075	4	10	2	10

Appendix C

1. Test apparatus

1.1. Open-ended steel cylinder

An open-ended steel cylinder is required to be used as the confinement chamber when crushing the aggregate. The cylinder should be approximately 150 mm in diameter. A separate plunger is required, with the same diameter as the cylinder, to be fitted on the open-ended side of the cylinder. Figure 86 displays the schematic of the steel cylinder with the accompanying plunger.

1.2. Taming rod

The tamping rod required should be made of metal with a diameter of 16 mm and a length of 450 to 600 mm. TMH1 (1986) also specifies that one end of the rod should be hemispherical.

1.3. Balance

A balance is required to weigh material up to 3000 g. The balance should be accurate to the nearest 1 gram.

1.4. Sieves

13.2 mm, 9.5 mm, and 2.36 mm sieves following the specification set out by SABS 197 are required to sieve the material before- and after the test.

1.5. Compression testing machine

A compression testing machine is required which should be able to apply a load of up to 400 kN. The machine should also be able to increase the load at a constant rate over 10 minutes.

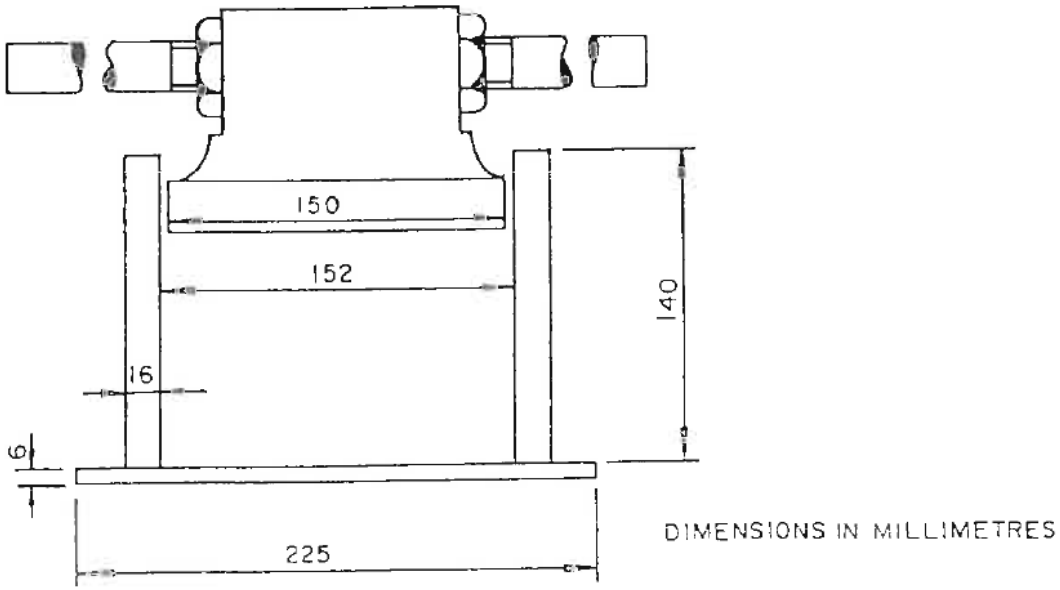

Figure 86 Steel cylinder with plunger and base plate (from TMH1, 1986).

2. Test procedure

For this test method, both a dry and wet version can be performed. The dry alternative will be discussed first, followed by the wet alternative.

To start, a representative sample should be acquired to perform the initial sieve process. The representative sample is put through a set of sieves and the fraction passing the 13.2 mm sieve but retained on the 9.5 mm sieve is used. This process should be repeated until enough material is available to fill up the cylindrical measure. Once enough material is procured, it is spread out on a thin tray a put in a force-draft oven at 110 ºC ± 1.0 ºC for at least 4 .

Once the material has been dried completely, the cylindrical measure can be filled in three separate layers. Each layer should be tamped with the tamping rod for 25 repetitions. With all three layers placed and tamped, the level side of the tamping rod is used to level off the surface of the material. With the material levelled off, the mass can be observed and tabulated. The same material can be inserted into the cylinder used for testing in three separate layers. Each layer should also be tamped for 25 repetitions. Once the material is tampered, the surface can be levelled and the plunger added.

With the material placed within the cylinder, the finished apparatus can be placed in the compression testing machine. A constantly increasing loading can be applied to the material until a maximum load of 400 kN is reached. The maximum load should be reached within a time frame of 10 minutes. As soon as the maximum load was achieved, the material can be removed and placed onto the 2.36 mm sieve. A sieve analysis is performed and the mass passing the 2.36 mm sieve is weighed. To calculate the percentage fines that was produced by the crushing, the following equation can be used.

$$ACV = \frac{M_{2.36mm}}{M_{total}} \times 100$$

Where

ACV	|Aggregate crushing value (%),
$M_{2.36mm}$	|Mass of material passing 2.36mm slots (g), and
M_{TOTAL}	|Total mass of material (g).

For the wet ACV test, the same general procedure can be followed, except for a few minor steps. Firstly, the material should not be dried but soaked in water for approximately 24 hours. After the material has been soaked, it should be allowed to drain for around 5 minutes and dried off with a damp cloth. Secondly, after the material has been crushed in the compression testing machine, the material should be dried in a forced-draft oven at 110 ºC for 24 hours before the material can be sieved.